Dynamic post-elastic response of transmission towers

By Xiaohong Zhang

Department of Civil Engineering an Applied Mechanics

McGill

December 2009

A Thesis submitted partial fulfillment of the requirements of the Degree of Doctor of Philosophy

To My Sons Zhihao and William

Abstract

Collapse of transmission towers can occur due to accidental loads such as conductor breakages, failures of insulators or other components, either under every day conditions (components with marginal strengths) or under extreme conditions such as ice storms, thunderstorms, tornadoes, fires, explosions, heavy mass impacts, etc. Furthermore, the trigger of one tower collapse may cause a catastrophic cascading failure of the whole transmission line section as was observed in the 1998 ice storm in Quebec, Canada. Knowledge of the post-elastic capacity of towers is necessary to mitigate the risk of cascading failures in overhead lines.

The thesis presents a detailed study of the post-elastic response of latticed towers combining advanced (highly nonlinear) finite element analysis and full-scale dynamic testing of four tower section prototypes. USFOS, commercial software developed for post-elastic analysis of offshore platform structures, was selected as the numerical analysis tool to perform the nonlinear static and transient dynamic analysis of transmission towers. USFOS good performance was demonstrated on several case studies. The lattice towers are modeled with special three-node beam elements that include nonlinear material constitutive models for post-elastic response and the geometric stiffness matrices for elements are progressively updated to account for the second order effects. The numerical models also include the effects of connection eccentricities between diagonal members and the main leg members. The numerical models have been used to plan the physical tests and for re-analysis of the models with the experimental loads as measured during the physical tests. Four full-scale transmission tower model sections were built and tested under different load scenarios to verify the results from the

numerical analysis. The prototypes were loaded at the tip of the cross arm, in the tower transverse direction (along the cross arm length) for the bending test and in the perpendicular direction, for the flexure-torsion test. Each of these loading cases was applied first in the quasi-static regime, in a pushover test, and then in the dynamic regime, under a strong dynamic pulse. These dynamic pulses were realized by dropping a large mass weighing 12.6kN from different heights (2 m for flexure-torsion and 6 m for bending).

The salient conclusions of the research as follows:

- The numerical models and the physical test results are in excellent agreement, both in terms of predicting the collapse loads and the sequence of element failures until collapse.

- The research demonstrates that it is possible to use post-elastic analysis to accurately predict the reserve strength of bolted lattice towers provided connection eccentricities are properly modeled at peaks or cross arms loading points and in diagonals connected only on one leg.

- Both the numerical model and experimental results indicate significant post-elastic reserve strength of the tower section. In the tower prototypes tested in this research, the post-elastic reserve strength was 1.22 for flexure-torsion (i.e. tower under longitudinal loading) governed by diagonals, and 1.37 for bending (i.e. tower in transverse loading) governed by inelastic buckling of the main legs.

- Diagonal members affect the failure modes of transmission towers and their connection design may be a weak link in the development of their post-elastic capacity. Diagonal members connected on one leg only are subject to biaxial

bending, they cannot develop the full strength of their cross section since the unconnected leg takes much less stress on its entire length.

- Consideration of the tower post-elastic capacity is necessary for realistic assessment of tower vulnerability to extreme loads.

- Accurate pushover post-elastic analysis is an essential design tool to ensure that the tower capacity is adequate and that failure modes are safe, i.e. not leading to progressive collapse. With appropriate training, such analysis is feasible in a design office.

- Observations from physical tests, confirmed by numerical simulations, suggest that failure modes under pushover static and dynamic pulse loading are similar.

- The ultimate loads sustained by the prototypes in the dynamic tests are higher than their static counterparts (162kN vs. 126kN in bending, and 57kN vs. 51.2kN in flexure-torsion); this can be explained by the strain rate effects, which were particularly large in the bending test due to a mass dropping height of 6 m.

- The numerical models could not accurately predict the displacements of the prototypes due to foundation movement and splice connection slippage, which were not modelled. However, such movements do not have a significant effect on the tower capacity and post-elastic response.

Sommaire

Les effondrements de pylônes de lignes de transport à haute tension peuvent se produire sous charges accidentelles de causes varies: ruptures de conducteurs, rupture de chaînes d'isolateurs ou autres accessoires ou pièces d'attache des conducteurs au pylône, sous des conditions d'utilisation journalière normale (bris de composants dont la résistance st marginale) ou sous des conditions extrêmes (tempête de verglas, tornade, incendie, explosion, impact d'objets lourds, etc. De plus, comme nous l'avons observé lors du Grand Verglas de janvier 1998 au Québec, un bris localisé peut déclencher une ruine en cascade de plusieurs supports.

Il est nécessaire de connaître la réserve de résistance post-élastique des pylônes afin de pouvoir concevoir efficacement des systèmes capables de résister aux effondrements progressifs en cascade.

Dans cette thèse, l'auteur présente une étude détaillée de la réponse post-élastique des pylônes à treillis en acier. L'étude combine les techniques avancées d'analyse non linéaire par éléments finis et la réalisation d'essais destructifs sur quatre prototypes de sections de pylônes à treillis en pleine grandeur. Le logiciel utilisé pour les analyses est USFOS, un produit développé en Norvège pour l'analyse post-élastique des plates-formes de forage offshore en haute mer.

La bonne performance du logiciel USFOS est démontrée à l'aide de plusieurs exemples. Les modèles sont basés sur l'utilisation d'un élément fini de cadre à trois nœuds qui inclut les non linéarités dues au comportement inélastique du matériau ainsi que les non linéarités géométriques. Les modèles incluent également les effets des excentricités de

connexions des membrures diagonales aux membrures principales. L'auteur a utilisé les modèles numériques détaillés des prototypes d'essais pour faire la planification détaillée des essais. Les modèles ont ensuite été ré-analysés en utilisant les charges mesurées lors des essais.

Quatre prototypes d'essais ont été construits et testés sous différents cas de charges afin de vérifier les résultats des analyses par éléments finis. Les charges étaient appliquées aux prototypes à l'aide d'un câble de chargement attaché au bout de la console, en direction transversale de la ligne (i.e. le long de la console) pour l'essai de flexion, et en direction perpendiculaire, pour l'essai de flexion-torsion. Ces deux cas de charges ont été appliqués en régime quasi-statique (*pushover* monotonique) et en régime dynamique par forte impulsion. Les charges dynamiques ont été réalisées en laissant tomber une masse de l'ordre d'une tonne (poids de 12.6 kN) d'une hauteur de 2 m pour l'essai de flexion-torsion et de 6 m pour l'essai de flexion.

Voici les principales conclusions de cette recherche :

- La concordance entre les résultats d'essais et les modèles numériques est excellente, tant pour les charges à la rupture que pour la séquence de ruine des membrures jusqu'à l'effondrement.

- Il est possible d'utiliser des analyses post-élastiques pour prédire avec précision la réserve de résistance des pylônes à treillis à condition d'inclure les excentricités de connexion des membrures des cornières des membrures diagonales connectées sur une seule aile ainsi qu'aux points de chargement au pylône en bout de console.

- Les modèles numériques et les résultats d'essais révèlent une réserve de résistance importante, de 1.22, pour les prototypes testés en flexion-torsion et gouvernés par les membrures diagonales, et de 1.37 dans le cas de flexion, gouverné par le flambage inélastique des montants.

- Les membrures diagonales des pylônes à treillis ont un rôle important dans leur mode de rupture et la résistance de leurs connexions peut s'avérer un maillon faible dans le développement de leur résistance post-élastique. Les diagonales connectées sur une seule aile sont incapables de développer la résistance maximale de leur section puisque l'aile non connectée n'est pratiquement pas sollicitée.

- Il est nécessaire de tenir compte de la réserve de résistance post-élastique des pylônes à treillis pour évaluer leur vulnérabilité sous charges extrêmes.

- L'analyse post-élastique de type *pushover* est un outil indispensable pour évaluer la résistance post-élastique des pylônes et vérifier que leur mode de rupture est sécuritaire, i.e. qu'il n'y a pas de risque d'effondrement progressif. Ce type d'analyse est accessible aux ingénieurs des bureaux d'étude et spécialistes en conception de lignes, avec une formation d'appoint.

- Les observations lors des essais, corroborées par les résultats des simulations par éléments finis, indiquent que les modes de rupture en *pushover* quasi-statique et en mode d'impulsion dynamique sont semblables.

- Les charges ultimes résistées par les prototypes lors des essais dynamiques sont supérieures aux charges ultimes quasi-statiques, (162kN vs. 126kN en flexion, et 57kN vs. 51.2kN en flexion-torsion). Ceci s'explique par les effets

d'augmentation de résistance liée au taux de déformation, lequel était particulièrement élevé dans l'essai de flexion dynamique avec hauteur de chute de 6 m.

- Toutefois, les modèles numériques n'ont pas permis de prédire le comportement en déplacement des prototypes, lesquels sont dominés par les effets du mouvement rotationnel de la fondation et le glissement des connexions boulonnées des montants permis par le surdimensionnement des trous dans les pièces connectées. Toutefois, ces déplacements additionnels n'ont pas d'influence significative sur la résistance ultime des pylônes et sur leur comportement post-élastique.

Originality of Research and Contributions to Knowledge

To the best of the author's knowledge, this research has the following original contributions:

- Full investigation of the ultimate capacity and failure modes of individual lattice steel towers both statically and dynamically in their post-elastic regime. At a lower loading rate (300 to 1000 kN/s), the dynamic and static failure modes are similar, but at a higher rate (10,000 to 30,000 kN/s) the dynamic failure mode is different and the local failure of diagonal members near their connections controls the global capacity. These localized failures are attributed to stress wave propagation. No similar detailed results are available in the scientific literature.

- Full pushover static and dynamic tower tests on prototypes of real-scale dimensions for the verification of the numerical analysis. The tests were planned by the author and conducted with the assistance of transmission engineers and technical personnel of Hydro-Québec. No similar detailed results are available in the scientific literature.

- An original modeling approach was proposed to account for loading eccentricities of single angle section members, which are largely used in transmission tower design.

- The numerical modeling methodology developed and validated in this research can readily be used by the transmission line industry to improve its design practice and take advantage of the tower post-elastic reserve under exceptional load. This will also help in designing towers and overhead lines by controlling failure modes to ensure that dangerous modes that may lead to progressive collapse are presented.

- The results of this research will likely have a great impact on overhead line design practice for consideration of extreme loads, and in particular in design to prevent line support cascades by efficient failure containment.

Acknowledgements

Table of Contents

List of Tables

List of Figures

Chapter 1 Introduction

1.1 General

Electric power plays an ever increasingly important role in keeping this world safe and in order; therefore, its reliable and continuous operation is essential. Transmission line systems relay the power from its production site closer to its users: malfunctioning of the transmission system, which feeds the subtransmission and distribution systems, may therefore lead to massive power outages. A better understanding of the structural response of transmission line systems under various extreme loading conditions is necessary to improve line safety and security. In order to fully understand this physical system, we need to expand our knowledge about the loadings, the structural strengths of its various components and their failure modes.

Climatic loads on overhead lines are defined using stochastic models, as presented for instance in the ASCE Manual on Engineering Practice No. 74 (ASCE 2001). In particular when defining extreme loads due to ice and wind, such models are still a research subject involving much cooperation between engineers and scientists. A lot of statistical data on climatic loads are continuously being collected and several past research results have been implemented into design procedures, for example, the recent updated wind maps and ice maps of the United States by the ASCE 7 Committee (ASCE/SEI 2005).

On the resistance side, numerous research papers dealing with structural capacity of individual components subjected to various loading conditions have been published and many experimental data are available, therefore it is possible to predict the resistance of components with reasonable accuracy. Specifically, when defining the strength of a transmission tower, conventional design will not allow the material to enter into the post-elastic regime. This is certainly justified in service load conditions, but in our opinion, this is not appropriate (and certainly not economical) for the whole transmission line to remain in the elastic regime when resisting the unlikely extreme loading scenarios. This

conventional elastic design can either overestimate the capacity of a single member by assuming an eccentrically loaded beam-column working as a simple truss member or underestimate the whole tower capacity by dismissing the extra capacity from post-elastic behavior. For a realistic assessment of line security, the full investigation of the ultimate capacity and failure modes of transmission towers under both static loading and dynamic impact is necessary. This research will demonstrate how such investigations can be carried out.

1.2 Background

As shown in Figure 1.1, a transmission line system is comprised of conductors, ground wires and their supporting structures. It is common in practice to refer to both electrical conductors and shield wires simply as conductors, but in this thesis we choose to distinguish them because they typically load the towers in different ways on suspension supports. The electrical conductors are always connected to the supporting structures via strings of insulators: these strings may be either mechanically suspended or anchored to the towers. Shield wires are typically suspended or anchored to ground wire peaks using axially rigid hardware components. When shield wires are suspended, the suspension links are typically quite short, thus providing little slack when they swing, and it is often assumed in analysis that they are anchored.

Transmission towers are classified into three main categories: dead-end towers, angle towers and suspension towers, which have different structural functions. Considering a family of towers of similar shapes, the dead-end tower (including its foundation) is the heaviest and most expensive, followed by the angle tower and the lightest and least expensive is the suspension tower. This is because towers with anchored conductors are subjected to large horizontal unbalanced loads, either due to unequal spans or to the components of cable tensions when the transmission line changes direction.

A classical lattice transmission tower (such as shown in Fig. 1.1) is a highly redundant structure with consideration of all its secondary bracing members, whose main function is to improve the stability of the main load-bearing members.
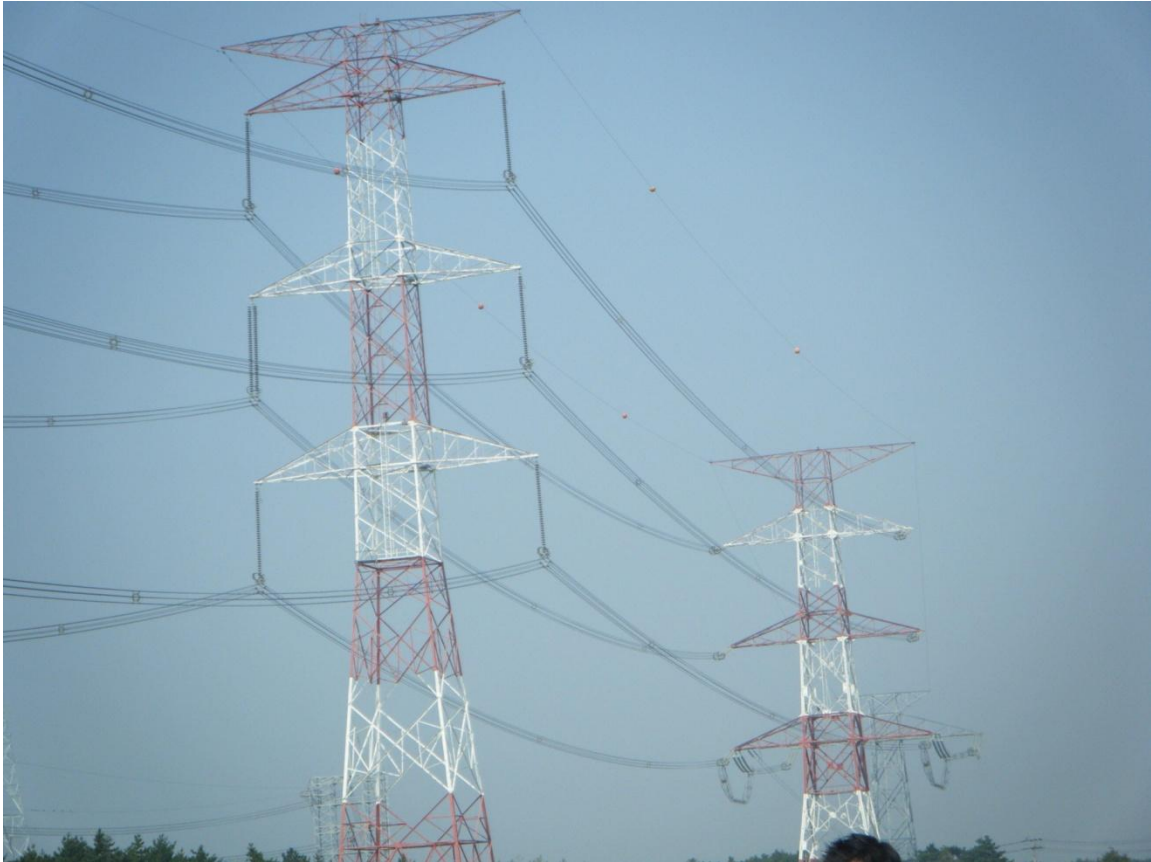
Figure 1.1 Transmission line section on lattice towers

A well-designed redundant structure should not collapse when only a few constituent members fail – this is the true benefit of redundancy. However, only a nonlinear post-elastic analysis can predict the behaviour of a redundant structure at its ultimate state. But in spite of the attractive rewards of conducting a nonlinear post-elastic analysis, most line engineers avoid using this type of analysis, for at least the following four reasons:

- The theory underlying nonlinear analysis is not familiar to most structural engineers.
- The time required for nonlinear post-elastic analysis is usually a multiple of that for a linear analysis, the extra time being mostly invested in the modeling phase and in the interpretation of analysis results.

- For such analysis, the detailed identification of material properties and imperfections is difficult.
- In transmission tower structural analysis, there is no widely accepted methodology or procedure for nonlinear analysis.

We believe that this last point is the real obstacle to more widespread post-elastic analysis.

The failure of a line system may be triggered by a variety of accidents: flashover, foundation failure, ice storms, strong wind storms (hurricane, downburst, and tornado), earthquakes, failure of weak mechanical component in the conductor assembly system, fire, impact by aircraft, sabotage, etc. A tower cascading failure is regarded by the industry as the most detrimental failure because of its direct high cost/time of repair and the ensuing long power outages likely to jeopardize human safety and to cause significant property losses (Commission – 1998 Ice Storm 1999). Since the beginning of the 20th century; line designers have tried to propose effective ways of designing economical lines able to prevent tower cascading failures (Peabody 2001). However, cascading failure prevention can be economically feasible only if the post-elastic response of towers can be accounted for.

As it will be summarized in the literature review of Chapter 2, some researchers have worked on the prediction of longitudinal unbalanced loads on lines while others have focused on reducing the maximum tension in the conductors so that the maximum loads transferred to the towers are controlled. But up to now, because of the modeling challenges and the difficulties to perform meaningful experiments, the understanding of line cascades and the methodology to prevent them are quite disperse: individual power utilities must decide if and how to protect their systems without specific guidelines. With the advanced state of computer simulation technology and the affordability of high-performance computing, including user-friendly graphical interfaces for data pre- and post-processing, the complete numerical modeling of a transmission line for nonlinear structural analysis is now possible. With adequate experimental validation, numerical

simulation tools can provide very realistic predictions of line response that will allow the improvement of design guidelines for extreme loading.

1.3 Statement of the Problem

An overhead transmission line is a highly interactive structural system. In addition, the overhead cables (the conductors and the ground wires) and their suspension insulator strings are highly geometrically nonlinear. For example, if one conductor (or a phase bundle) breaks, the whole line section (bounded by strain towers) will readjust its configuration, and these changes in geometry will in turn affect intact cable tensions. As a result, the loads on the towers will also change. It is very important to account for these interactions when performing structural analysis of a line section, even when its individual components remain elastic. To fully understand the cascade failure mechanism – and to devise means to stop cascades – it is essential to describe these interactions when some of the line components undergo permanent deformations, in both the quasi-static and dynamic load regimes. In this thesis, the specific objective is to study the post-elastic response of classical lattice towers.

A lattice steel tower is an assembly of many (typically hundreds) of angle (L-section) members, which are eccentrically connected by using bolts and plates. It is a well known fact that the lattice tower structures with thin-walled angle members are very difficult to analyze accurately, in particular with consideration of the large deformation and inelastic material properties and inelastic buckling (Lee and McClure 2006). As far as the author knows, there is no commonly accepted finite element for second-order nonlinear analysis of angle sections which is able to predict the buckling load by using only one element.

A very common practice in lattice transmission tower design is that all the members are considered as ideal pin-ended truss elements. This practice dates back to the early 20th century when graphical methods (polygons of forces) were used for structural analysis. Since redundant truss members take zero load in linear analysis, they are designed using empirical formulas (IEC60826, CENELECEN-50341-1, and ASCE Manual 52 and

ASCE10), which are based on a fraction of the compressive force to be resisted by the main member which they support laterally. Even with the advent of matrix analysis and computer methods in the 1970s, this approach was still used for tower design because it yielded satisfactory performance for the usual static loading conditions combined to the allowable stress design method. After 1970 most designs were based on a yield design method (essentially allowable stress design method without safety factors), which is still in use today in the U.S.A. n, After the limit state design method was introduced in the 1980s for building design, the transmission line industry adapted with special consideration of return periods for various climatic loads. All of these methods are inappropriate for collapse analysis. From a mechanical security perspective, it becomes important to know how the traditionally-designed towers - hundreds of thousands of them are in operation worldwide - will behave (and fail) under extreme loads, both in the static and dynamic regimes.

This thesis presents an analysis methodology that will provide answers to the following questions:

- What is the strength reserve in classical lattice towers if the post elastic behaviour of all the main legs and redundant members together is considered?
- What are the tower failure modes that are to be considered safe?
- Will the tower failure mode differ if the loading is applied by static pushover (actually applied by displacement-control in tower-test stations) or by dynamic shock loading?

The study of lattice tower failure modes, i.e. understanding the chain of successive component failure events that will lead to tower collapse, is a central goal of this research. This is paramount for rational line security management – this lack of knowledge explains why transmission line towers continue to fail, every year, often at load levels well below their design values.

In the real world, designing transmission lines with zero probability of collapse is neither feasible nor possible. There always exists a risk of failure under some uncertainty. In

reliability words, the likelihood of failure, though very small, always exists. When failure happens despite its low likelihood, engineers say it is accidental. But accidents do happen. So the engineering challenge is to predict the failure modes accurately and design structures to fail in a specific way which can prevent the most severe damages, minimize the cost of repairs, or to provide a countermeasure to prevent tower cascades.

1.4 Some Definitions

Material Nonlinearity

For mild structural steel typically used in transmission towers, laboratory tensile tests on coupons show that the yielding limit is in the order of 50% less than the ultimate limit which is obtained with large strains of 30 to 40% (Kulak and Grondin, 2006). In traditional linear elastic analysis, it is assumed that the material stresses are directly proportional to strains and remain below the yielding limit, and no permanent deformations are left after unloading. Only a materially nonlinear analysis can take into consideration the post-yielding response, where stresses exceed the proportionality limit and permanent deformations remain after unloading. For large transmission towers, the modeling of material nonlinearity is important for the prediction of their ultimate capacity. (Albermani and Kitipornchai 2003)

Geometric Nonlinearity

Transmission line systems are highly geometrically nonlinear and their equilibrium must be verified in their deformed state. In matrix structural analysis, geometric nonlinearity is reflected in the formulation of the stiffness matrix of the system, which requires updating as the structure deforms. The global stiffness matrix of the system can be decomposed into three constituents: the linear stiffness (initial or secant), the geometric stiffness and the deformation stiffness due to the coupling between the axial stretch and the flexural and torsional deformations (Bathe 1996).

Progressive Collapse/Cascading Failure

Progressive collapse is a chain reaction of structural element failures, disproportionate to the initial damage (usually a local component failure), resulting in partial or full collapse

of the transmission line section. When the triggering failure happens in the system maintaining the conductor tension (conductor or hardware failure), the progressive collapse is a dynamic event involving vibrations of transmission line components and dynamic internal forces, such as inertia and damping forces, whose energy may or may not be absorbed by the structure. Progressive collapse may also happen in a quasi-static manner when no significant inertia forces are induced: an example of such a "slow" collapse would be the progressive longitudinal failure of adjacent supports whose longitudinal capacity would be inferior to the unbalanced load created by the initial support failure. Progressive collapse, be it dynamic or quasi-static - is a nonlinear event in which some of the structural elements are stressed beyond their elastic limit to failure.

Progressive collapse involves two types of loadings on the supports: the load that causes the first structural element to fail (for example the extreme ice load on the conductor that increases the cable tension) and the loads that are generated due to the structural motions or load imbalances caused by the first element failure (secondary loads). External abnormal loads, such as blast, ice storm, etc. may be the source of primary loads, while secondary loads result from internal static or dynamic loads and are caused by (slow or sudden) changes in the load path through the structure geometry. Although estimation of primary loads is important, this research is focused on the effects of secondary loads.

The best way to mitigate the effects of progressive collapse is to prevent it altogether; however, total prevention, i.e., reducing the probability of occurrence to zero is not feasible. Alternatively, proper structural design can greatly reduce the probability of progressive collapse through attention to structural details and material properties. Progressive collapse analysis is necessary to evaluate whether the initiating damage would propagate throughout the transmission line section.

A cascading failure is the description of the progressive failure for an overhead line system, which means one critical component failure (for example a conductor breakage) will trigger the collapse of a tower, which will in turn cause the collapse of an adjacent tower, and in a domino effect this second tower failure will trigger the collapse of the

8

next tower, and so on. A line cascade failure may vary from several spans (say about 10 towers) to hundreds of spans. For example, during the January 1998 ice storm, 256 structures on Hydro-Québec's Yamaska to Saint-Césaire line were lost in several cascades (Commission - 1998 ice storm, 1999)

1.5   Research Objectives

This research project has two main objectives:

- To investigate the ultimate strength reserve of a classical steel lattice tower with consideration of post-elastic effects by full-scale static and dynamic tests and by detailed computational models.

- To determine and compare the static and dynamic failure modes of the tower.

1.6   Research Significance and Original Contributions to Knowledge

This research is original in many respects. This is the first time that an experiment is carried out on a full-scale classical tower section in both the static and dynamic regimes of loading. The author has planned the entire testing program using initial detailed numerical simulations of the post-elastic response of the tower prototype.

The author has established a post-elastic modelling approach, using commercial finite element analysis software originally developed for offshore platforms: all the important modelling aspects are discussed in the thesis. Only careful modelling can lead to accurate prediction of the post-elastic ultimate capacity of transmission towers and their failure modes. The computational models are fully verified by the test results, and the author believes that the approach developed is valid to apply to other classical towers of similar construction, i.e. made of bolted angle steel sections.

This is also the first time that lattice tower failure modes are observed and predicted in both the dynamic regime (shock loads) and the static regime (pushover loads). The shock loads selected model an impact horizontal load possibly caused by a conductor failure

inducing torsion and bending on the tower, or by a transverse shock inducing mostly bending effects.

This research and the modelling methodology that is proposed and validated have very important practical applications. The author has shown that it is possible to use computational mechanics to analyze the complex effects resulting from shock load scenarios on the transmission towers with the full consideration of nonlinearities and structural interactions among the line section components. If adopted by the transmission line industry, post-elastic computational modelling will become a powerful tool to improve tower failure confinement design and reduce the occurrence of catastrophic tower failures.

1.7 Organization of the Thesis

After this introduction, Chapter 2 will present a literature review focusing on the post-elastic analysis method for classical lattice steel towers used in transmission lines. Important published work on static post-elastic structural analysis applicable to planar and spatial structures will be reviewed first. Then, some detailed understanding of the behaviour of structural angle sections will be presented. It is noted that there are only a few references addressing the full scale dynamic testing of towers, and they do not present many details.

In Chapter 3, several specific topics will be discussed regarding the computational modelling techniques and the many challenges in modelling transmission line structures.

Chapter 4 will present the full scale tests. Four 10-m high tower section prototypes were tested at the site of IREQ (Hydro Québec's Research Institute in Varennes, Québec). The prototypes and testing protocols will be described first. Then, the experimental results will be presented in some details in terms of ultimate strength, failure modes, force-displacement relationships, to name the most important aspects.

Chapter 5 is dedicated to the results of the numerical simulations. At the beginning of this research, very careful attention was paid to the verification of the software selected (USFOS developed by SINTEF, Norway www.usfos.com). We first compared the static analysis results of USFOS with the results obtained from two North American general-purpose finite element software available in the Department, SAP2000 (www.sap.com) and ADINA (www.adina.com). With a favorable agreement both in the static domain and for the natural frequency analysis results, we began our dynamic numerical simulations to investigate the best approach to model the force time history function as the main external load applied at the tip of the cross-arm. After numerical experiments on small tower sections, we moved to the full-scale tower test simulations and obtained the results of four simulations corresponding to their experimental counterparts.

Chapter 6 is the detailed discussion and comparison of the numerical results and the experimental results. As mentioned in Chapters 4 and 5, it is quite a challenging task for the full-scale dynamic tests. The work presented in this chapter proves that careful numerical simulations can be reliable and more economical than prototype tests.

Finally, Chapter 7 presents the summary of the main observations and conclusions of the research.

Chapter 2 Review of Literature

2.1 Overview

As mentioned in the introduction, this research has two main objectives: the first is to determine the reserve capacity of a typical lattice tower with consideration of its post-elastic behaviour, and the second objective is to compare the dynamic failure modes under impact loading and the static failure modes under monotonic pushover loading. In this chapter, the post-elastic analysis method and the general theory applicable to steel structures will be reviewed first, followed by a presentation of the different models and material constitutive laws most commonly used in steel structures. Dynamic analysis aspects of transmission tower structures will be covered after, noting that published research on the subject is very scarce. Of particular relevance are a description of the conventional analysis method of transmission towers and the evolution in transmission structure design practice. The chapter ends with a specific review of analysis procedures for angle section members used in conventional lattice transmission towers.

2.2 Static Post-Elastic Analysis of Lattice Towers

The research papers related to this topic may be classified into two categories. The first category is related to ideal truss structures, either space truss or plane truss, as the main analytical assumption: the tower members are assumed to be developing only axial and centric internal forces. The second category is related to frame structural analysis, where the tower members can also resist shear forces and moments, depending on their end connections.

Truss Models

With the ideal truss model, the complexity of the problem can be reduced significantly without compromising design safety for normal loading conditions where the tower is expected to remain elastic. As all the elastic strain energy is resisted by axial effects in

members, the ideal truss assumption will lead to conservative values of member forces. The simple truss model can also be used with success in post-elastic analysis.

The analytical work related to materially nonlinear truss analysis done before 1996 was summarized by Blandford (1997) who covered most of the important aspects of the theory. The Green-Lagrange representation of the axial strain, $\bar{\varepsilon}_x$, is required for materially nonlinear analysis of members in uniaxial loading:

$$\bar{\varepsilon}_x = \varepsilon_x + 2\eta_x \qquad \text{(Eq. 2.1)}$$

in which ε_x =du/dx is the linear or engineering strain and

$$2\eta_x = \left[(du/dx)^2 + (dv/dx)^2 + (dw/dx)^2 \right] \qquad \text{(Eq. 2.2)}$$

$\bar{\varepsilon}_x$ is the nonlinear strain; and u, v and w are translations along the local element coordinates x, y and z. Blandford also discussed member failure models including elastic postbuckling, inelastic postbuckling and constitutive modeling of the truss material behaviour. He reported using successfully the arc length control nonlinear algorithm in the equilibrium iterations required to trace the response in the post elastic phase. (Blandford 1997)

The simplicity of truss analysis is appealing to tower designers: as a matter of fact, before the advent of computer methods, this was the standard approach with graphical equilibrium solution of force polygons. However, this approach can overestimate the strength of the tower because in reality several connection eccentricities may exist, which introduce secondary moments in the members. These eccentricities tend to reduce significantly the compression capacity of slender members, in particular. Dynamic analysis of trusses becomes in fact a problem of dynamic stability, where one wants to determine the influence of a sudden member failure or snap-through member buckling on the neighbouring members.

Do *et al.* (1993) reported the results of a full-scale static test on a 31.4 m high microwave tower owned by the Bonneville Power Administration (BPA) in the USA. The test was

performed in order to generate data for the calibration of BPA's post-elastic tower analysis software LIMIT. Based on this test, they have found that the actual failure load was 1.54 times the value predicted at first yield (by linear elastic analysis). Their software was specifically developed to analyze lattice towers as space trusses using a first-order nonlinear analysis taking into account the post-buckling performance of steel angle (L-section) members. No mention is made regarding the modeling of connection eccentricities.

Frame Models

Al-Mashary and Chen (1990) have studied a simplified method for static second-order elastic analysis of two-dimensional frames based on the matrix formulation of beam-column stability functions. To reduce computational demand, the method used only one step of iteration in addition to the preliminary step of the first-order analysis. Its application to more realistic three-dimensional structures and frame-truss lattice towers was not addressed.

Andrew *et al.* (1991) have developed a one-element-per-member method aimed at improving the efficiency and user-friendliness of nonlinear finite element analysis programs for frame structures. The interpolation functions of these higher-order elements enabled to model each member by one element only and were proposed to replace the conventional Hermitian cubic functions. Their goal was to reduce the computation time, which at the moment of their research was an important practical issue. They confirmed that in most cases, a single fourth-order element was sufficient to model a member in a static buckling analysis, which meant a significant saving in computer time, data input and interpretation efforts.

Plastic Hinge Methods

A common approach used in plastic analysis of steel frames is to consider that material nonlinearities are concentrated at the location of a hinge carrying a maximum plastic moment. As mentioned in White (1993) some important issues are associated with plastic hinge methods. In the *elastic-plastic hinge method*, the members are modeled as fully elastic elements between the plastic-hinge locations. This simplifying assumption can provide essentially the same load-deflection predictions as refined plastic-zone methods for many practical design cases, but it is not adequate to represent the response of individual members of the frame.

As an improvement, the *tangent-modulus- plastic hinge method* uses a tangent modulus expression for the member stiffness between plastic hinge locations. This approach does not account for the effects of distributed yielding along the member length due to flexure since the tangent modulus is not reduced from its elastic value until the applied load exceeds 50% of the yield load. These distributed yielding effects have a major influence on the inelastic stability of weak-axis bending cases, where the difference between the initial yielding and the cross-section straight curve is large. According to White (1993), when restricted to strong axis bending cases, the method is slightly unconservative (by about 7%) in the assessment of the ultimate strength. This range of error is similar for both the beam-column capacity as well as the pure axial strength of columns. Further improvements of the method are possible by accounting for the additional distributed plasticity effects associated with flexural action, but these have not been implemented.

Advanced inelastic analysis of transmission towers

Albermani and Kitipornchai (1992) have applied advanced nonlinear analysis to transmission towers. They emphasized that the problem is complicated by the spatial nature of the configuration and by the fact that individual components are asymmetric angle shapes that are eccentrically connected. The elements are then subjected to uniaxial loading and biaxial bending effects, which are impossible to model using conventional 3D elastic truss-type methods. The same author later suggested to model steel lattice

15

towers with beam-column elements according to a "lumped plasticity coupled with the concept of yield surface in force space" approach (Albermani and Kitipornchai 1997).

Liew *et al.* (2000) have provided a state-of-the-art summary on inelastic analysis of three-dimensional frame structures. For comparison purposes, a three-dimensional truss was modeled using the conventional strut-and-tie model, and rigid space frames were modeled using the Hermitian beam-column element. Particular attention was devoted to inelastic material modeling of the components for accurate representation of the formation of plastic hinges in large-scale frameworks. Important issues discussed related to inelastic buckling and post-buckling unloading of struts, modeling gradual yielding in steel beam-columns, inelastic modeling of composite (concrete-steel) floor beams subject to sagging and hogging moments, modeling of building core walls and semi-rigid beam-to-column connections in three-dimensional structures. Numerical examples were provided to illustrate the acceptability of the use of the inelastic material models in predicting the ultimate strength and inelastic behavior of spatial frameworks. This approach was intended to make the tool of plasticity analysis available for the practicing engineers. Eventually, the conventional two-step or multi-step design procedure could be consolidated into a one-step analysis tool that would directly handle both the limit state (first yield) and the ultimate state (collapse).

Only a few examples of lattice tower models are presented in the literature where detailed nonlinear static analysis results are verified by full-scale test results. In Robert *et al.* (2002), nonlinear analysis results are compared between a truss model and a frame model where the tower legs are represented with frame elements while the secondary bracing members (redundant members ignored in linear analysis) were also taken into consideration. Both models yielded similar results but the frame method is preferable because it allows checking whether flexural effects may lead to premature failure.

Kempner *et al.* (2002) have expressed the opinion that with the maturity of the transmission tower engineering profession and the advances in computational solution power, the transmission tower designers can now look into the marginal strength beyond

the simple truss model. They have compared the numerical predictions of three advanced transmission tower analysis computer programs for one benchmark tower problem that was to be tested at the full scale.

Albermani and Kitipornchai (2003) have devoted several years of research to nonlinear analysis of lattice transmission structures. They concluded that these structures were sensitive to imperfections and that nonlinear analysis must be applied to investigate their ultimate strength. They have studied the effects of geometric and material nonlinearities, and joint flexibilities on the static ultimate strengths of towers. These effects are especially important when considering the buckling of leg members and cross-arm bottom members, and traditional individual component design procedures may be misleading if such effects are ignored.

It should be emphasized that in all the above mentioned papers, the influence of connections in static post-elastic analysis is not considered and it is assumed that the connection should not fail before the structural members. In this research, the ultimate strength of the connections is not investigated, and it is assumed that the connections should not fail. However, it is important to keep this assumption in mind when assessing the ultimate strength of existing towers which may have been designed with connections weaker than the connected members.

2.3 Dynamic Analysis of Lattice Towers

Very few research papers have addressed dynamic analysis of transmission lattice towers, which may be explained by the fact that it is not usually required by transmission tower design codes and commercial or industry software dedicated (PLS CADD 2006) to tower analysis typically do not cover structural dynamics options. Also, the dynamic work reviewed was limited to the linear elastic regime due to the complexity of predicting the post-elastic behavior of steel angle shapes. It is evident that dynamic analysis of latticed structures can be performed with general-purpose finite element computer programs. However, utilities have no indication that such analysis is necessary for design purposes.

To the best knowledge of the author, there was no experiment done prior to this research which was dedicated to the investigation of the ultimate strength of real scale lattice towers. Real scale tests had been performed by EPRI (Mozer 1978) but their purpose was to investigate the dynamic amplification factor of the peak conductor tension due to the broken conductors, and the towers adjacent to the breakage did not fail – and no tower damage was reported.

Current electric utility practices on how to design towers for longitudinal impact loads due to broken conductors can be described according to three approaches:

- Use of residual static load method
- Use of stop structures
- Use of load-limiting devices.

In the first approach, each suspension tower is designed to resist the static unbalanced load induced by a broken phase, assuming that towers close to the source of the shock load may be destroyed but that the failure will not propagate in a cascade. The main difficulty with this approach is that it cannot prevent tower cascading failures unless sufficient reserve strength is present. It can be argued that the 1978 EPRI tests (Mozer 1978) are an example where enough reserve strength was present for conductor loads in the bare condition. The issue is therefore to determine how much reserve strength is available in the post-elastic range of the response and what is happening after the first failure. The current design approach is considering individual members and ignores the fact that the load path may be changed significantly by changes in the tower configuration even when the global stiffness parameters are unchanged.

In the second design approach, stop structures are introduced with the intent to stop a cascading failure and absorb any dynamic shock, while the weaker structures of a line section between the stop structures may fail. The issue is then to determine what are the appropriate loads to consider for the design of these stop structures. An approach that became popular in the last decades because of its simplicity is the impact load method

18

(Govers, 1970). This way, the unbalanced design load on the tower adjacent to the failure point is taken as the static unbalanced load multiplied by an impact load factor greater than unity. This method is very convenient because it does not require utilities to determine more realistic dynamic loads using advanced nonlinear analysis software. Therefore, the understanding of tower survival to accidental load events is to consider that the ultimate strength of the tower will exceed the amplified load in a quasi-static manner, without specific investigation of the failure modes.

The impact factor method used by the Bonneville Power Administration and further developed by EPRI is also based on the assumption that when light suspension towers fail in-between stop structures, they absorb some of the strain energy induced by the initial failure and therefore reduce the load on subsequent towers. The impact factor introduced by BPA is of the order of 1.33 only, based on a series of reduced-scale tests (Kempner 1997). It is believed that this value is too low for typical steel lattice towers and the extrapolation of the results from reduced-scale tests to real line sections is questionable. The main difficulty with this approach is in the appropriate choice of the impact load factor. In fact, there are very few published data to validate the magnitude of the dynamic longitudinal impact loading at the real scale from a broken conductor and tower failure scenarios. Application of the research presented in this thesis can produce this kind of data considering different combinations of towers/conductors failure; in fact, it is proposed to use advanced computational mechanics to generate "numerical" experiments of tower failure scenarios.

It is worthy of note that Hydro-Québec TransÉnergie carried out a full-scale destructive test of a steel lattice tower at the St. Luc-de-Vincennes experimental line in 2002 (Guilbault *et al.* 2004) and an impact factor of 2.8 was observed with respect to the residual static load at the tower cross-arm next to the cable breakage induced. Although some load cells and strain gages had been installed on the tower next to the direct impact point and beyond, the investigation of the detailed tower behaviour was not reported in the open literature.

Ramesh *et al.* (1993) discussed the dynamic effects of progressive member failure of truss structures. They considered two types of possible dynamic member failure one is the brittle-type and the other a member snap-through or dynamic jump due to buckling/post-buckling. Their method is to replace the damaged member by the adequate external force functions at its end joints. They studied the transient dynamic effects of member failures including time variations of joint displacements and member stresses, and the changes in natural frequencies of the damaged truss structures. They have observed that sudden buckling failures can cause significant stress redistributions near adjacent members and might cause a second member failure, and possibly trigger progressive collapse.

Sekulovic *et al.* (2002) studied the effects of connection flexibility and damping on the dynamic behaviour of plane steel frames used in buildings in seismic areas. They modeled the eccentric connections by a nonlinear rotational spring and dashpot in parallel. By introducing a complex dynamic stiffness matrix, they have shown several examples to prove their modeling technique. They concluded that the joint flexibility most significantly influences the dynamic behavior of the steel frame by lowering its natural frequencies. This further emphasizes that connection design and modeling have a great practical importance, as we have observed from our experiments.

Mizuno *et al.* (1998) presented a two-surface plasticity model in the force space for steel members; they used it to analyze a steel frame under cyclic loading and the numerical results were in good agreement with their experimental results. This particular concept is implemented in the USFOS software (USFOS 1994) which is used in this research: it will therefore be discussed in more details in Chapter 3 on modeling considerations.

2.4 Angle Section Static Buckling

An angle shape member subjected to axial compression and some amount of bending can fail in the following modes:
- Excessive yielding;

- Overall elastic, inelastic or plastic buckling, governed by the slenderness ratio, the end restraints and the loading;
- Local buckling of angle legs.

Urbano (2001) mentioned that the design criteria for hot rolled angles used in transmission towers are based on the following: the basic column stability curves which account for loading eccentricities and residual stresses, the slenderness ratio, the partial safety factor for strength and the local elastic plate buckling criterion for thin-walled members. However, he commented that different specifications are used in different countries that emphasize different aspects of column design, which results in different approaches in the United States and in Europe.

Earls (2001) used nonlinear finite element analysis in the study of equal leg single angle geometric axis flexure (actually bi-axial bending). His numerical techniques have been validated (with favourable agreement) using a series of experimental results found in the literature related to the ultimate response of angles bent in this manner. The angle shapes used in the study had plate slenderness values (b/t) ranging from 6 to 20, global slenderness values (L/r_z) ranging from 50 to 200, and minimum specified yield stress between 276 MPa and 552 MPa. From the study of the results of more than 500 finite element models, conservative design equations were formulated. The new equations provide for more accurate designs as compared with the current provisions in AISC (1994) section 5.2 of the Specification for the Load and Resistance Factor Design of Single-Angle Members. (AISC 1994).

It is worthy of note that geometric-axis bending of angle sections is the actual failure mode observed in bracing members used in transmission tower structures. Although several tests have been done on individual angle members, they are of limited value to this study because they focus on finding the single member strength without consideration of the real connection complexity found in transmission towers.

As analytical methods are becoming more prevalent in research, it is believed that the conventional slenderness ratio/column curve method is going to be verified by computer simulation. An example of such effort is described in Lee and McClure (2006, 2007). With their model, it is possible to simulate many different loading scenarios and find out the resulting failure modes. Knowledge of these failure modes is important to improve design since dangerous collapse modes must be avoided.

Kemp *et al* (1998) presented the results of a series of 13 tests of latticed tower cross-bracings, and associated theoretical analyses have confirmed the complexity of the behaviour of these apparently simple member arrangements (members connected back-to-back by a single bolt on one leg). For slenderness ratios between 100 and 160, it was found that the cross-over joint acts as an effective restraint to out-of-plane buckling of the strut. The ultimate strength was increased by up to 17% by increasing the number of bolts in the end connection from one to two. A flexibility-based model provided the most accurate representation of the test results. This model confirmed the dominant influence of bending about the orthogonal x-axis on first yield of the section. Due to the dominant effects of the end eccentricity, the secant formula can be used to provide a design formulation for the cross-bracing members in the slenderness ratio range studied. This refined approach provides a more accurate representation than the provisions in the American and European design manuals.

Latticed transmission tower members are galvanized. Abdel-Rahim (1996) studied the effect of galvanizing on the mechanical properties of angle shapes, by comparing the properties of coupons cut from galvanized members with those of coupons cut from the same locations of non galvanized members and tested at the same temperature. The results indicated that galvanized coupons had an increase in yield strength by as much as 36%, an increase in the ultimate strength by as much as 20%, and an increase in the elastic modulus by as much as 39%. However, galvanizing resulted in a decrease in the percent elongation (ductility) by as much as 15%. In the same study, the effect of low temperature on the mechanical properties of cold-formed steel was obtained by the same approach as for galvanized steel. The results indicated that comparing to the room

temperature, the yield stress, ultimate stress and elastic modulus at -50°C are increased by 13%, 14% and 24% respectively. But the elongation decreased by as much as 35% at this low temperature.

Several additional studies too numerous to be reported here have addressed the ultimate capacity of individual angle compression members. Kitipornchai (1983) studied torsional flexural buckling and suggested a parametric solution to determine the buckling load. Madugula and Kennedy (1985) studied the behaviour of single and compound angles under elastic and inelastic conditions. Kitipornchai and Lee (1986) compared experimental results with the theoretical predictions of AISC (United States), AS-1250 (Australia) and SSRC formulae (United States) for the design of single angle struts, they proposed to use an SSRC curve 2 for the design of single and double angle struts and curve 3 for tee struts.

Adluri *et al*. (1996) studied the compressive strength of steel angles failing in the flexural buckling mode. They conducted 71 tests with nine sizes ranging from 64x64x9.5 mm to 152x152x9.5 mm and a new column curve was developed as guidance for calibration with actual designs. The behaviour of all test specimens showed consistently lower capacity than the predicted load mainly because of initial imperfections. The overestimation of the load by the theory was within 20%, and the observed and predicted strain values correlated well (within 10-20%). The load reversal caused stiffness degradation irrespective of the type of load transfer (through shear centre or through gusset plate). However, gusset plate loading caused a notable reduction in capacity after three cycles. Loading through unsymmetrical axis (minor axis) was found to cause severe buckling and limit the energy absorption capacity.

Rao *et al.* (2001) conducted nonlinear FEM analysis on different levels of lattice structures: single angle members, single panel of angle members, and three-dimensional lattice frames as used in typical steel transmission towers. They had concluded that design code provisions were highly unconservative compared to the test results because of the loading eccentricities, member imperfections, and residual stress effects.

2.6 Angle Section Dynamic Buckling Modes

Only a few published studies have investigated the dynamic buckling of simple shapes, and they are summarized next.

Kenny et al (2000) investigated the dynamic buckling of a flat bar impacted on the top and observed generally improved member performance in dynamic conditions compared to static loading: the dynamic yield stress, the ultimate stress and the modulus of elasticity were all increased.

In an experimental study carried out by Hydro-Québec in 2003 (Charbonneau *et al.,* 2006), several angle section samples were tested in order to investigate the loading rate effects and assess the difference between their dynamic and static failure modes. This was an exploratory study with a small number of specimens and it was concluded that within the range of the tested specimens, the loading rate effects appeared significant while the dynamic failure modes did not differ from the static ones. During the tests, a ball joint was used to maintain the applied load concentric, and minor axis buckling was observed, which can be verified by the theory. In reality, this condition is hardly ever achieved and further tests simulating real tower connections should provide more reliable conclusions.

2.7 Lattice Tower Modeling Review

Lattice transmission towers have been modeled as elastic space trusses for decades, and it is only in recent years that some researchers have exposed the shortcomings of this practice and modeling has been shifting from truss to frame-truss or framed members.

In the traditional approach, a latticed tower is described by a one-line design drawing (tower outline) that shows overall dimensions, member sizes and locations. This outline drawing is used to prepare a computer model of straight members pin-connected at joints.

Moments resulting from normal framing eccentricities are not typically calculated in the analysis. A first-order linear elastic analysis is used (capable of carrying compression as well as tension), and assumes that the loaded configuration of the structure (used to verify final equilibrium) is identical to its unloaded configuration.

In a second-order (geometrically nonlinear) elastic analysis, structure displacements under loads induce member forces in addition to those obtained in a first-order analysis. These additional member forces are called the P-Δ effects in building frameworks or transmission pole structures. A second-order elastic analysis may show that the redundant members carry some loads. Very flexible self-supporting structures (such as tubular frames and poles) and guyed structures normally require a second-order analysis; however, such an analysis is not necessary for self-supporting lattice towers.

Specialized computer programs for the analysis of latticed transmission structures typically include the following features: automatic generation of nodes and members that utilize linear interpolations and symmetries, interactive graphics to ascertain model correctness, provisions for tension-only members and for automatic handling of planar nodes, and unstable subassemblies that may develop in a small group of nodes and members. Out-of-plane instabilities or mechanisms are generally prevented in actual structures by the bending stiffness of continuous members that pass through the joints.

In a research report published by EPRI (1986), it was clearly shown that the traditional analysis and design methods cannot be used to accurately predict the capacity of transmission towers, and the necessity of full-scale tower testing was emphasized. Urbano (2001) also concluded that for mass-produced towers, representative full-scale prototypes destructive tests are still needed to verify the design.

Albermani and Kitipornchai (2003) described a nonlinear analytical technique for simulating the ultimate static response of latticed transmission towers. They concluded that geometric and material nonlinearities play a very important role in determining the ultimate response of these structures. They verified that the approach could be used to i)

verify new tower designs, ii) strengthen existing towers and iii) upgrade old towers. However, they support the need for full-scale prototype design tests as sophisticated numerical tools are not commonly used nor understood in practice.

As mentioned earlier, stress calculations in the tower are normally obtained from a linear elastic analysis where members are assumed to be concentrically loaded and, in the majority of cases, to have pinned connections. In practice, such conditions do not exist and towers are detailed to minimize bending stresses in individual members. Results from full-scale tower tests often indicate that bending stresses in members could be as high as axial stresses (Roy *et al* 1984). EPRI (1986) compared data from full-scale tests with predicted results using the method proposed in Albermani *et al* (2003) and concluded that the behaviour of transmission towers under complex loading conditions cannot be consistently predicted using this method: they found that almost 25% of the towers tested failed below design loads and often at unexpected locations (that is in different failure modes than expected).

2.9 Conclusion

The literature review has shown evidence that the traditional analysis and design methods of lattice transmission towers are inadequate to predict their ultimate static response and capacity and their response to dynamic loads, especially in the post-elastic range of response. Our research will show that careful numerical modelling can provide answers that are validated by full-scale physical tests. Accurate post-elastic analysis of new towers can lead to improved design and can serve to evaluate the post-elastic strength reserve of existing towers.

Chapter 3 Modeling challenges

3.1 Selection of nonlinear analysis software

McGill University researchers have been successful at using the ADINA commercial software for cable dynamics and transmission line analysis. The main shortcoming of ADINA at the time this research was conducted was that it did not allow plastic analysis in an easy manner for tower members: It is noted that the work of Lee (Lee and McClure 2006, 2007) was not available then. After comparing with other available commercial software, USFOS (version 8.0, SINTEF, 2003 www.usfos.no) was selected as the numerical simulation tool for this research.

USFOS stands for Ultimate Software package for nonlinear static and dynamic analysis for Offshore Structures. The software has been developed by SINTEF Civil and Environmental Engineering, Structural Engineering and the Department of Marine Structure at the Norwegian University of Science and Technology, NTU, in Trondheim. The main scope of this software is to provide the fully nonlinear analysis (geometric and material) capabilities for complex offshore platform structures under static and dynamic loadings, with post-elastic response tracking features and post-processing options. After some preliminary trials, it became clear that its application to static pushover analysis of latticed transmission towers was very successful, although a few problems remained with conductor dynamics as will be explained later.

3.2 Modeling capabilities of USFOS

3.2.1 General incremental formulation

Equation 3.1 represents the incremental form of static equilibrium in a nonlinear problem at iteration k:

$$K_n \Delta U_n^{(k)} = R_{n+1} - F_{n+1}^{(k-1)} \tag{3.1}$$

Where K_n is the tangent stiffness matrix at load increment n, ΔU_n is the approximate incremental displacement vector, and the terms of the right-hand-side are the out-of-balance loads. For solving these nonlinear equilibrium equations, incremental-iterative methods have been so far the most commonly used algorithm. Loads are applied in small increments, and at each load level several iterations are performed to satisfy the equilibrium and the structural geometry is constantly updated. (Bathe, 1996)

In general, the Euler-Cauchy incrementation algorithm is used but it causes a drift-off from the exact solution path. Corrections for this deviation can be taken care of by specifying equilibrium iterations on the unbalance between the external loads and internal forces after each step. The approach used in USFOS is the original Newton-Raphson method with arc length control. In other words, instead of keeping the load constant during the iteration, the external load and displacement vectors vary according to a prescribed function in "load-displacement space." The tangent stiffness matrix, K_n, in Equation 3.1 is updated after each iteration level. The diagrams in Figures 3.1 a) and b) illustrate the differences between the two approaches, namely the pure incremental solution with a drift-off effect and a modified algorithm with equilibrium iterations.

An interesting feature of USFOS is that each physical element (each tower member in lattice towers) is represented by a single three-node finite element, which facilitates the transfer of input models from conventional linear analysis with minor modifications.

a) Purely incremental solution

b) Incremental solution with load corrections (Eq. 3.1)
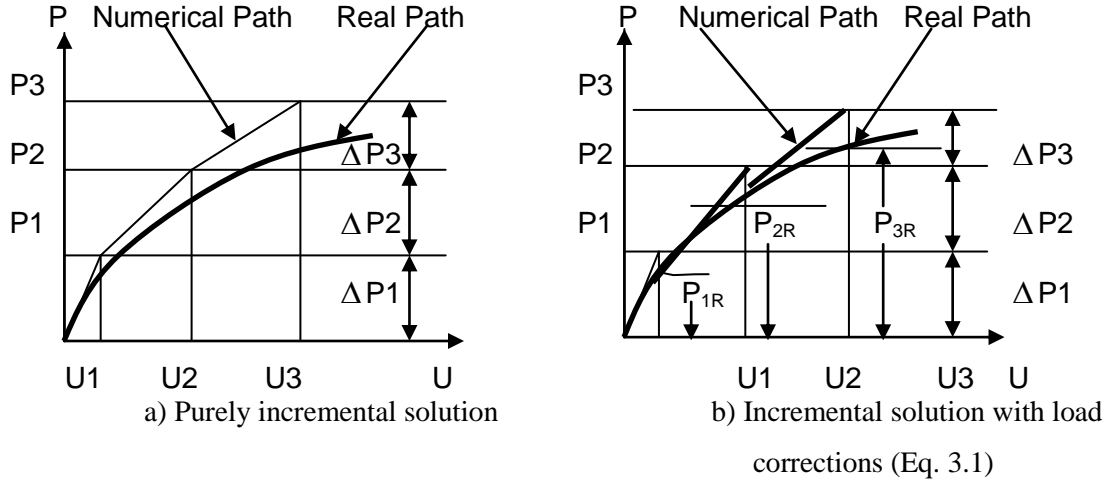
Figure 3.1 Incremental solution of the equilibrium equation *P = f(u)*

3.2.2 Geometric and material nonlinearities

The effects of large displacements and coupling between lateral deflection and axial strain are included by using nonlinear strain relations (Green strain) (Fung, 1965)

$$\text{Green Strain } E_X = \frac{1}{2}\left[\frac{(ds)^2 - (ds_0)^2}{(ds_0)^2}\right] \quad (3.2)$$

where ds_0 and ds are infinitesimal line segments in the initial and current configurations respectively, instead of conventional linear strain (engineering strain):

$$\text{Engineering strain } \varepsilon_X = \frac{ds - ds_0}{ds_0} \quad (3.3)$$

This gives a very accurate representation of the element behaviour, including membrane effects and column buckling.

The relation of Green strain to engineering strain is

$$E_X = \varepsilon_X + \frac{1}{2}\varepsilon_X{}^2 \tag{3.4}$$

In the total Lagrangian formulation (Bathe, 1996), all displacement derivatives calculated at the element level are computed in the original coordinate system regardless of how large a rigid-body deformation may be superposed on the deformations of the element. However, USFOS uses an updated Lagrangian formulation where all the displacement derivatives are calculated according to the last step of the calculated configuration instead of the original configuration, since the element reference axes are updated throughout deformation. At the element level, large kinematics effects are incorporated by additional second order strain terms while the global effects are taken into consideration by updating nodal coordinates of the structure.

The tangent stiffness matrices, corresponding to the derivatives of the internal element nodal point forces F_t with respect to the nodal point displacements U_t, are derived in a consistent manner from energy principles. This preserves symmetry in the equations, and allows for the use of an efficient skyline equation solver. The elastic tangent stiffness matrices are calculated for Hermitian beams.

Linear, geometric and deformation stiffness matrices are used to describe the geometric nonlinear behaviour of these elements in the updated Lagrangian framework. The formulation can include nonlinear geometric effects at the local element level and large kinematics at the global structure level. Geometric nonlinearity accounts for the effects of accumulated stress on the stiffness of the elements and the effect of the continuing changes in the geometry as the applied load is increased. The buckling of structural

members can therefore be detected during the incremental load application. The material nonlinearity accounts for the effect of combined stresses as plastification of the element cross-section occurs.

3.2.3 Numerical algorithm for solving dynamic equations

For nonlinear dynamic problems with large nonlinearities, the only solution approach to the equations of motion is the direct time-step method. Several algorithms exist which are implemented in commercial software, most of them based on the Newmark method which makes assumptions on the variation of the acceleration response in subsequent time steps. (Newmark, 1959)

The method used in the present study was developed by Hilbert, Hughes and Taylor (1977) and is called the $HHT - \alpha$ method. As described next, this method employs some time averaging of the damping, stiffness and load term expressed by the α-parameter. A beneficial feature of the method is that it introduces artificial damping of higher frequency modes without degrading the accuracy. The governing equilibrium equation is:

$$M \ddot{r}_{t+\Delta t} + (1+\alpha)C \dot{r}_{t+\Delta t} - \alpha C \dot{r}_t + (1+\alpha)Kr_{t+\Delta t} - \alpha Kr_t = (1+\alpha)R_{t+\Delta t} - \alpha R_t \tag{3.5}$$

Where M, C and K are the mass, damping and stiffness matrix, respectively, r is the displacement vector, and R is the applied load vector, at time $t + \Delta t$.

The velocity vector at time step $t + \Delta t$ is

$$\dot{r}_{t+\Delta t} = \dot{r}_t + \Delta t(\gamma)\ddot{r}_t + \Delta t\gamma \ddot{r}_{t+\Delta t} \tag{3.6}$$

And the displacement vector is

$$r_{t+\Delta t} = r_t + \Delta t \dot{r}_t + \frac{\Delta t^2 \gamma}{2}(1-2\beta)\ddot{r}_t + \Delta t^2 \beta \ddot{r}_{t+\Delta t} \tag{3.7}$$

The factors γ and β in Eqs. (3.6) and (3.7) are the free parameters in the Newmark-β method which, along with α, determine the stability and accuracy of the quadrature formula. In the original average-acceleration Newmark-β method ($\alpha = 0$), γ is set equal to 0.5 to avoid artificial damping and β=1/4. Depending on the value of β different integration methods are retrieved, such as the second central difference method (β =0), and the linear acceleration (β=1/6) method. Only the integration with constant average acceleration is unconditionally stable, otherwise the method is conditionally stable. In the HHT-α method, unconditional stability is obtained when the following conditions are satisfied:

$$-\frac{1}{3} \prec \alpha \prec 0, \ \gamma = \frac{1}{2}(1-2\alpha), \ and \ \beta = \frac{1}{4}(1-\alpha)^2. \tag{3.8}$$

In this research the HHT method is used with α = -0.3, and according to Eq.(3.8), γ =0.8 and β =0.4225.

3.2.4 Automatic incremental loading

An automatic incremental load procedure provides for a robust solution and makes the program safe and easy to use by engineers inexperienced in nonlinear analysis. The size of the increments may be varied along the deformation path i.e. large steps in the linear range, and smaller steps with increasingly nonlinear behaviour. If the forces in some element cross-sections exceed the yield surface (inner circle in Figure 3.3), the load increment is automatically reduced to make the forces comply "exactly" with the yield surface. The load increment is automatically reversed if global instability is detected.

There are two general ways to simulate a pushover load test: by controlling the applied load or the displacement at some reference point. In USFOS, there is one more option: velocity control, which we have used in this research to simulate as exactly as possible the experimental conditions of the tower section tests, which are described in Chapter 4.

3.2.5 Material nonlinearity and plasticity control

USFOS includes material models both for elastic-perfectly plastic behavior, and gradual plastification with strain hardening. These are illustrated schematically in Figure 3.2.

a) Elastic-Perfectly-Plastic   **b) Plastic with Strain Hardening**
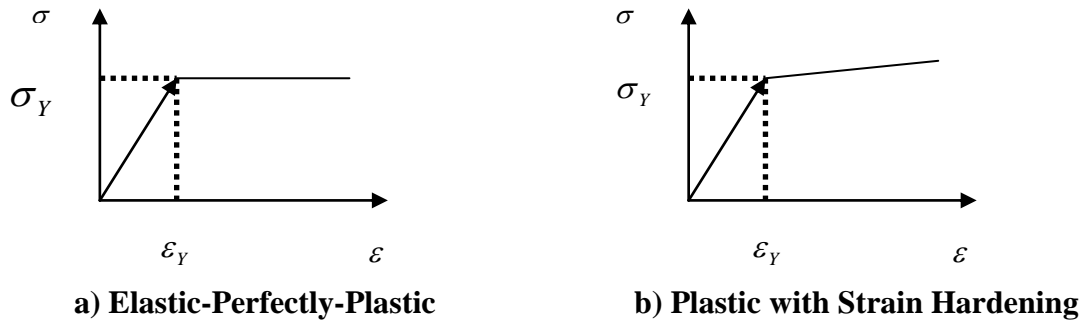
Figure 3.2 Constitutive models

The yield stress and strain hardening modulus were obtained from detailed stress strain curves available from uniaxial loading tests. The plastic model used is formulated in the stress resultant force space (S_1, S_2) and is based on the bounding surface concept as shown in Figure 3.3 and explained next.
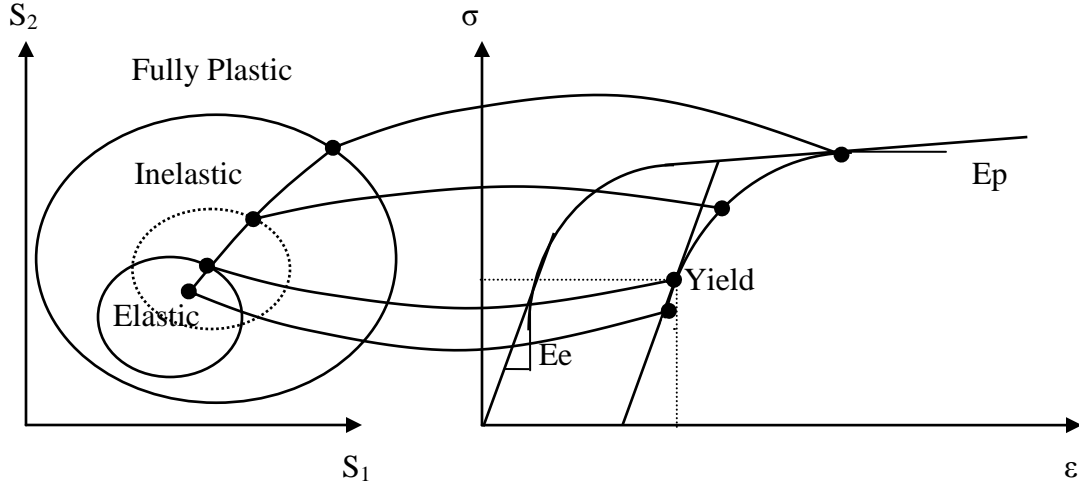
Figure 3.3 Analogy between multidimensional stress-space (left) and

uniaxial stress-strain curve (right).

Figure 3.3 is a schematic representation of relation between axial stress states and stress strain curve. Four different stress points are considered: one in the elastic domain, one on the yield surface, one in the inelastic domain and finally one in the fully plastic domain corresponding to the ultimate stress.

- For elastic-perfectly-plastic behaviour, the plastification state function Γ is :

$$\Gamma = f\left[\frac{N}{N_P}, \frac{Q_Y}{Q_{YP}}, \frac{Q_Z}{Q_{ZP}}, \frac{M_X}{M_{XP}}, \frac{M_Y}{M_{YP}}, \frac{M_Z}{M_{ZP}}\right] - 1 \tag{3.9}$$

$\Gamma = 0$ for all combinations of forces giving full plastification of the cross section and

$\Gamma = -1$ is the initial value of a stress-free cross section.

The usual stress resultants are defined on the cross section:

N: axial force; Q_Y, Q_Z shear forces along transverse Y and Z principal axes; M_x: torsional moment; M_y, M_z: bending moment about Y and Z axes. The corresponding stress resultants at full plastification are:

34

$$N_P = \sigma_Y A; \quad Q_{YP} = \tau_Y A_Y; \quad Q_{ZP} = \tau_Y A_Z$$
$$M_{XP} = \sigma_Y W_X; \quad M_{YP} = \sigma_Y W_Y; \quad M_{XP} = \sigma_Y W_Z. \tag{3.10}$$

Where A is the cross-sectional area, A_y and A_z are the effective shear areas for transverse shearing in directions y and z, σ_y and τ_y are the normal and shear stresses at yield, W_x is the plastic torsional constant, and W_y and W_z are the plastic second moments of area of the cross section.

- For strain hardening materials, the yield surface has equation

$$F_Y = f_Y[n, q_Y, q_Z, m_X, m_Y, m_Z] - 1 = 0 \tag{3.11}$$

where:

$$n = \frac{N - \beta_1}{N_P z_Y}, \quad q_Y = \frac{Q_Y - \beta_2}{Q_{PY} z_Y}, \quad q_Z = \frac{Q_Z - \beta_3}{A_{PZ} z_Y}$$
$$m_X = \frac{M_X - \beta_4}{M_{XP} z_Y}, \quad m_Y = \frac{M_Y - \beta_5}{M_{YP} z_Y}, \quad m_Z = \frac{M_Z - \beta_6}{M_{ZP} z_Y}. \tag{3.12}$$

where $0 < z_Y < 1$ denotes the yield surface extension parameter. $\beta_{i, i=1,6}$ is the translation of the yield surface in the stress-resultant space from the initial position corresponding to a stress-free cross section. The bounding surface determines the state of full plastification of the cross section. This surface, which has the same shape as the yield surface, is defined by the function:

$$F_b = f_b[n, q_Y, q_Z, m_X, m_Y, m_Z, z_b] - 1 = 0 \tag{3.13}$$

where $0 < z_b < 1$ denotes the bounding surface parameter.

When plastic hinges are introduced, the element tangent stiffness matrices are modified according to the conventional plastic flow theory, which is based on the following three assumptions (Bathe 1996):

a) There exists an initial yield condition which in stress space can be illustrated by an initial yield surface;

b) There exists a flow rule relating plastic strain increment to stress increment and

c) A hardening rule is defined relating the translation of yield surface to the amount of plastic deformation, and the element forces remain on the yield surface, unless the element is unloaded and returns to the elastic state.

The plastic hinging theory presented above is used in USFOS for materially nonlinear analysis. Each beam element is formulated with three nodes, two end joints and a middle node. However, the middle node is automatically generated and needs not be defined by the user. Of course, it is also possible to model each component with a refined mesh of several basic elements for a more detailed tracking of the failure. When yielding starts to occur in a member, the program automatically inserts plastic hinges at the element nodes where yielding is occurring. If the yielding is taking place at the middle of the member, the program will automatically divide the member into two elements adding an additional node at the mid-span where the plastic hinge has developed. This plastic hinge insertion feature enables large models to be analyzed very fast compared to general non-linear analysis programs based on detailed stress-strain analysis. The post-buckling behaviour of the member is modeled assuming the insertion of a plastic hinge at any of the three nodes. This way, a separate check on the stability of the member is not necessary. For members undergoing excessive straining resulting in fracture, USFOS proceeds to the automatic removal of the fractured member and redistribution of its internal stress resultants to the adjoining nodes.

3.2.6 Powerful user interface

Most commercial software share the common theoretical background which supports the sophisticated analysis of structures or loading systems, but when it is time for the application engineers to choose the proper numerical tool, the quality of the user interface and numerical and graphical post-processing features become very important in practice. An ideal post-processor should allow the engineers to check with their own database or experiences with the structural behavior of their designs. USFOS comprises an advanced interactive graphical post-processor based on Windows. The post-processor enables to display the configuration of the damaged structure at any step during the load application by simply pointing at the load-displacement curve available in a different widow. The deformed configuration is shown with colour fringes to enable the user to see the exact point in the load history when plastic hinges begin to form and the structure starts to collapse. These capabilities are very useful to understand the failure modes and their propagation in the structure: several illustrations presented in the thesis are taken directly from this post-processor.

3.3 Validation of the analysis of angle members

Angle section structural members have been a long time interest for structural engineers because of their simplicity of fabrication and assembly. But as indicated in the literature review of Chapter 2, their response under complex loading and their failure modes make them very challenging to study.

The failure modes of compressed angle members can be classified into two main categories: global failure and local failure. The local failure is essentially a plate buckling

problem, most often in the inelastic range of response. Local buckling is controlled at the design stage by limiting the width-to-thickness ratio of the angle legs. In USFOS, the member is assumed to fail in its global mode.

Figures 3.4 to 3.6 illustrate the results of a comparative study (Lee *et al*., 2005) of the numerical solutions obtained for a pin-ended angle shape (2"x2"x1/8") with length of 0.25 m, 1 m and 4 m, respectively modeled with USFOS and ADINA. The mesh size is indicated in parentheses next to the model type in the legend. For example, in Figure 3.4, the USFOS model comprises 4 beam elements while three different finite element models have been created in ADINA: two Hermitian beam models with 4 and 8 elements, and a more sophisticated thin shell model comprising 10 shell elements (5 per angle leg). The ADINA shell model is considered the most accurate model in the comparison.

These results indicate the good performance of the USFOS models to predict the member capacity, with the exception of the single-element model in Figure 3.6. The full load-deformation history is difficult to render with equivalent beam models, but it is seen that the USFOS models perform very well compared to the ADINA beam elements in the initial range of the post-elastic response. Clearly, refining the mesh size in members identified as critical in a preliminary analysis is very cost-effective in USFOS.
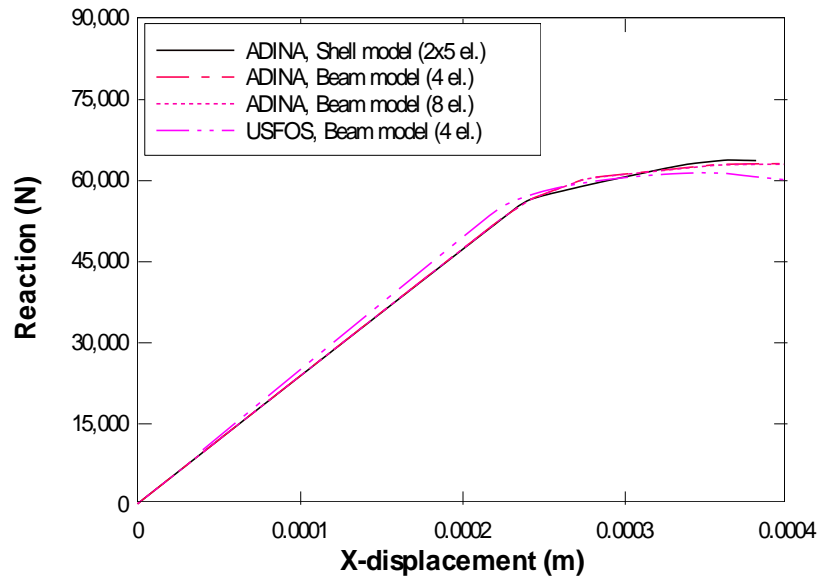
Figure 3.4 Load-displacement for 0.25 m angle section (Lee *et al.*, 2005)
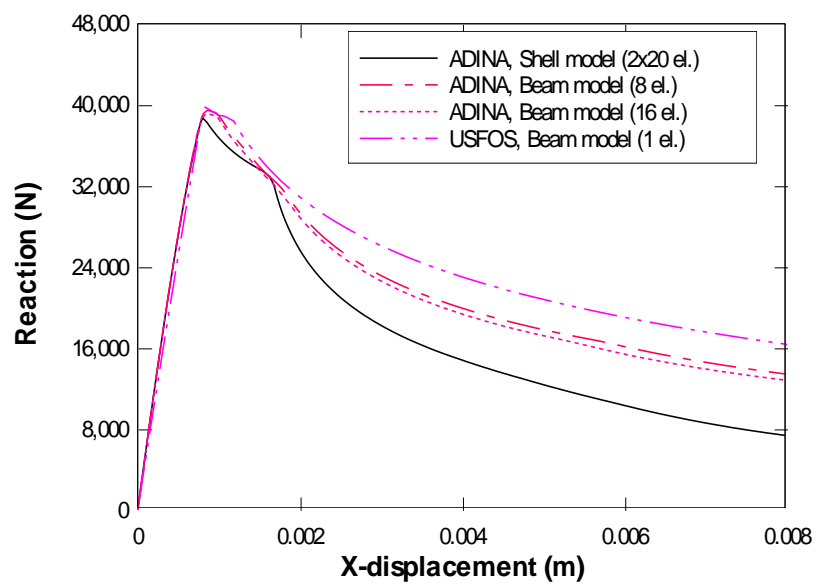
Figure 3.5 Load-displacement for 1 m angle section (Lee *et al.*, 2005)
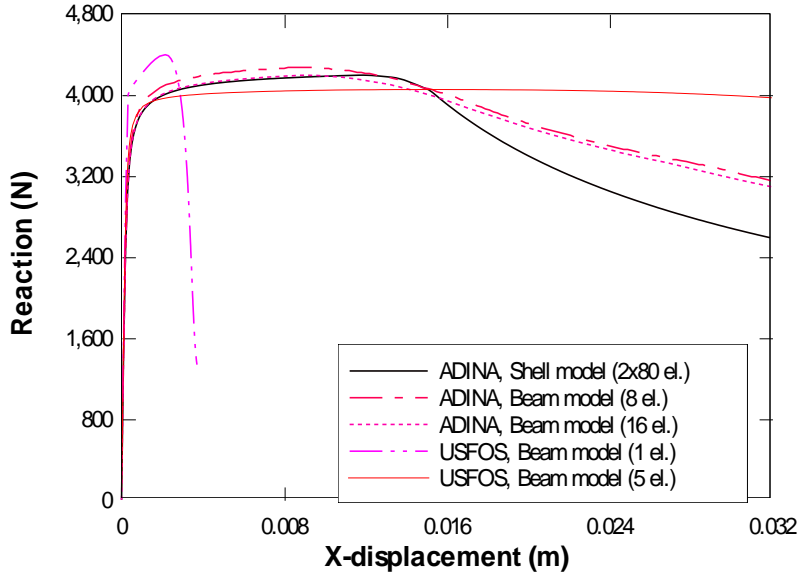
Figure 3.6 Load-displacement for 4 m angle section (Lee *et al.*, 2005)

3.4 Validation of the analysis of truss models

The first USFOS validation example used in this study was a portion of lattice tower, the ground wire peak of the Canadian Bridge 735 kV single-circuit tower used by Hydro-Québec on its Churchill-Manicouagan-Montreal lines. Complete agreement between ADINA and USFOS results was obtained in both the elastic regime and the frequency analysis. This ground wire peak tower section was also analyzed separately by Guo (2004) using ADINA.

Then another ground wire peak section of another type of Hydro-Québec 735 kV single-circuit latticed tower, SAE1968, was analyzed by USFOS, and this time the analysis results were compared with full scale tests done at IREQ in Varennes, Québec (Guilbault and Picard 2000). There was excellent agreement (95%) between the numerical

prediction of the ultimate strength of the reinforced peak and the value obtained in the test. The sequence of failure was exactly the same in the two cases.

These two case studies confirmed that the post-elastic static analysis (static pushover) simulations using USFOS were accurate and reliable.

The next step was to experiment with dynamic post-elastic analysis. A 2D transmission line section model was analyzed for both the static analysis and a cable rupture analysis. The results were compared with those obtained from ADINA and good agreement was obtained. This proved very promising for future post-elastic simulations of the whole line section under dynamic loads.

The numerical results of these validation models are presented in Chapter 5 of the thesis.

3.5 Connections and eccentricities

Kemp *et al* (1998) have proposed the following empirical relationships to represent the observed flexural stiffness (bending moment / flexural rotation), M / θ, of the restraint at each end of a simple strut depending on the number of bolts in the end-connection (the two ends having the same connection type):

$M / \theta = 0.02 EI_{xl} / L$ for one bolt in each end connection (3.14 a)

$M / \theta = 0.04 EI_{xl} / L$ for two bolts in each end connection (3.14 b)

where E is the modulus of elasticity and I_{xl} is the second moment of area of the main leg about the geometrical transverse axis, and L is the total length of the strut. A spring stiffness equal to 70% of the full theoretical restraint provided by the tie at the cross-over joint, including tension stiffening, was also found to reflect the experimental results. This apparent 30% loss of full stiffness may represent the influence of clearance in the bolt

41

holes on the tension stiffening provided by the tie, examples of typical connections in transmission towers are presented in Figure 5.10.

Note that connection flexibility was not modeled at individual joints because of the lack of an automated procedure. Some special joint elements are available in USFOS for typical connections used in offshore platform applications, but not for bolted angles.

The main reason why the behaviour of the strut in a cross-bracing arrangement differs from the conventional codified single strut theory is the dominant effect of the end eccentricity in the bolted connection to the main legs. This important connection eccentricity is modeled in USFOS by defining a series of eccentricity vectors pointing from the original nodal coordinates towards their offset construction joints; this is discussed in more details in Chapter 5 (see Figure 5.11). For the four tower section prototypes that were physically tested (see Chapter 4), each vector was verified with the as-built drawings and eccentricity measurements on the prototypes.

3.6 Structural damping

Latticed transmission towers are assembled from many different sizes of angle sections, splice joints, gusset plates, bolts, washers and nuts, which introduce a frictional resistance to motion and therefore create internal structural damping. Modeling of such damping effects is very difficult due to the incomplete experimental data (even the experiment itself is very difficult and expensive). Knowledge of damping in as many natural vibration modes as possible is certainly desired for a realistic formulation of damping matrix used for numerical analysis, but, unfortunately, field measurements of conductor

damping have been limited to only the lowest frequency, purely vertical (plunge) and solely torsional motion. McClure et al. (2003) mentioned that the damping of a transmission system mainly came from the cables and the structures, for example: the friction between the cable strands but very limited information was available for this kind of damping effects. Based on numerical experiments, they proposed an equivalent viscous damping ratio can vary between 2% to 10%. On the other hand, was discussed in Section 3.2.3, application of the HHT-α method for dynamic analysis automatically introduced numerical damping for high frequency contents. Since field observation data could not be found for damping of transmission line structures during accidental loading conditions, only this algorithmic damping was used.

3.7 Other considerations and limitations

Other limitations pertaining to the modeling of the latticed tower section prototypes are as follows:

- All the eccentricities in the tower could not be modeled due to the complexity of the problem: only those eccentricities in bracing member joints to the main legs were introduced.

- The nominal material properties are used in the simulations to prepare the tests.

- For the verification simulations carried out after the tests, detailed stress-strain curve data were used, which were obtained from uniaxial loading tests. Different sizes of angle members were therefore assigned specific properties; in total nine detailed material curves were used.

- The net area of the members due to bolting was not modeled and the gross cross-sectional area was considered. Net section fracture was not a concern due to the detailed design of prototypes.

- The loading eccentricity at the cross arm tip of the prototype was not modeled.

- Nominal angle dimensions were used and no provision was made for out-of-straightness tolerances.

Chapter 4 Experimental Study

4.1 Introduction

Sophisticated commercial finite element analysis tools like USFOS (SINTEF, 2003) and ADINA (ADINA R&D, 2003) have been verified with benchmark problems as well as classical solutions. Still, when it comes to their application to a new engineering area, experimental studies to verify and calibrate the numerical models are essential. As far as the author knows, it is the first time that USFOS is applied to transmission structures. Therefore, a series of numerical simulations using other software and full-scale tests were designed to validate the models created with USFOS.

Full scale tests are ideal as validation tools since they allow adjusting simulation models to closely represent the real engineering project, provided the tests are kept simple (i.e. amenable to modeling) in terms of loading and boundary conditions. But the high cost of full-scale tower tests makes them impossible to achieve in most research institutions. Insofar as the author knows, most of the full-scale transmission tower tests are carried out in specialized testing centers (there are few worldwide) or on old existing towers in line sections to be dismantled.

Full-scale tests on new tower designs are mostly aimed at checking construction details to detect detrimental eccentricities and premature failure modes. They are not aimed at finding the post-elastic capacity of towers as testing installations are usually limited in accommodating large deformations and displacements. Modeling of new designs can be very accurate because most of the information on geometry, connections and material properties is readily available from accurate drawing and mill tests. On the other hand, tests on existing older structures are difficult to model accurately because of

45

the variability of the member properties that are very difficult to measure. However, as pointed out by Kempner Jr. (2002), the full line system analysis is becoming in demand by utilities for the designers to obtain a better understanding of the ultimate strength of the line structures with the full investigation of the transmission line structures under different loadings.

In 2002-2003, Hydro-Québec TransÉnergie invested in a series of full-scale tests to validate its advanced numerical procedures of dynamic analysis of lines under shock loads (Lapointe, 2003, McClure and Lapointe 2003). The tests were carried out in the fall of 2003 on a 230 kV un-used transmission line with 12 towers and 11 spans in total length of 3.4 km line in Saint-Luc-de-Vincennes (Guilbault et al. 2003): the author is using some of these results in Section 5.3 to verify the analytical models created in USFOS.

A second series of pushover tests on latticed tower sections was performed by TransÉnergie during the summer of 2004 in Varennes, Québec. These tests were designed by the author and form the basis of this thesis. Figure 4.1 (in Section 4.2) shows a general view of the test site with one of the latticed tower prototype in place.

The whole test program took about one year from the design of the tests to the completion of data processing. These tests demanded a lot of cooperation between McGill researchers and Hydro Québec specialists in tower design and testing. The contributions of the various participants are stated in the acknowledgments section. Mr. Pierre Vincent was the engineer in charge of the project management. The test prototype was designed by Hydro-Québec line engineer Mr. Marc Charbonneau; this is an adaptation of a real tower (BBB Tower) whose design was supervised by engineer Mr. Denis Banville. All the testing operations were under the direction of the expert testing

engineer Pierre Guilbault of the Varennes test line. In addition to all the numerical modeling and simulations which assisted in the test planning phase, the author has designed the instrumentation layout and testing protocols in collaboration with the TransÉnergie experts mentioned above.

4.2 Testing objectives and procedures

The main objectives of the full scale tests are:

 1) To determine the basic dynamic parameters such as natural frequencies and structural damping ratios, of the tower section prototype for future numerical simulations;

2) To determine the ultimate strength of the prototype with post-elastic effects in a static pushover test;

3) To determine the ultimate strength of the prototype with post-elastic effects in a dynamic pushover test;

4) To compare the static and dynamic behaviour of the prototypes in the post-elastic regime;

5) To provide experimental data for validation of the numerical models created with USFOS (See Chapter 5).

Four nominally identical tower section prototypes were built for the tests. The prototypes are the top 10 m section of the BBB tower adapted for the test: they consist of a prismatic square plan section of 1.25 m side dimension with a single triangular cross arm. The external loads are applied at the tip of the cross arm located at 9 m above the tower base. More details about the test prototype are provided in Section 4.5.

After a series of characterization tests (static and dynamic) in the elastic regime, the prototypes were subjected to destructive push over tests under four different loading

configurations, among which two are static and two dynamic. Several tests were also done in the elastic regime to adjust the testing instrumentation and loading procedures. The two basic loading cases for the pushover tests are a biaxial bending and torsion test (referred to as torsion test) and a transverse bending test. The torsion test is achieved by applying a horizontal load at the tip of the cross arm, in the longitudinal direction (i.e. perpendicular to the axis of symmetry of the prototype), as shown in the set-up of Figure 4.1. The bending test is achieved by applying a horizontal load at the tip of the cross arm, along the axis of symmetry of the tower prototype. In total, 11 tests were carried out as described in Table 4.1. The testing layout and placement of instrumentation for the tests are described in Sections 4.3 and 4.4.
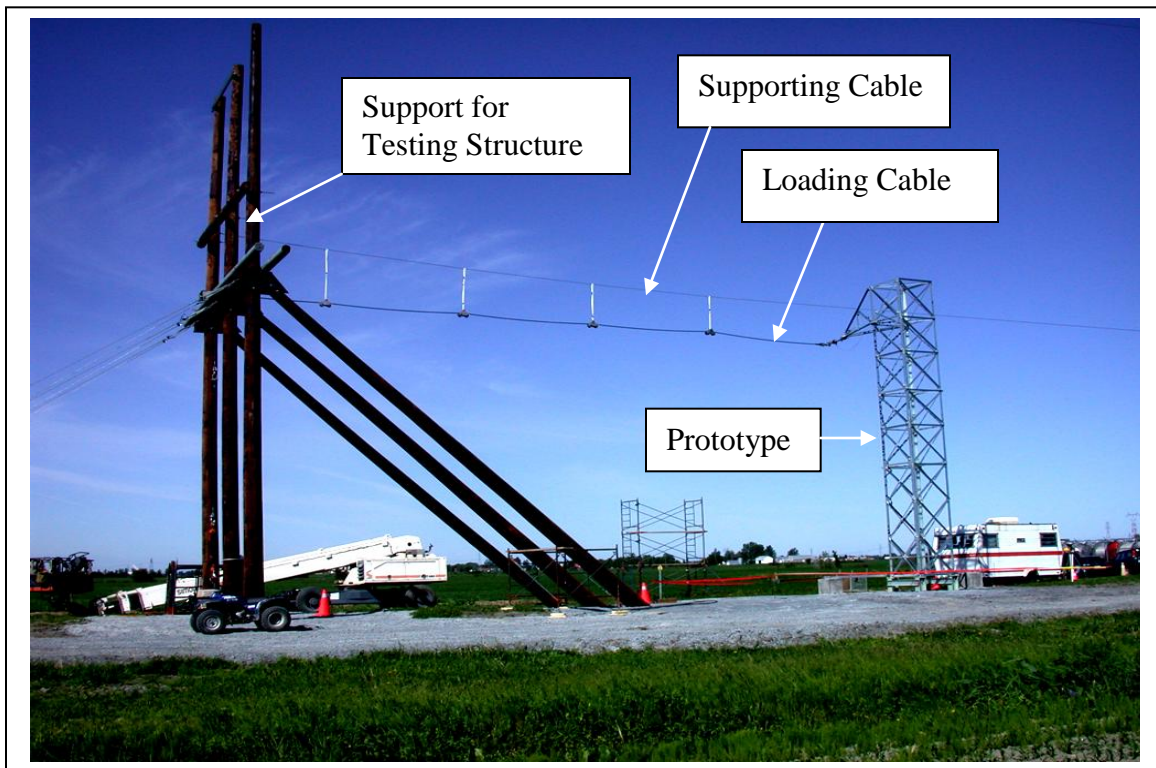
Figure 4.1 Overview of the test structures and facilities

Table 4.1 Testing program

Test No.	Loading regime	Description
1	Free vibration	A weight of 10.00 kN is dropped from the tip of the cross arm to excite flexural and torsional tower modes.
2	Free vibration	Repetition of Test 1.
3	Dynamic	Preliminary test. Dropping of the 10.00 kN from a height of 105 mm.
4	Cancelled.	
5	Static torsion	Bi-axial bending and torsion push over test. The test is velocity-controlled. A longitudinal force is applied at the tip of the cross arm by a towing truck at a constant speed of 2 mm/s. The maximum longitudinal displacement is 800 mm.
6	Dynamic torsion	Destructive test. A longitudinal shock load is applied to the tip of the cross arm by dropping a weight of 12.65 kN from a height of 2 m.
7	Free vibration	Release of transverse load of 12.65 kN to excite transverse bending modes.
8	Free vibration	Repetition of Test 7.
9	Dynamic bending	A transverse shock load is applied to the tip of the cross arm by dropping a weight of 12.65 kN from a height of 202 mm.
10	Dynamic bending	Repetition of Test 9 with a dropping height of 227 mm.
11	Static bending	Transverse bending push over test. The test is velocity-controlled. A transverse force is applied at the tip of the cross arm by a towing truck at a constant speed of 2 mm/s. The force is increased until failure of the tower.
12	Dynamic bending	Destructive bending test. The 12.65 kN weight is dropped from a height of 6 m.

4.3 Testing layouts

The testing layouts of the various tests are presented in Figures 4.2 to 4.8. Figure 4.2 shows the general layout comprising three structures. From left to right: the reaction tower (not shown in Figure 4.1), the BBB tower section prototype (test structure), and the portal frame with longitudinal struts. The reaction tower anchors the horizontal cable support system, while the portal frame accommodates various loading configurations on the cross arm of the tested prototype.
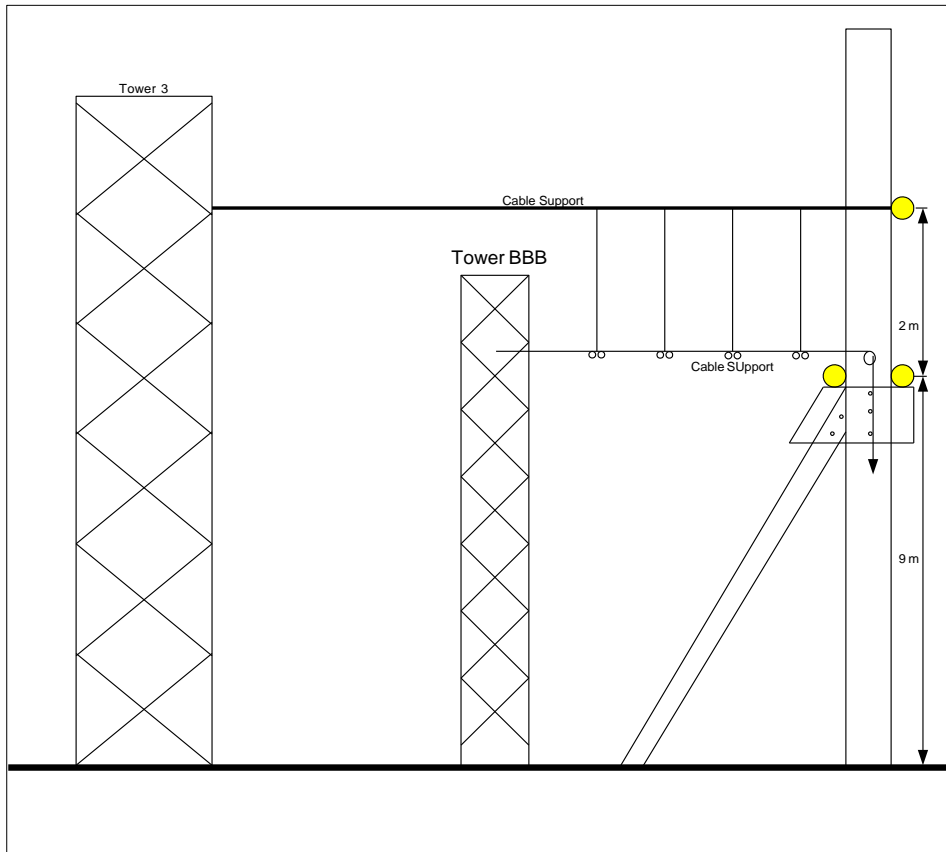
**Figure 4.2 General sketch of the testing layout
(TransÉnergie report no. 53024187, 2004).**

Figure 4.3 shows a plan view of the cross arm configurations for the torsion (in red) and transverse bending (in blue) with the position of the towing truck (*remorqueuse*) used in the static and dynamic pushover tests. The elevation views are shown in Figures 4.4 to 4.7, which also indicate the placement of the displacement instrumentation (described in Section 4.4) including high speed cameras and LVDTs.
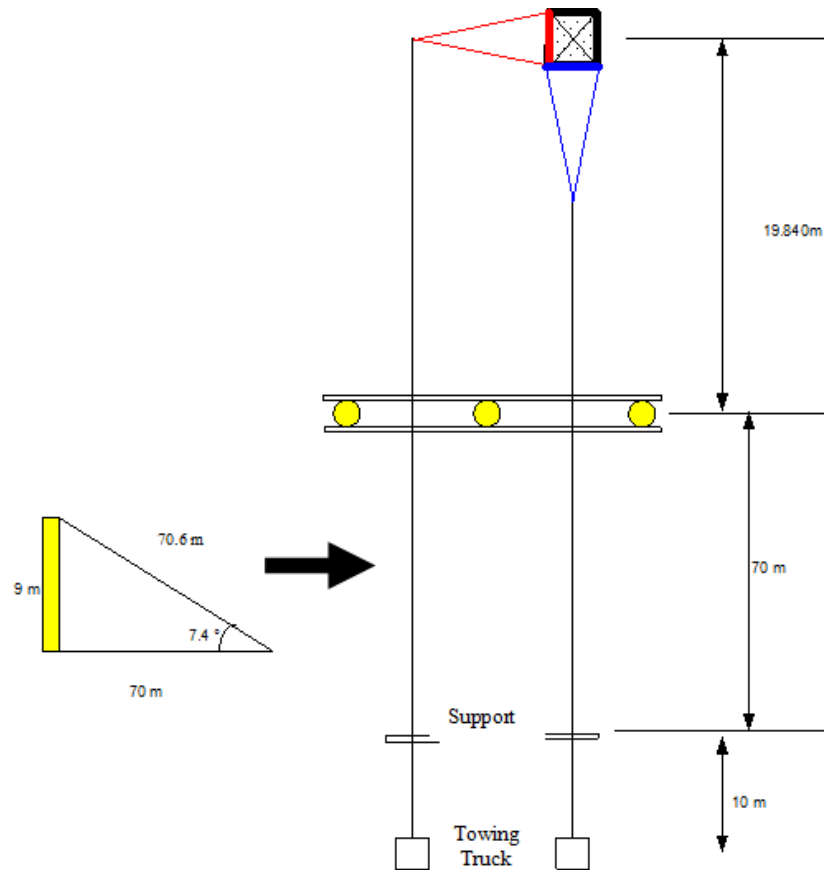
Figure 4.3 Plan view of pulling system for pushover tests
(TransÉnergie report no. 53024187, 2004)

Tower 1
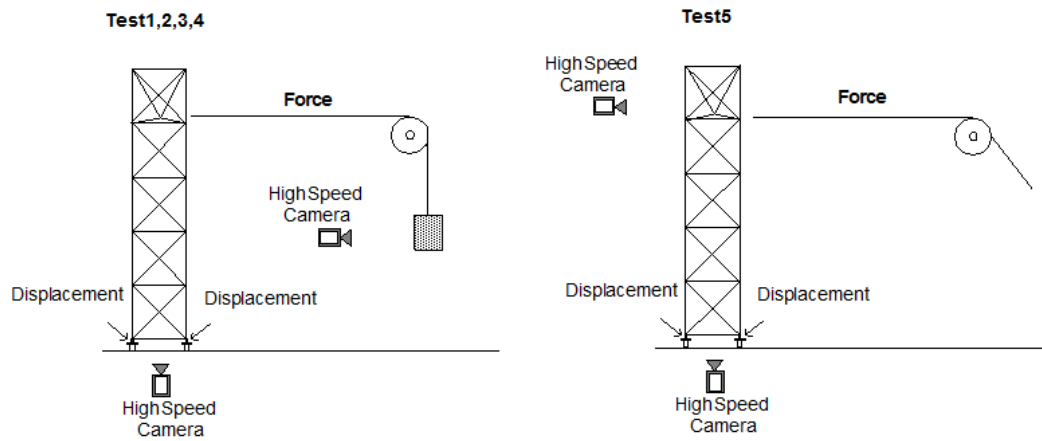
Figure 4.4 Elevation view of pulling system for pushover tests – Tests 1 to 5.

Tower 2
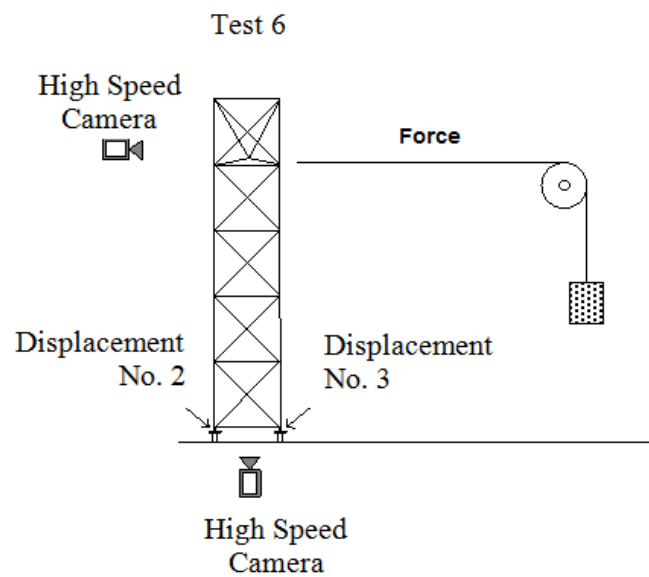
Figure 4.5 Configuration for destructive dynamic Test 6 (weight drop of 2 m)

Tower 3

Test 7, 8, 9, 10
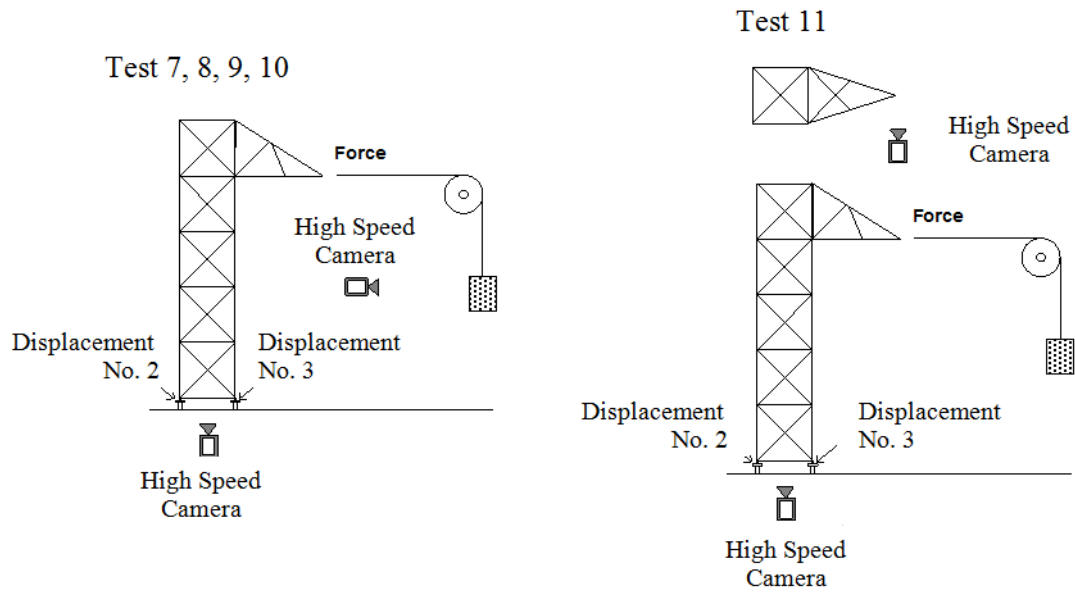
Test 11

Figure 4.6 Configurations for Tests 7 to 11

Tower 4
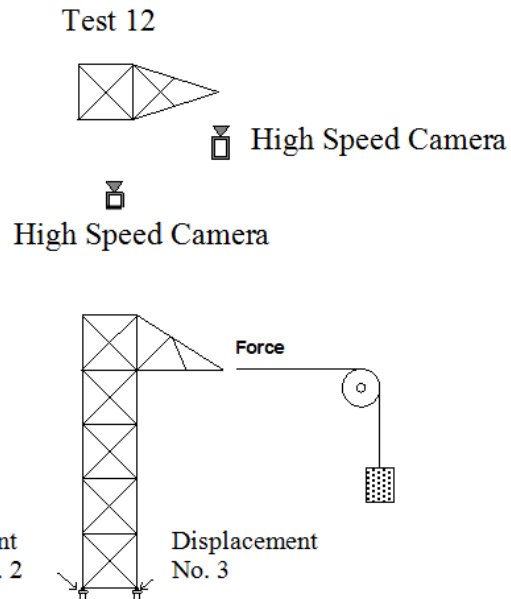
Test 12

Figure 4.7 Configuration for destructive dynamic Test 12 (weight drop of 6 m)

4.4 Instrumentation

During the planning of the tests, very little information regarding the instrumentation of full-scale post-elastic and dynamic tests was found in the literature. The design of the monitoring set-up was done in collaboration with the chief test line engineer and a subcontractor of TransÉnergie specialized in advanced monitoring technology, Scientech Multimedia Inc., who handled the high-speed video camera system and its related data processing. It is noteworthy that all the destructive tests have been video-recorded and a DVD has been produced. The instrumentation employed during the testing program is summarized next.

Loading Apparatus:

Figure 4.8a shows the mechanism for dynamic impulse tests (a sudden release of a deadweight), for the pushover tests, a towing truck (Figure 4.8b) was deployed to pull on the tower cross arm through a specifically designed pulley system until the structure failed. The applied load is monitored by a load cell shown in Figure 4.8c.

a) Weight release mechanism   b) Towing pulling system
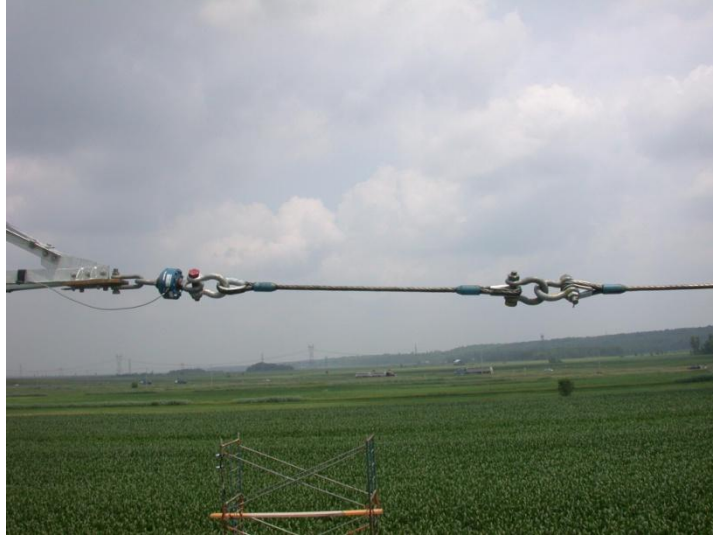
c) Load cell at cross arm tip

Figure 4.8 Loading apparatus

Monitoring system:

Figure 4.9 shows a schematic of the data acquisition system linking the high speed video cameras, the strain gauges installed on the prototype, the displacement transducers, and the load cell installed on the pulling cable.
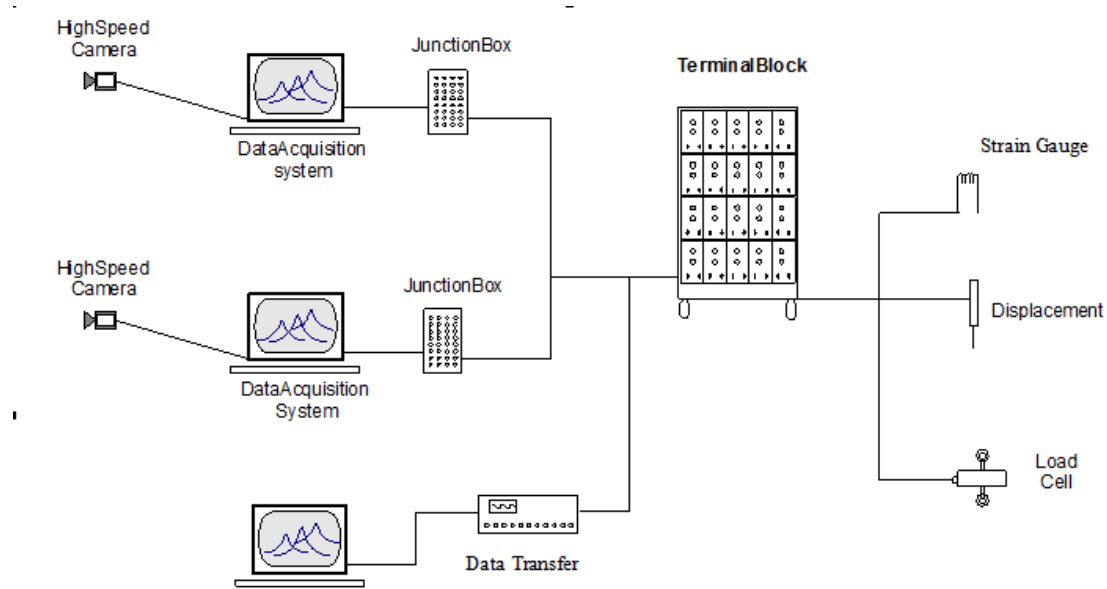
Figure 4.9 Global data acquisition system

Strain gauges:

The strain gauges are unidirectional and measure the axial stresses at the outer surface of the angle shapes as indicated in Figure 4.12. The sampling frequency of the strain gauges was 200 readings per second. Figures 4.10 to 4.12 show the arrangements of the strain gauges used on the prototype for the various tests. These arrangements were planned by the author based on the results obtained from numerical simulations conducted prior to the tests.

TORSIONAL INSTRUMENTATION LAYOUT TEST 1
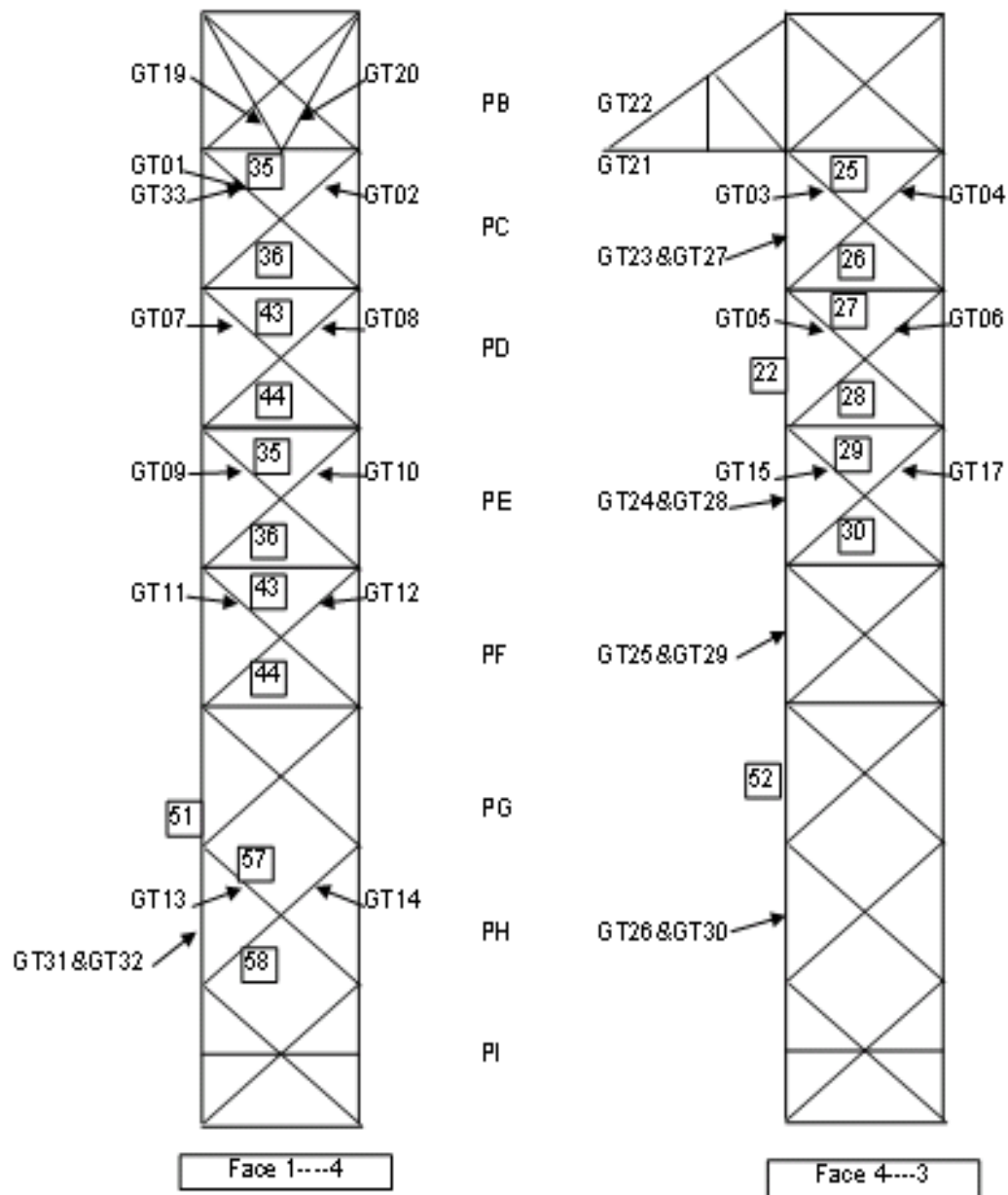
Figure 4.10 Strain gauge locations for Tests 1, 2, 3 and 4

TORSIONAL INSTRUMENTATION LAYOUT TEST 2

GT19 GT20
GT01 GT14
GT33 GT02
GT07 GT08
GT34 GT35
GT09 GT10
GT11 GT12
GT13
GT31&GT32

PB
PC
PD
PE
PF
PG
PH
PI

Face 1—4

GT22
GT21
GT03 GT04
GT23&GT27
GT05 GT06
GT15 GT17
GT24&GT28
GT25&GT29
GT26&GT30

Face 4—3
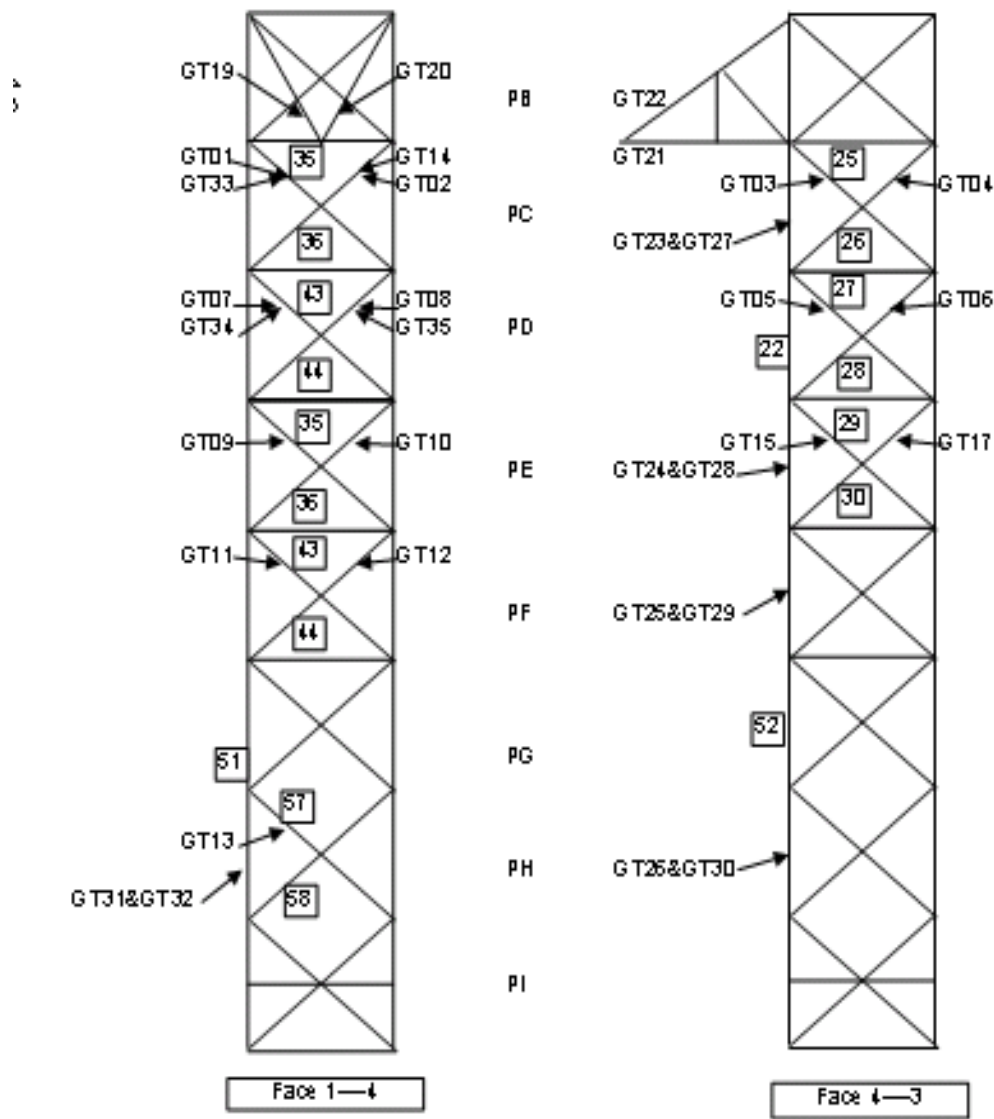
Figure 4.11 Strain gauge locations for Tests 5 and 6

58
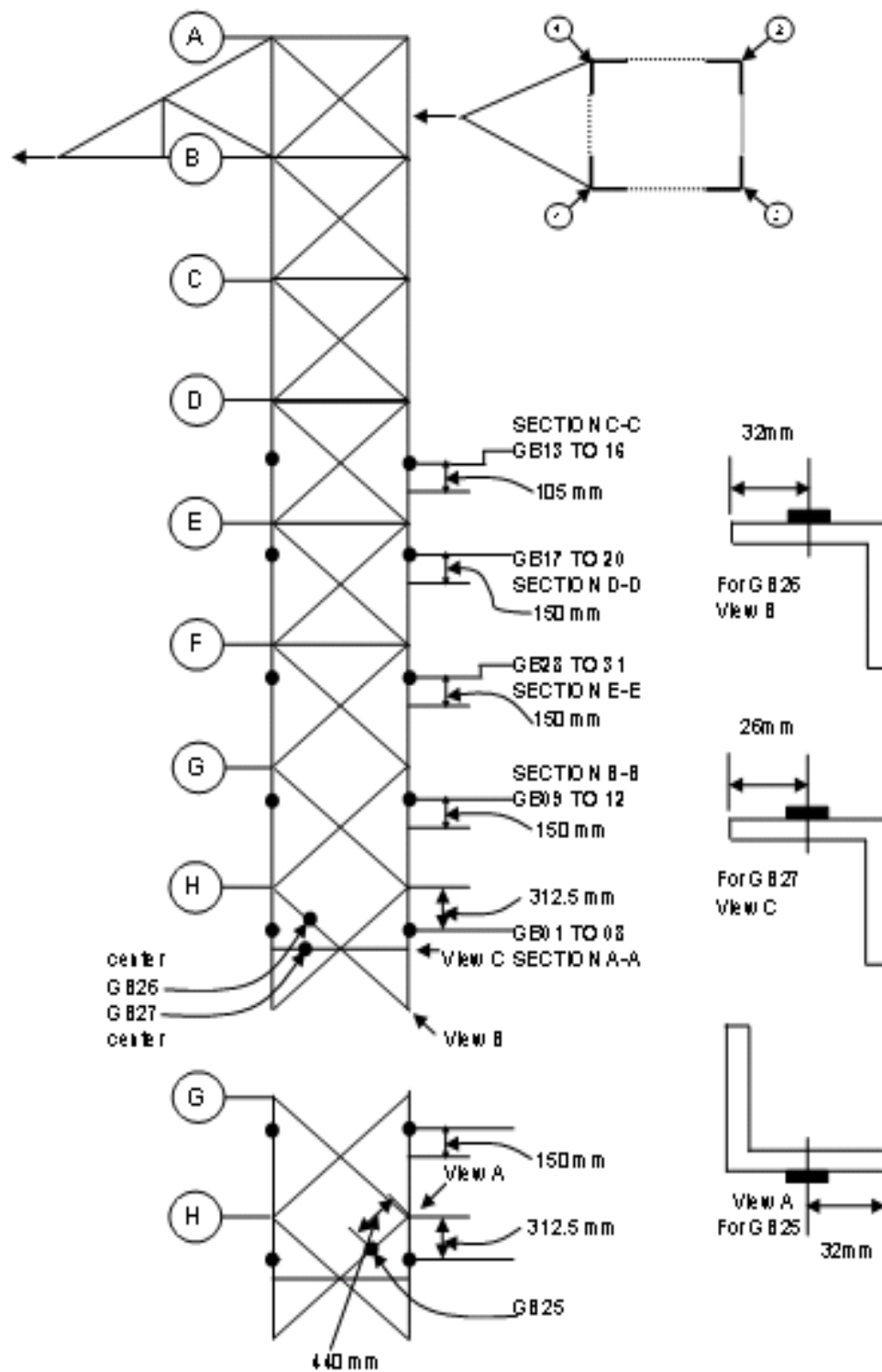
Figure 4.12 Strain gauge locations for bending tests (Tests 7 to 12)

Displacement transducers (LVDTs):

Two LVDTs were installed at the foundation level to record the foundation movement during the tests. This information is very important for safety reasons; the onset of any abnormal movement (overturning, slippage) can be detected and the chief testing engineer may use this information to decide to stop the testing procedure. The base displacement data is also important when comparing numerical results with experimental results.

High speed cameras:

Two high speed cameras (2500 frames per second) were installed. One is to monitor the displacement of the cross arm tip in both directions during the pushover tests. The other one is installed on the ground to trace the failure sequence: this is especially important for the dynamic tests considering the high load rate.

Monitoring cameras:

In addition to the high speed cameras, 16 Canon ZR90 video cameras (sampling frequency 30 frames per second) were installed on each side of the rectangular tower (4 cameras on each side) to monitor the motion of two vertical panels (2.5 m high by 1.25 m wide). This will track the failure sequences with relation to the testing time coordinates, therefore allowing us to relate the applied load and recorded displacements with the failure modes when carrying out data analysis after the tests. Three more video cameras were installed at three more distant locations to record the full tower motion during the tests.

4.5 Prototype design

The test tower prototype was the upper section (8 panel sections in total) of the standard Hydro-Québec TransÉnergie BBB suspension tower with narrow base for single-circuit 235 kV lines. The outline drawing of the prototype is shown in Figure 4.13. As mentioned in the introduction, the prototype was adapted by engineer Marc Charbonneau from the original design. The main changes related to the reinforcement of the bracing members at the joints to prevent localized failures. New structural drawings had to be prepared which are numbered **G61160111047-010-HQ0 to G61160111054-010-HQ0.** The design calculations are shown on drawing **G61160111048-020-HQ0.** The calculated elastic limit loads for static loading at the cross arm are 42 kN for longitudinal loading (combined bending and torsion) and 92 kN for transverse loading (bending only). No loading factor was considered in the design, to provide a reference for the actual loads that can be applied during the tests.

A special foundation had to be designed to ensure that there would not be a foundation failure during the tests. Details are not given here for conciseness but the governing foundation loads obtained from the numerical models are discussed in Chapter 5. The reader interested in detailed prototype geometry is invited to contact Hydro-Québec TransÉnergie.
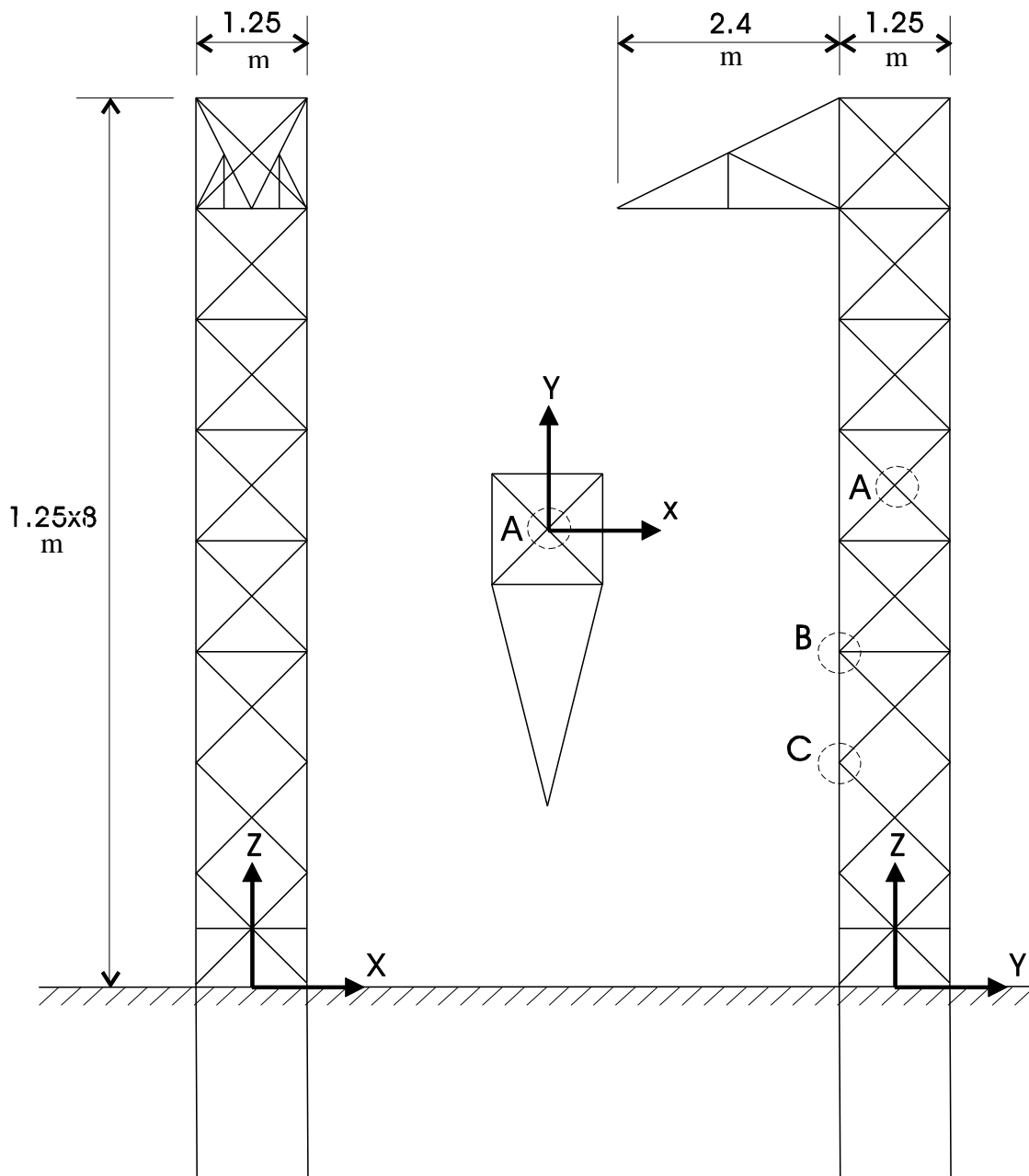
Figure 4.13 Outline of the BBB Tower test prototype

4.6 Results

4.6.1 Natural frequency tests and damping measurement

Prior to the four main pushover tests, several dynamic tests were done within the elastic regime to get the natural frequencies of different vibration modes and the structural damping ratios. Under each loading scenario, torsion and bending, two free vibration tests were done to measure the natural frequencies and damping ratios: one without added weight, and the other with the dropping mass staying attached directly at the tip of the cross arm, as described next.

The tower was first excited by tensioning a cable attached to the tip of the tower cross arm with a mass of approximately 1000 kg (a concrete block) and suddenly dropping it. The static vertical deflection before the mass was dropped was measured as 2.96 cm. The free vibration movement of the tower tip was measured using a high speed camera from two directions as shown in Figure 4.4, for the two loading protocols.

The period of the first transverse sway mode of the tower was found to be identical for the two different procedures of excitation, at 0.135s (7.4 Hz). However, the presence of the added weight influenced the damping ratio, which was obtained from the logarithmic decrement of the recorded displacements. Damping was found to be 3% for the prototype without added weight and 7% with the attached weight. This indicates that damping in the prototypes is increasing with the magnitude of the applied loads.

The period of the second mode (longitudinal sway) without added mass is 0.125s (8.0 Hz) with a damping ratio of 4%. In the second approach, with added mass, the period is 0.129s (7.75 Hz) with the same damping ratio. This suggests that damping in the higher modes is not as sensitive to the magnitude of the force applied to the tower as in the fundamental mode.

The period of the third mode (torsion) is 0.068s (14.8 Hz) measured in both the longitudinal torsion- flexure excitation and the transverse flexure excitation.

4.6.2 Static torsion pushover test (Test 5)

Figure 4.14 shows the load-displacement curve obtained for this test. It is seen that the maximum load is of 51.4 kN but the residual capacity is of the order of 30 kN. The displacement observed at maximum load is 476 mm. Figure 4.15 shows different views of the deformed shape of the prototype at the end of the test.
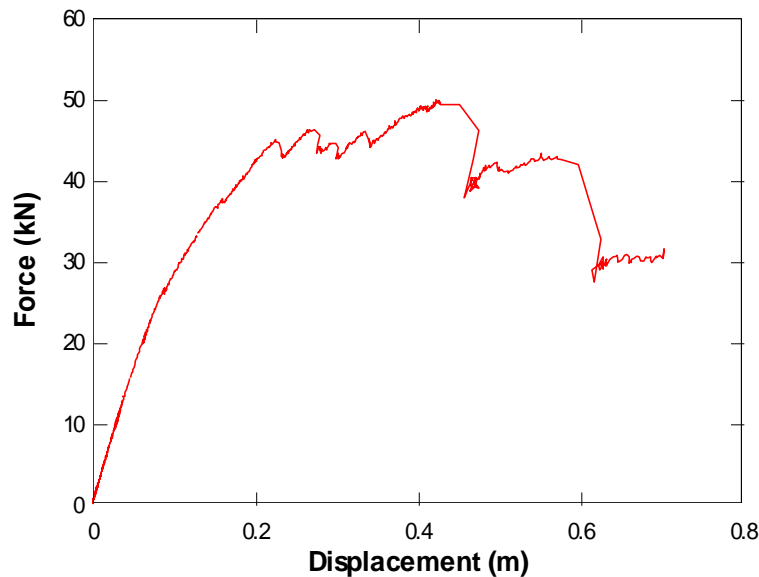
Figure 4.14 Load-displacement for static torsion (Test 5)

a)
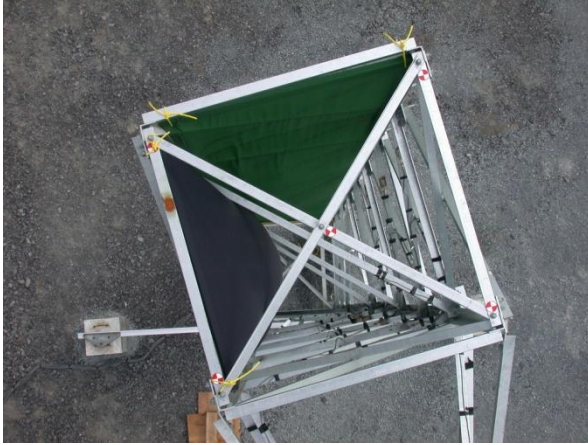
b)

c)

Figure 4.15 Deformed structure in pushover static torsion (Test 5)

Table 4.2 summarizes the sequence of member failures as recorded by the strain gauges. Note that the strain gauge and member numberings refer to Figure 4.11. The failure begins from the 5th panel under the cross arm and then goes to 6th panel, the 7th

and then to the 3rd panel. The maximum capacity is reached when the 8th panel fails as

indicated in Table 4.2. The failure sequence is also indicted in Figure 4.16.

Table 4.2 Sequence of member failures in Test 5

Gauge No.	Element No.	Time (s)	Applied load (kN)	Remarks
GT08	43	187.61	45.9	
GT07	44	187.64	45.4	Video D4
GT10	41	197.81	47.0	
GT09	42	197.84	44.7	Video E4
GT12	39	201.66	44.5	
GT11	40	201.68	44.5	Video F4
GT02	45	210.30	47.0	
GT01	46	210.33	46.0	Video C4
GT13	36	237.60	50.9	Video G4
GT14	35	238.06	50.5	

Figure 4.17 shows the failure of the diagonal members, close to the connection to

the main legs, in plastic buckling.
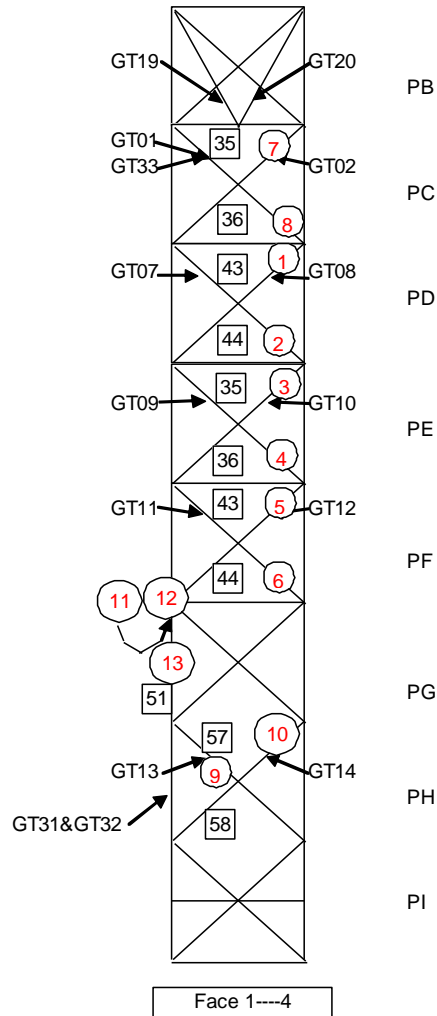
Figure 4.16 Failure sequence for static torsion test 5

It is interesting to compare, in Figure 4.18, the readings from the two strain gauges installed on the same diagonal member but on the different legs of the angle, namely gauge numbers GT01 and GT33. Clearly, there is unequal load sharing between the two legs, as the connected leg (GT33) initially takes almost the entire load. After the member failed, the strains decreased significantly and eventually, one leg (GT33) is under small tension and another under compression (GT01).

a)

b)

c)

d)

Figure 4.17 Failure of bracing members in Test 5
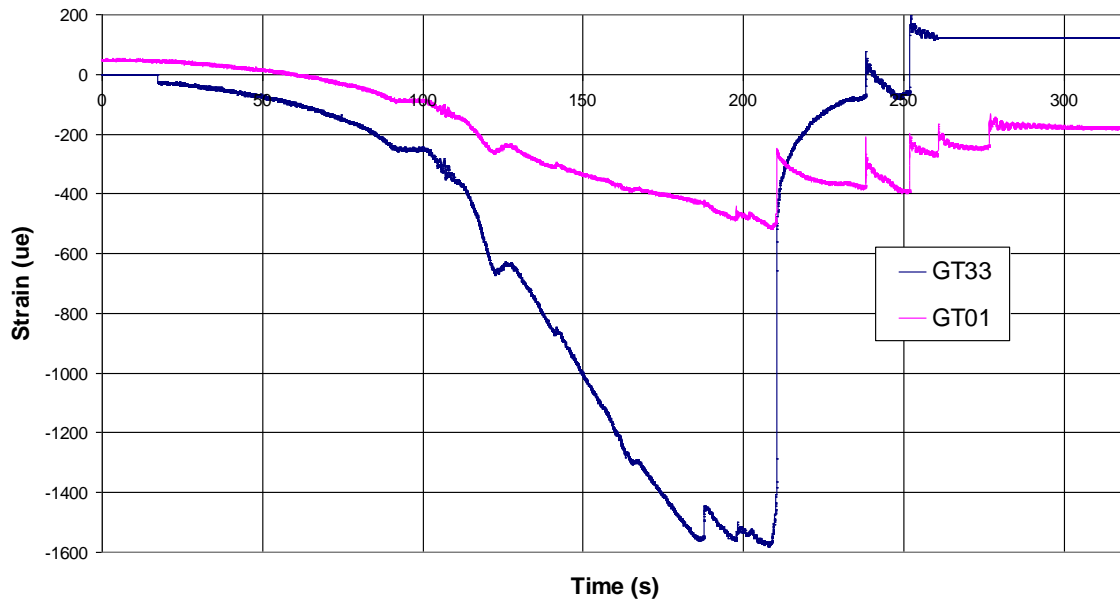
Figure 4.18 Unequal load sharing among the two legs of angle bracing No. 35 (GT01 and GT33)

Despite very careful design of the prototypes, some unpredictable failure events were observed. During this test, the final collapse of the tower was triggered by a localized brittle rupture of net section of the diagonal member at the bottom panel at the connection point. If not for this local failure, it is likely that the ultimate capacity would have been higher than that from the test; therefore, the ultimate strength from this test is a conservative value.

4.6.3 Dynamic torsion test (Test 6)

It was difficult to determine the drop height of the weight to produce an appropriate shock load in this test. The pulse load had to produce enough energy to fail the tower but losses in the loading system were difficult to quantify. A simple calculation based on the work done by the external loads was used to estimate the amount of strain energy reached at failure in the static pushover test (Test 5). The elastic strain energy

69

(reached with the first member failure) is estimated at 5.52 kJ. However, when the several post-elastic events are included, the energy dissipated is much higher, at about 18.40 kJ. Then, assuming the efficiency η (ratio between the actual strain energy dissipated and the work done by the external load) is varying between 0.5 and 0.8, the following empirical formula was used to calculate the drop height (H_{drop}) of the weight (mg = 12.65 kN):

$$H_{drop} = \frac{E_{total}}{\eta\, mg} \qquad (4.1)$$

The efficiency parameter depends on the rigidity of the secondary structures of the testing setup. As the impact load is generated, the energy is transferred in the global system and part of it is absorbed by components other than the tested prototype. Finally, a dropping height of 2 m was selected for this test.

From the information obtained from the static pushover Test 5, the strain gauge placement was refined to get more data for the verification of our numerical models; three critical diagonal members were installed with two gauges to obtain the stress distribution on the different legs of the angle section members. All the other equipment and instruments were the same as for Test 5.

Figure 4.19 presents the time history of the loading as measured by the load cell. It is seen that the loading rates are different after the initial impact: the maximum rate is 967 kN/s and the average is around 366 kN/s.
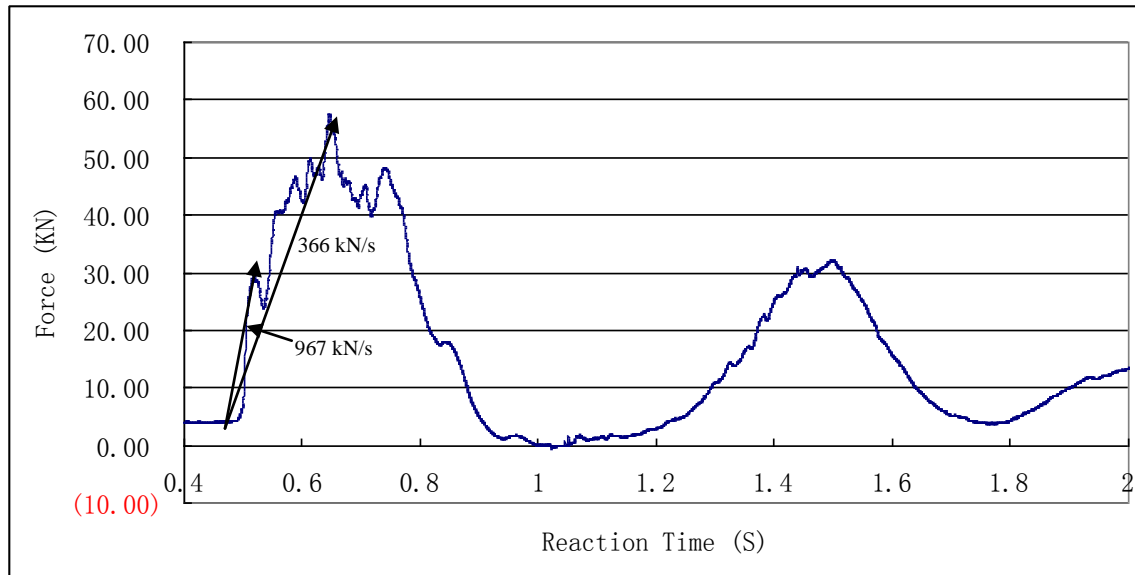
Figure 4.19 Loading time history at the cross arm in dynamic torsion (Test 6)

The load-displacement at the tip of the cross arm for this test is shown in Figure 4.20, in superposition with the curve obtained for the static test (Test 5). It is seen from the dynamic test curve that the effective stiffness of the structure is almost the same as the static stiffness. During the test, after 300 to 500 ms, the structure was in free vibration for more than 10 seconds. After the motion was damped out, the structure stopped at the static equilibrium position.
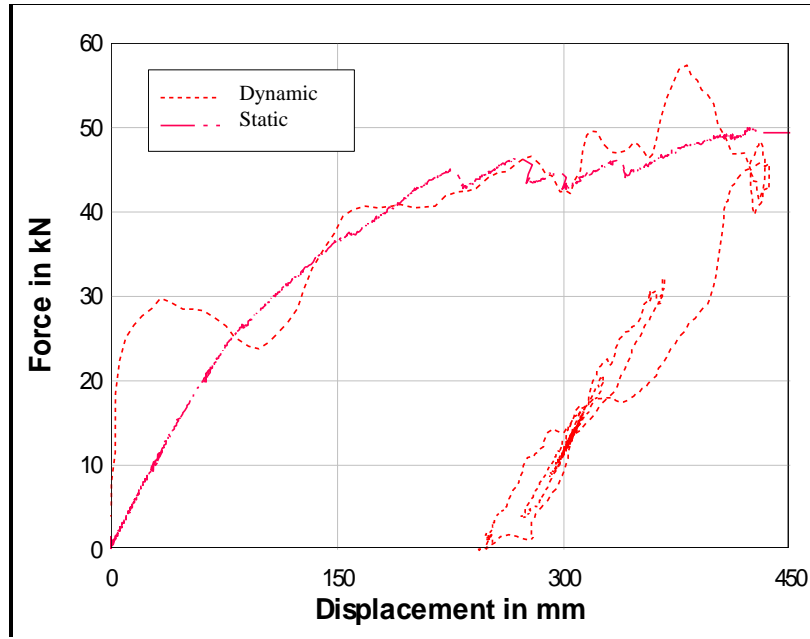
Figure 4.20 Load-displacement for dynamic and static torsion tests

Figure 4.21 shows a general view of the prototype at the end of the test. It is seen that the displacements are not large, barely visible on the photo. However, the observed sequence of member failures (presented in Table 4.3) is almost the same as in the static test. The load at failure measured in the dynamic test is slightly (11%) larger than the static value (57 kN vs. 51 kN from Figure 4.20). Apparently the structure was still able to resist some external load after the shock loading since the tower did not collapse.

Figure 4.22 shows the failure sequence comparison between the static and dynamic test and Figure 4.23 shows the failure in plastic buckling of the diagonal members, close to the connection to the main legs, similarly as observed in Test 5.

Figure 4.21 Deformed structure in dynamic torsion (Test 6)

Table 4.3 Sequence of member failures in Test 6

Gauge No.	Element No.	Time (s)	Applied load (kN)	Remarks
GT35	43	0.5992	42.6	
GT34	44	0.6164	47.8	Video D4
GT10	41	0.6016	42.0	
GT09	42	0.6220	47.2	Video E4
GT12	39	0.6236	47.1	
GT11	40	0.6284	47.8	Video F4
GT14	45	0.6664	46.5	
GT33	46	0.6716	45.9	Video C4
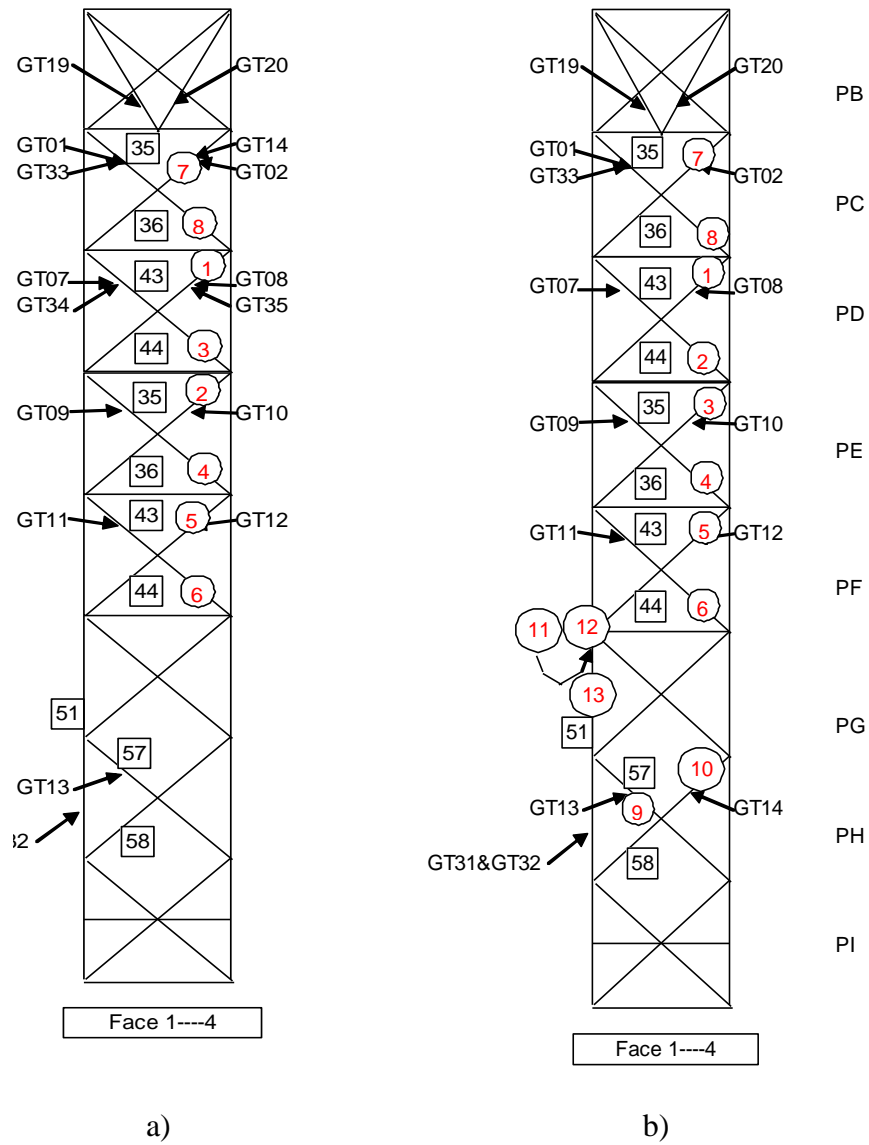
Figure 4.22 Failure sequence from dynamic test (a) vs. static test (b)

a)

b)

c)

d)

Figure 4.23 Failure of bracing members in Test 6

Since the results of static tests indicated unequal load sharing among the legs of the bracing members located in the longitudinal face below the cross arm, more strain gauges were installed on those diagonal members to verify this behaviour in the dynamic regime. As shown in Figure 4.24, the ratios obtained between the longitudinal axial strains on the two legs of the same angle at the same relative position are of 4.1, 3.5, 4.3 and 2.9 for members 35, 36, 43 and 44, respectively (see Figure 4.11). These results confirm the response observed during the static test. This observation is very important because those diagonal members control several failure scenarios and are typically the main damaged elements at ultimate loads. Unequal axial stress distribution in the legs

75

essentially comes from eccentric loading of the members, which are subject to bi-axial bending and axial force. It should be noted that conventional lattice tower design does not take this nominal eccentricity into account when calculating member stresses; this approach should be reconsidered. Since the strain gauges were installed approximately 300 mm to the connections and angle leg sizes were in the range of 50 mm, the strain gauge distance from the connection is about 6 times the leg size, shear lag effects have no influence on the measurements.

a)
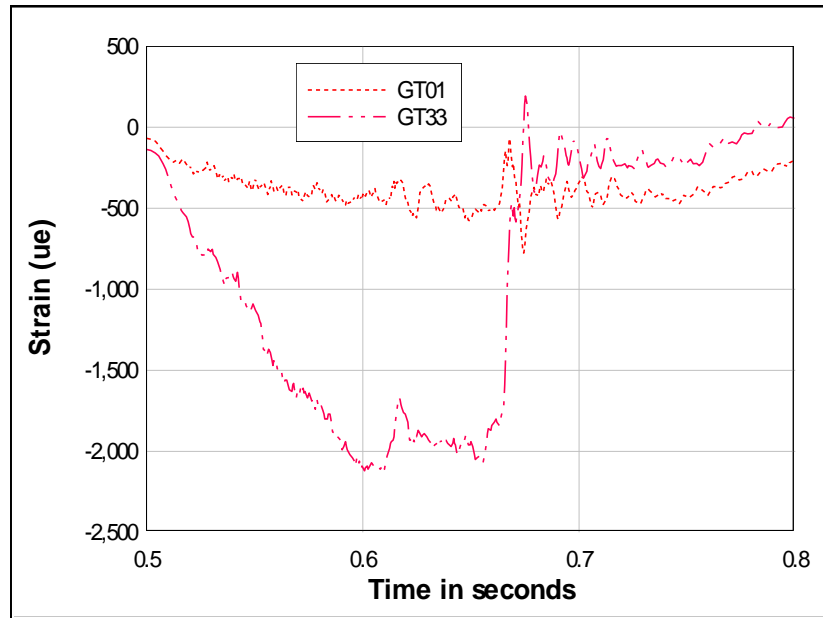
b)
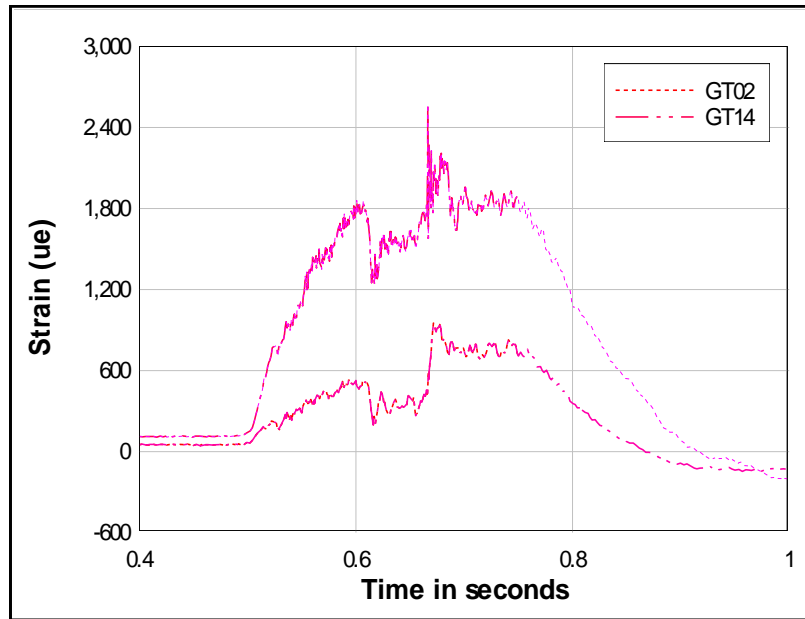
c)
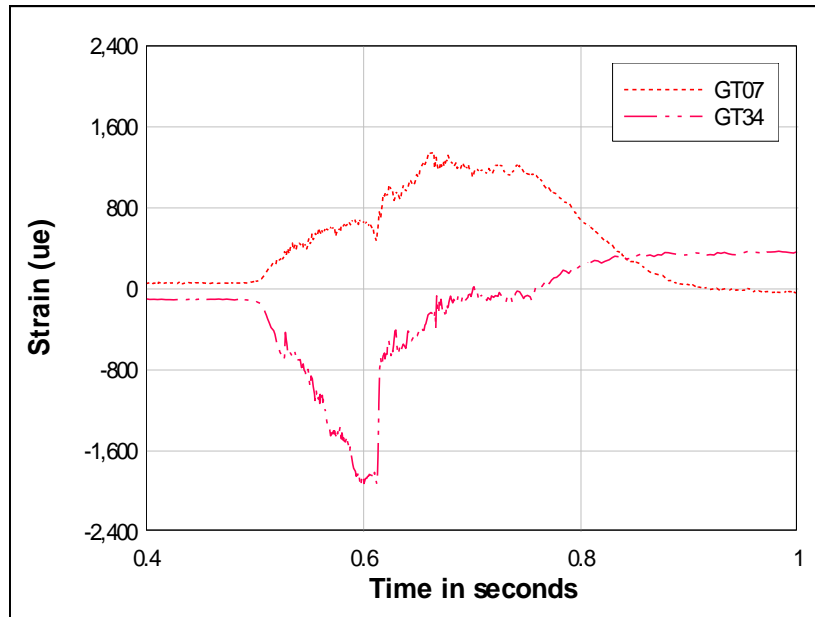
d)
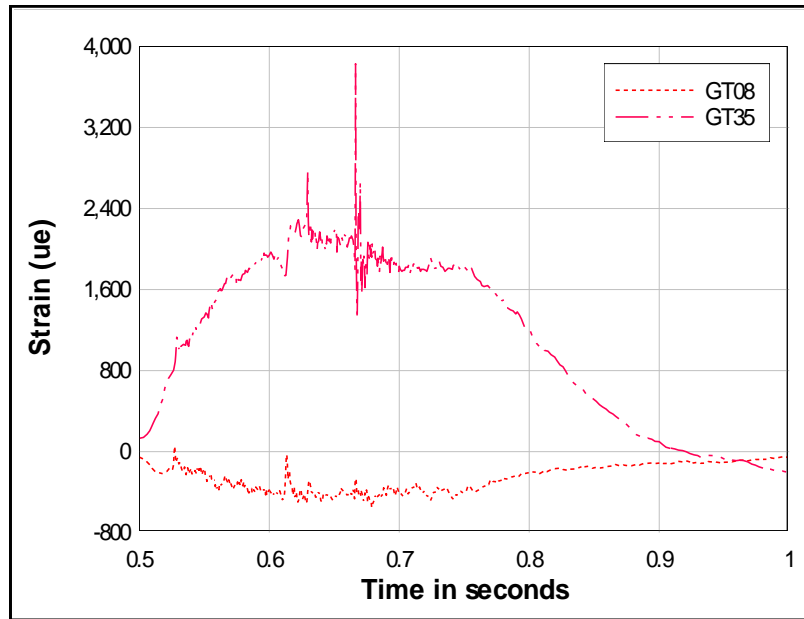
**Figure 4.24 Uneven load sharing among the two legs of angle bracings:
a) Member 35; b) Member 36; c) Member 43 and d) Member 44**

It was concluded from those comparisons that due to their connection eccentricities, all the diagonals under this loading are in fact subjected to combined axial and bending effects, which cannot be represented by an ideal truss model. This is an important consideration because these bracing members control the post-elastic response and failure of the tower in both the static and dynamic torsion tests. This will be discussed further in Chapter 5 when the numerical models were verified.

4.6.4 Static bending pushover test (Test 11)

The numerical simulations performed in preparation for the transverse bending test indicated that the failure would be initiated in the main legs of the bottom section where the overall bending moment reaches a maximum. As shown in Figure 4.12, the strain gauge placement was adapted for this loading case, according to the predictions of

78

the numerical simulations. A total of 31 strain gauges were installed on the leg members to monitor the load paths from the panel below the cross arm to the base.

Before performing the static pushover test, two non-destructive mass dropping tests (Tests 9 and 10) were carried out to get an indication of the loading rates that could be achieved. In Test 9, the mass was dropped from 202 mm: the maximum loading rate was 600kN/s, and the minimum, 201kN/s. In Test 10, the mass was dropped from 227 mm and the maximum loading rate recorded was 1250kN/s, and the minimum was 311kN/s. During both tests, no damage or excessive strain was observed and the structure responded elastically.

The same loading apparatus used in the static torsion test was applied to the bending test; the pushover bending test was realized by pulling on the tip of the cross arm with a towing machine at the speed of 2mm/s until the full collapse of the tower. The load-displacement curve measured at the tip of the cross arm is shown in Figure 4.25. The initial portion of the curve in Figure a) is enlarged in Figure b). The maximum load recorded is 126 kN.

a)
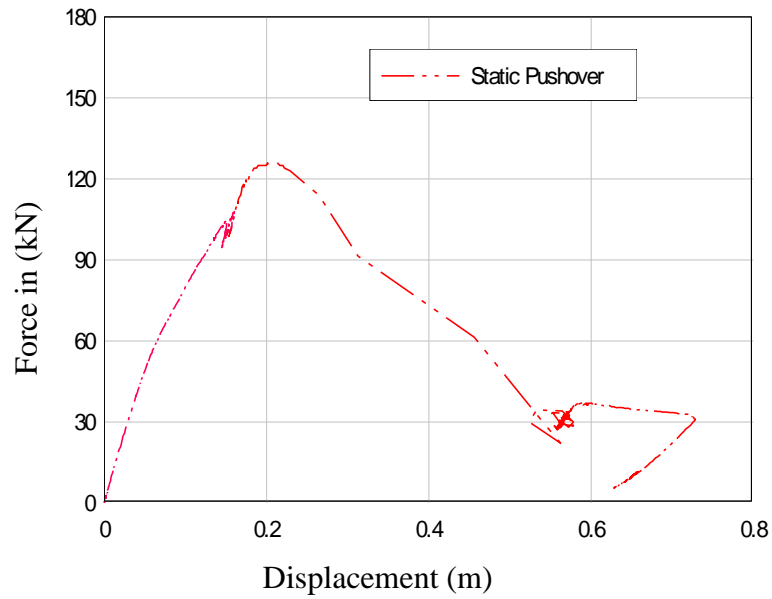
b)
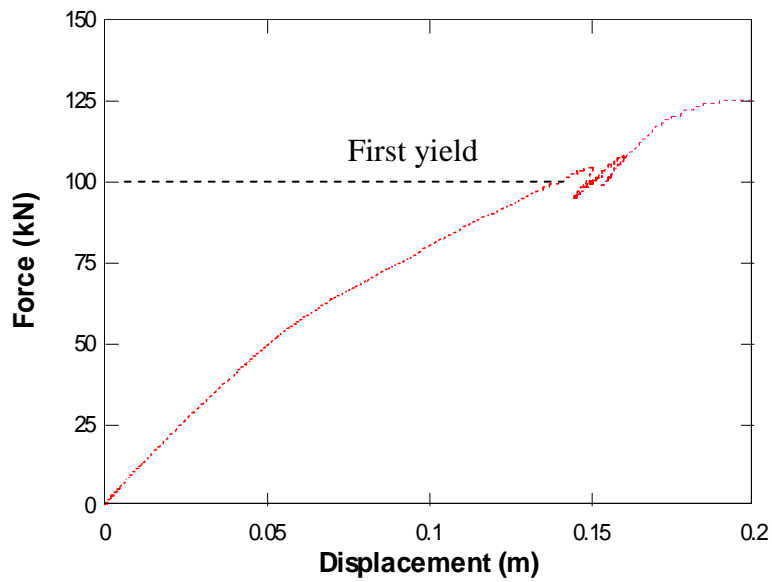
Figure 4.25 Load-displacement for static bending (Test 11)

When pulling the tower to fail we had to interrupt the test due to the insufficient capacity of the loading equipment attached to the towing truck (the towing truck moved backwards); this explains the erratic discontinuity in the curve around the displacement of 0.15 m.

As expected, the failure propagated from the bottom main leg members to the second panel. The final collapse was triggered by the rupture of a diagonal member at a connection. Figure 4.26 shows the residual deformed shape of the structure at the end of the test. Close-up views are shown in Figure 4.27.

Figure 4.26 Deformed structure in static pushover bending (Test 11)
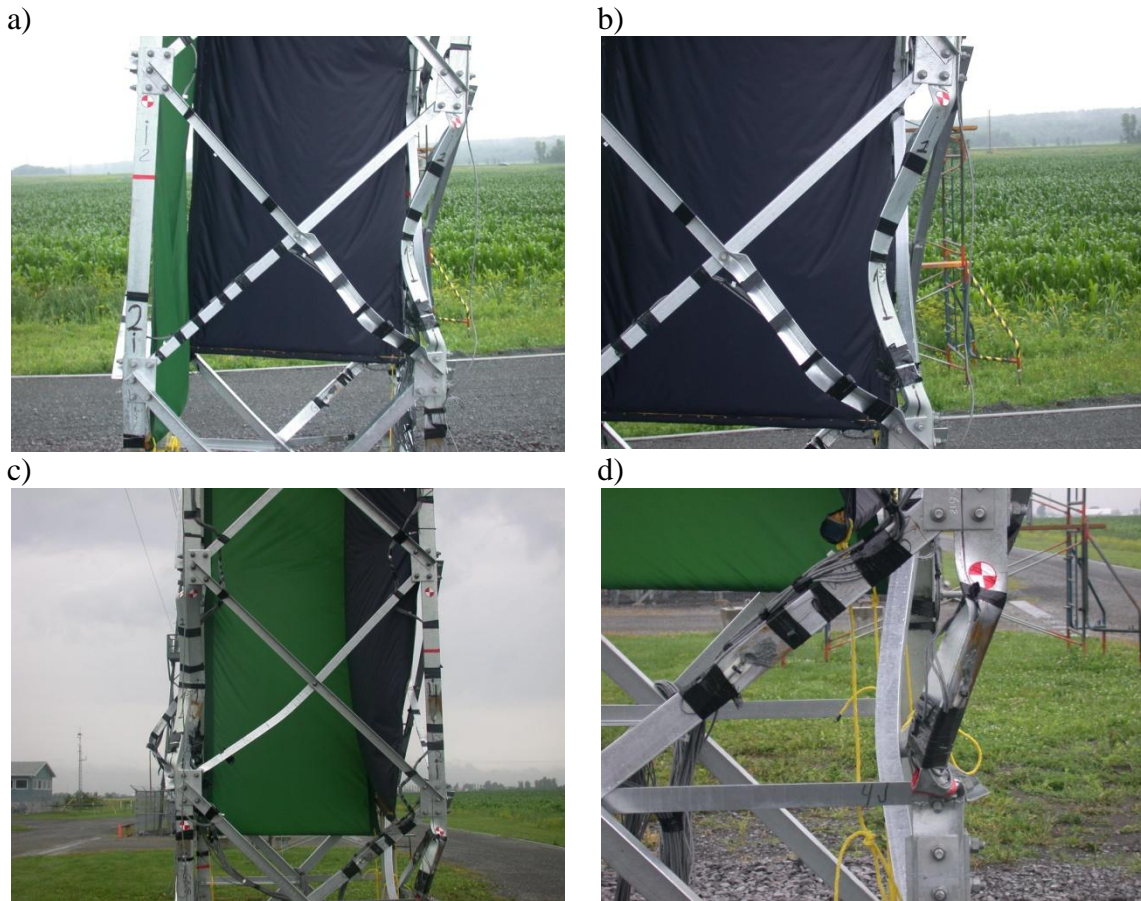
Figure 4.27 Close-up views of leg damage in Test 11

The sequence of member failures is indicated in Table 4.4 and Figure 4.28. From the strain gauge readings, it was established that the first plastic hinge occurred for a load of 123 kN, which is 1.34 times higher than the design limit of 92 kN. However, it is difficult to identify the first yield; based on strain measurements, it was found that first yield occurred around 100 kN (see Figure 4.25b). Therefore, the strength reserve is 23 kN (25% of the design capacity) between the first yield and the first plastic hinge.

It is seen that the main leg members are beam-column elements connected on their two legs. Figure 4.29 shows the strain gauge readings on the different legs of the same angle section (member no. 112) located at the same distance from the ends. Clearly, the evolution of the strains is similar in the two legs and the difference in strain readings

reflects the amount of bending in the angle member. After the failure, there is a transient response (failure shock) in both strain gauges before the steady state is reached (Figure 4.29). Refer to Figure 4.28 for strain gauge numbers and Appendix A for corresponding element numbering.

Table 4.4 Sequence of member failures in Test 11

Gauge No.	Element No.	Time (s)	Applied load (kN)
GB01	189	27.30	123.0
GB02	189	42.51	121.0
GB03	188	26.23	122.0
GB04	188	37.80	126.0
GB05	187	30.37	124.0
GB06	187	30.37	124.0
GB07	186	28.20	123.0
GB08	186	28.20	123.0
GB09	108	42.54	123.0
GB10	107	36.71	126.0
GB11	106	36.71	126.0
GB12	105	42.54	123.0
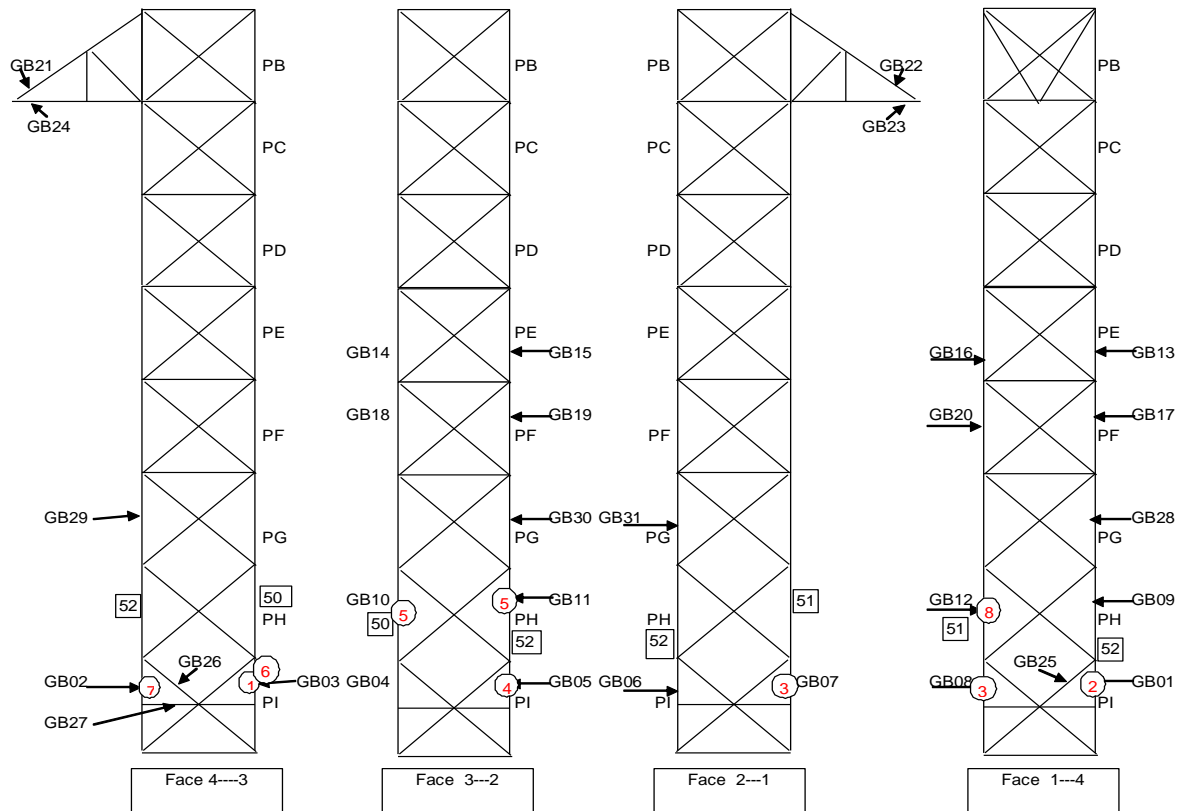
Figure 4.28 Failure sequence of static bending test (Test 11)
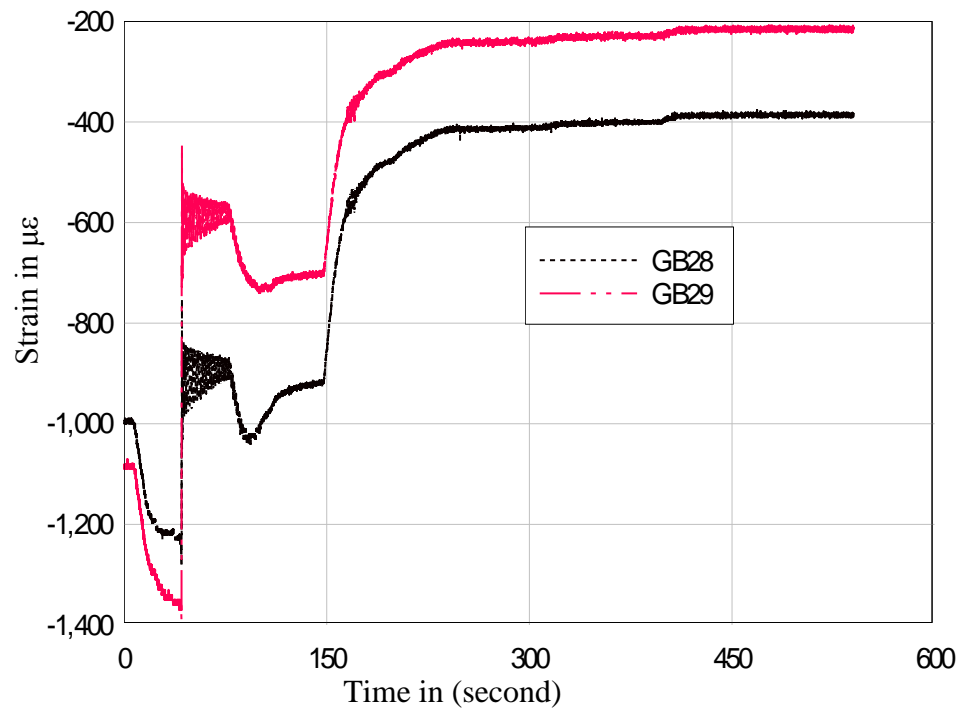
Figure 4.29 Comparison of strain gauge readings on the legs of angle member 112

4.6.5 Dynamic bending test (Test 12)

As explained in Section 4.6.3 for the dynamic torsion test, the shock load is applied by dropping a weight from a controlled height. Considering that the bending strength of the tower is much larger than its torsion-flexure strength, more energy is necessary to fail it in Test 12 and a larger dropping height must be determined. A value of 6 m was selected, which is also the practical upper limit of the experimental set-up. Different dropping heights will induce different loading pulses on the cross arm tip. Our concern was to choose a value that would actually cause strong dynamic effects without total collapse of the tower and prevent damaging the testing apparatus. The transient response of the tower following the shock load lasted for only a few milliseconds and the tower had fully collapsed.

The residual deformed shape of the structure is shown in Figure 4.30 with close-up views in Figure 4.31. The load-displacement curve at the tip of the loaded cross arm is shown in Figure 4.32, in superposition to the curve obtained for the static pushover test.

Figure 4.30 Deformed structure in dynamic bending (Test 12)

a)   b)

Figure 4.31 Close-up views of leg damage in Test 12

86
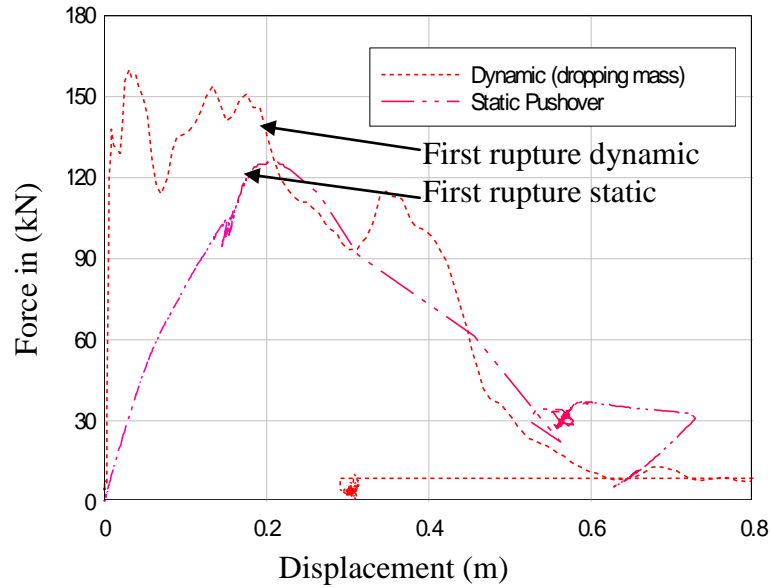
Figure 4.32 Load-displacement for dynamic and static bending tests

The maximum load recorded in the dynamic test is 162kN. The first rupture happened at 142kN and the corresponding displacement of the cross arm tip was 200 mm. The maximum loading rate is 58,000 kN/s, the minimum is 4,000 kN/s and the average is 10,400 kN/s. This is seen on the graph of Figure 4.33 which is a time history plot of the cross arm displacement.
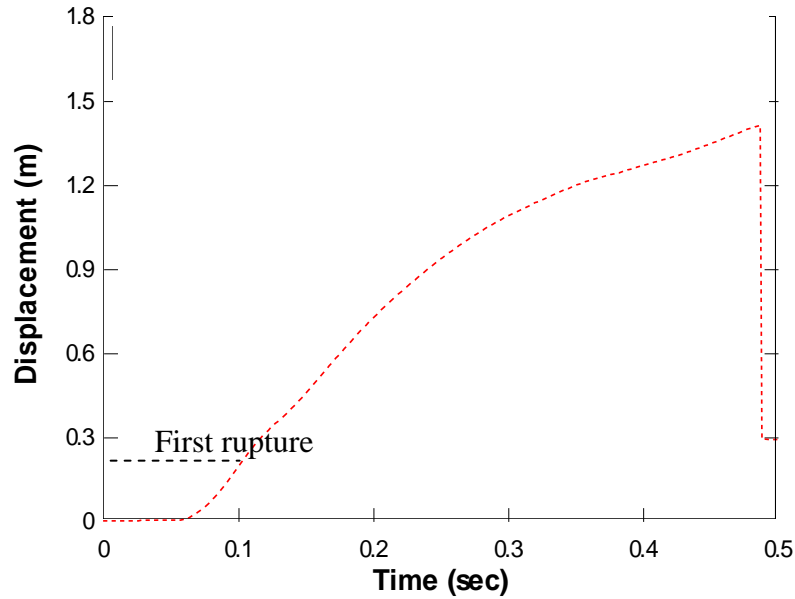
Figure 4.33 Cross arm displacement in Test 12

The dynamic failure modes and sequences are quite different from their static counterparts, as indicated in Table 4.5 and Figure 4.34. The dynamic test failure starts from the local joints, not from the main leg as observed in the static test. For this test, failure starts from the sudden rupture of a diagonal member connected to the main leg under compression, then the main leg connected to this diagonal ruptured and the whole structure lost the strength and stability in just tens of milliseconds. It is very difficult to predict this kind of local failure.

Table 4.5 Sequence of member failures in Test 12

Strain Gauge No.	Element No.	Time (s)	Applied load at cross arm (kN)	Failure Sequence
GB03	188	0.083	**119.3**	
	106	0.085	**129.0**	
	105	0.090	**137.5**	
No Strain				localized
gage	336	0.094	**136.8**	failure
	4058	0.096	**129.1**	
	108	0.097	**127.1**	
	112	0.103	**117.3**	
No Strain				Rupture of
gage	335	0.104	**115.9**	connection
	185	0.105	**114.2**	
	401	0.106	**112.5**	

Figure 4.34 Failure Sequence from Test 12 (dynamic bending)

As in the static test, a strain level needed to be defined to represent the development of the first yield and first plastic hinge. In this case, with the results from the mill tests, 1700 µε was used as first yield level (using Hooke's law) and 20% more (2040 µε) as the strain level for the first plastification. These are key references in the evaluation of the strength reserve and the failure sequence development; this choice of values was confirmed with the experiments.

The strain gauge results plotted in Figure 4.35 show the typical behaviour of main leg members; before the shock and ensuing failure, the two main legs share the stress (and strain) equally, but after failure, one main leg has lost its capacity (zero stress/strain) while the other is still able to resist a residual compressive stress because the structure

90

itself did not fully collapse. From the aftermath of the test, one side of this main leg member (angle 89x89x6.4mm, length 1.25 meters) was deformed wide open and the L-shape of the angle section was not preserved. Unfortunately this detail was not captured on a photo, but still it can be seen on a video record.
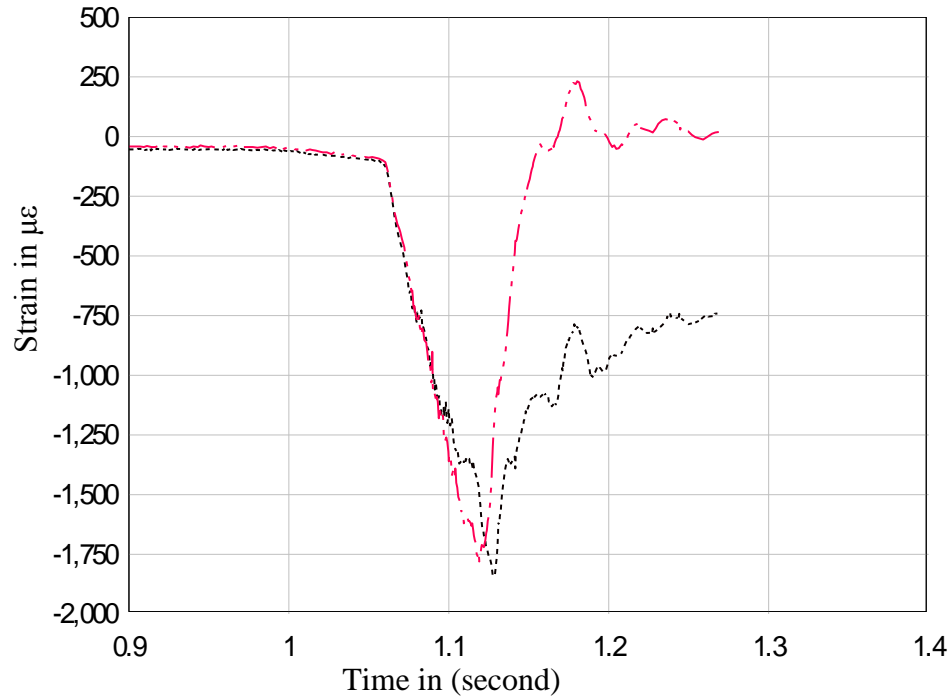
Figure 4.35 Strain gauge readings on member 112 GB28 and GB29

4.7 Discussion

The following summarize the salient observations on the experimental study:

4.7.1 Vulnerability of diagonal members

Diagonal members played quite different roles in different loading cases and they should be designed accordingly. Under the torsion case, the diagonals controlled the ultimate strength of the tower with local ruptures in post-elastic buckling. Since these members are usually connected only on one leg (if they are angle shapes as in the tested

91

prototypes), connection eccentricities cause significant bending in the members and it is the connected leg that contributes most of the internal resistance. The axial stress in the net area of the connected leg is larger than in the gross area at strain gauge location. These observations suggest that it would be possible to avoid these local ruptures by proper design considering bi-axial bending effects to further increase the ultimate capacity of the tower. This is quite different for the bending case where the diagonal members played a secondary role to the main legs (acting as beam columns), and did not control the capacity.

4.7.2 Post-elastic strength reserve

The post-elastic strength reserve is the additional static load that the structure can sustain after the first yielding of a member, until collapse. Since usual tower design is based on elastic limits, this is a reserve on the calculated design capacity. In the two static tests, significant strength reserves were observed, above 20%, as indicated in Table 4.6. The values in parentheses are ratios to the corresponding design value (First Yielding).

Table 4.6 Maximum applied loads (in kN) for static tests

Test	First Yielding	First Plastic	First Buckling	Collapse Load
Torsion Test 5	42 (design)	45 (1.07)	47 (1.12)	51.4 (1.22)
Bending Test 11	92 (design)	110 (1.20)	119 (1.29)	126 (1.37)

4.7.3 Strain rate effects

For the tested prototypes, it was found that globally the static failure modes are the same as the dynamic failure modes. The strain rate as measured during the dynamic bending test is the highest, with values in the range of 0.05/s to 0.14/s. The value of 0.05/s is typical for this test and it was concluded that the strain rate is not significantly influencing the ultimate dynamic strength of the structures. During the dynamic bending, the loading rate was very large, with a maximum of the order of 30,000kN/s. The load effects of a conductor rupture on a suspension tower are much slower; in the full scale tests carried out by Hydro Québec TransÉnergie in St-Luc-de-Vincennes (TransÉnergie, 2003), the loading rate was 150 kN/s approximately.

4.7.4 Static vs. dynamic failure modes

The loading rate plays an important role in the load paths and ensuing failure modes. For the torsion loading case, the dynamic loading rate was relatively low (less than 600 kN/s), and the failure modes are similar to those observed in the static test. However, for the bending case, the dynamic loading rate is about 17 times higher (10,400 kN/s on average) and stress wave propagation likely played an important role in the failure modes. During the dynamic bending test, local failures of the diagonal members at the connection areas near the main leg members appeared first and then very fast triggered the main leg failure; the collapse of the whole tower occurred within milliseconds. This is an important finding which suggests that whenever accidental loading occurs on transmission towers, consideration of the loading rates is very important. For instance, a "slow" unbalanced load generated by the collapse of an

adjacent tower will trigger failure modes that are quasi-static. In the St. Luc-de-Vincennes test (TransÉnergie Report No. 53014683, 2003), the loading rate applied on the tower cross arm adjacent to the cable breakage point was of the order of 150kN/s only. At this loading rate, the dynamic failure modes are expected to be the same as the static modes.

4.7.5 *Static vs. dynamic strength*

The interpretation of the test results must be put in the context of each test. The static tests are pushover tests, and the load is increased gradually until the tower fails to resist a higher load, and large deformations occur in the final collapse state. The dynamic tests are impact tests: the tower responds and fails following the application of an impact load that is in fact a pulse load created by the drop of a large weight from a prescribed height. Therefore, the maximum load applied during a dynamic test cannot be interpreted as the dynamic strength of the prototype, and the static strength value represents a lower bound of the pulse load that can be resisted. For the torsion test, the drop height selected has resulted in maximum loads almost equal in both static and dynamic tests (57 kN vs. 51 kN): a larger drop height would have resulted in a higher load. This gain in dynamic strength under impact was observed for the bending case, with a measured dynamic load at failure of 162 kN vs. a static pushover capacity of 126 kN.

Since there is no information in the literature on full scale dynamic tests of lattice towers, it was very difficult to plan and carry out the tests. In retrospect, it was confirmed that the preliminary numerical simulation models have been crucial to plan the tests and

find estimates of failure loads. They were also very useful to decide on the strain gauging of the relevant members. An especially difficult issue, related to the difficulty of predicting the foundation movement, was to estimate the maximum displacements needed to fail the tower so that the general layout of the test line could be properly designed. The selection of the maximum weight dropping height for the impact tests was also a delicate task and selection of adequate weight-height combinations was very important. In conclusion, we believe that the tests were very successful and all these results will be used to verify our numerical models in Chapter 6.

Chapter 5 Numerical Study

5.1 Introduction

One important objective of this research is to develop a numerical modelling approach applicable by practising engineers to perform post-elastic analysis of towers. Such an analysis is a relatively small investment to evaluate the post-elastic reserve strength of towers available to resist extreme and accidental loadings. In current design practice, the capacity of towers is taken as their elastic limit, i.e. the load that will cause the first yield in any member.

As mentioned in Section 3.2, two simple ground wire peak structures were analyzed first to validate the USFOS software (Section 5.2). Following that, the dynamic features of the software were also checked with a cable breakage problem studied by McClure and Lapointe (2003) (Section 5.3). This dynamic validation was essential to carry out the simulations on the BBB prototypes in preparation for the tests (Section 5.4). Finally, re-analyses of the BBB Tower prototypes were done by applying the load functions as measured during the tests (Section 6.1.3). From the simulation results, a general discussion about the testing infrastructure design and instrumentation concludes the chapter (Section 5.5).

5.2 Numerical Simulations on Latticed Ground Wire Peaks

5.2.1 Frequency Analysis of Canadian Bridge Ground Wire Peak

The first numerical test with USFOS was to model the ground wire peak structure shown in Figure 5.1 (which was obtained with USFOS post-processor). The dimensions of the tower peak are as follows: the base is 3.747 m x 3.048 m, the height is 3.78 m and the total mass is 203.7 kg. The material is steel with the following nominal properties: yield stress of 300 MPa, ultimate tensile stress of 450MPa, density of 7850kg/m^3 and modulus of elasticity is 2.1E11Pa, and Poisson's ratio of 0.3. Data for this tower peak sub-structure were provided by Hydro-Québec TransÉnergie. The model joints are numbered as shown in Figure 5.1. The reader interested in more detailed information about the test specimen should contact Hydro-Québec TransÉnergie.
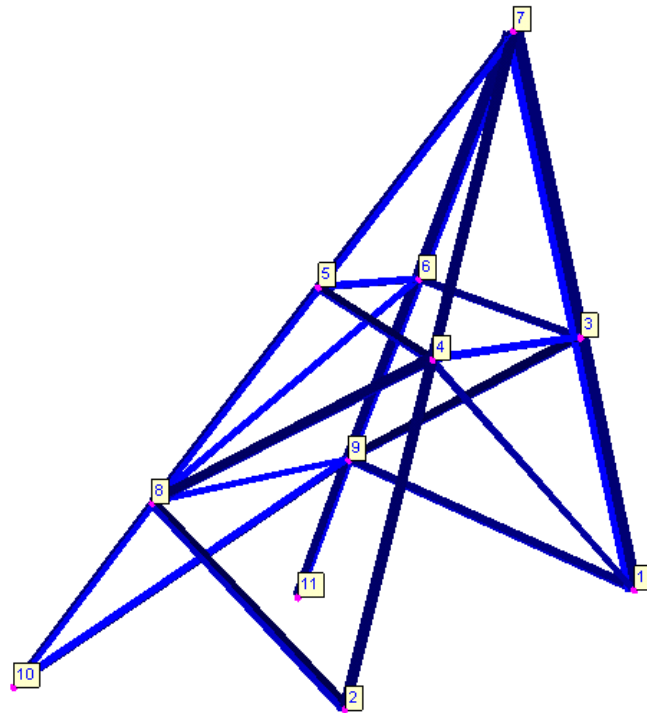
Figure 5.1 Geometric model of the Canadian Bridge ground wire peak

This model had been studied earlier by Guo (2003) with ADINA (ADINA R&D, 2003) and the main objective here was to replicate her frequency analysis results with the USFOS model. Table 5.1 summarizes the comparison of the natural frequency results. Essentially, the two numerical models give the same results for the lowest five natural frequencies and mode shapes. No experimental data are available to validate these results.

Table 5.1 Verification of the Canadian Bridge ground wire peak natural periods

Mode Number	T_{ADINA} (s)	T_{USFOS} (s)	T_{USFOS}/T_{ADINA}
1	0.01524	0.01514	0.993
2	0.01165	0.01161	0.997
3	0.01043	0.01041	0.998
4	0.01016	0.01016	1.000
5	0.00937	0.00940	1.003

5.2.2 Pushover Simulation of SAE1968 Ground Wire Peak

The second numerical model studied with USFOS is another ground wire peak structure. During the January 1998 ice storm in Quebec (McClure et al. 2002), many of the ground wire peaks of the SAE1968 735kV tower used on the 735 kV Churchill-Montreal lines were damaged and had to be replaced. In 2000, Hydro-Quebec tested this ground wire peak up to failure (Guilbault and Picard, 2000) and it was observed that important connection eccentricities at the tip of the peak were limiting the resistance of the structure. A new design was implemented and tested up to failure, which confirmed the increased ultimate capacity of the ground wire peak from the original 28.9kN to 65.5kN. Both the old design and the new design were used to create USFOS finite element models for post-elastic analysis.

The material properties (steel) are the same as in the model of Section 5.2.1. A three-dimensional view of the peak structure is shown in Figure 5.2 with display of member indices.
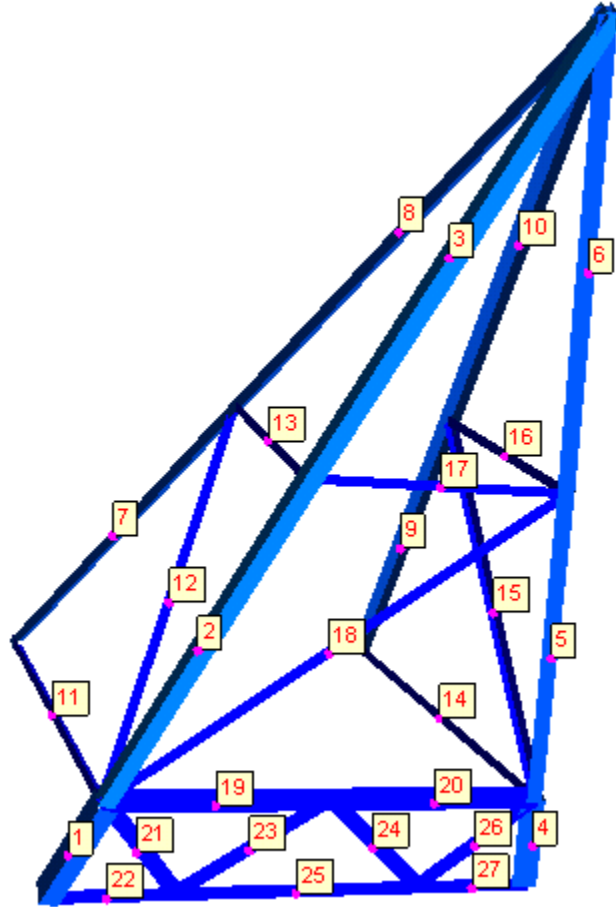
Figure 5.2 Geometric model of the SAE 1968 ground wire peak

The numerical prediction of the ultimate strength of the original design is 35.7 kN while the full scale test yielded 28.9kN. The major source of the discrepancy is the eccentricity in connections at the tip of the structure, which amplified secondary bending effects in the members; in this model, the connection eccentricities were not yet implemented. With the modified design (reducing the loading eccentricity), the post-elastic capacity

predicted by the numerical simulation with nominal properties is 68.9 kN and the test capacity is 65.5 kN. The failure mode obtained from the test is in agreement with the numerical prediction. The field observations after the 1998 ice storm also confirmed the accuracy of the failure mode predicted by the USFOS model of the original design.

Both the experimental and numerical results obtained from this small ground wire peak structure show that considerable strength reserve is accessible in the post-elastic range of response. USFOS models can predict this post-elastic response accurately if the failure modes do not involve any premature connection failures. These important findings have been a source of motivation to pursue the investigation of the post-elastic capacity of the BBB tower structure.

5.3 Simulation of Cable Rupture of a line Section

This simulation project proved very challenging. The objective was to replicate the numerical results obtained with ADINA models by Lapointe (2003) on a six-span line section (shown in Figure 5.3) subjected to conductor breakage in Span #5. For convenience, the tower model geometry was directly imported from the ADINA input text file. The conductor was modeled with cable elements while the insulator strings were modeled by a single rigid truss element.

In the ADINA models, the option of element-death is used to simulate the sudden rupture of a conductor element at any particular time and location (McClure and Lapointe 2003) – this causes the stiffness and the mass of the element to vanish at the specified instant,
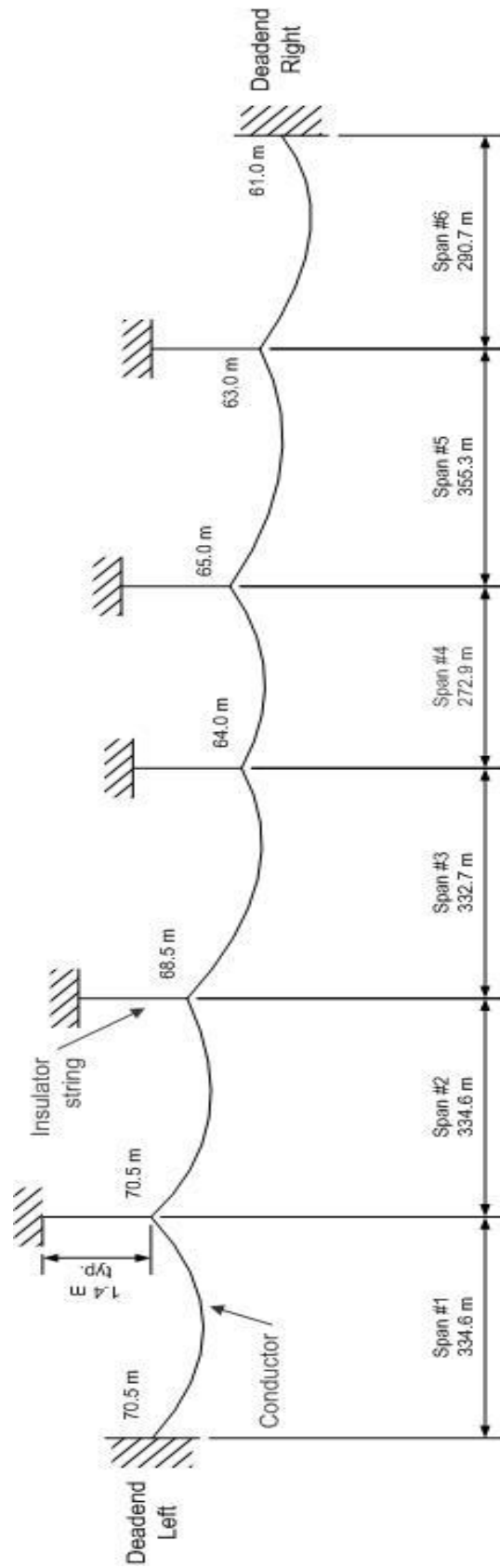
Figure 5.3   Profile of a two-dimensional line section model (Lapointe 2003)

which causes a sudden imbalance. However, this option is not available in USFOS and this effect was modeled as external dynamic load acting on the cross arms adjacent to the conductor breakage point in USFOS. Figure 5.4 shows the tension in the conductor of Span #2 and Figure 5.5 shows the tension in the insulator string next to the breakage point (Span #1 is failing) simulated by USFOS. It should be noted that in all the time history response graphs shown below (in Figures 5.4 to 5.8), the conductor rupture is simulated to occur at time t = 10 s and the response is calculated for a duration of 7 s following the shock for the convenience of comparison with the results of Lapointe (2003)
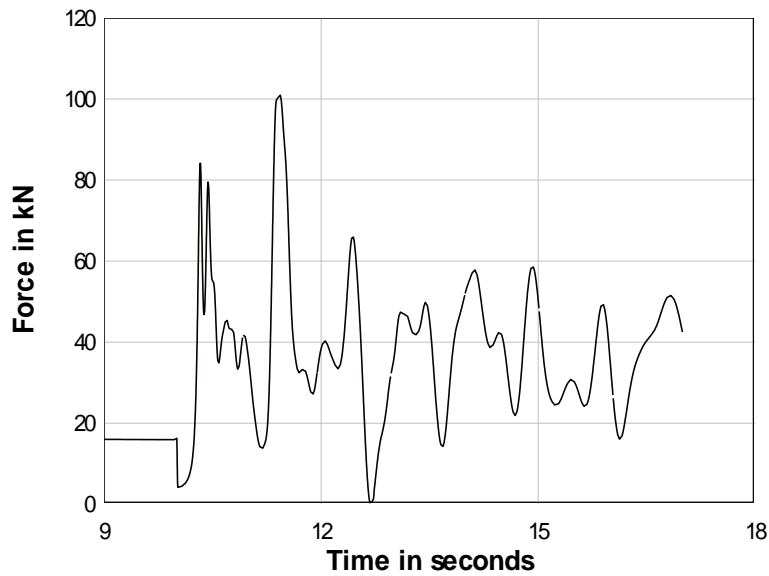
Figure 5.4 Conductor tension in Span #2 (left end) from USFOS model
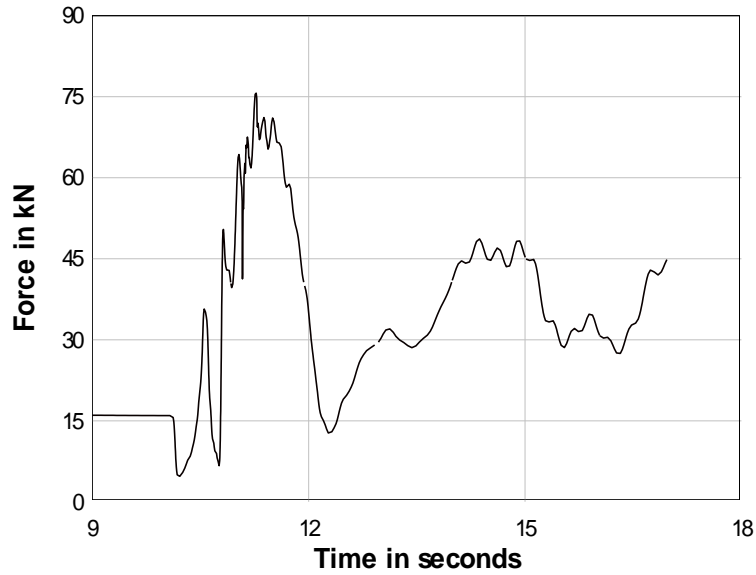
Figure 5.5 Insulator string tension next to breakage point from USFOS model

Figure 5.6, obtained with ADINA from Lapointe (2003), and Figure 5.7, obtained with USFOS, show the longitudinal forces generated after a conductor rupture at the cross arm adjacent to the failure point, for three different ice loading scenarios. It is seen that the USFOS and ADINA simulations yield very similar results despite the differences in load modeling. Figure 5.8 shows the time history of the conductor tensions under the 25mm ice condition, where the results from the two simulation models are superimposed.

From this set of simulations, it was verified that the cable element of USFOS is workable for dynamic analysis. This cable failure approach will be applied later to simulate the shock loads for the BBB Tower for dynamic tests.
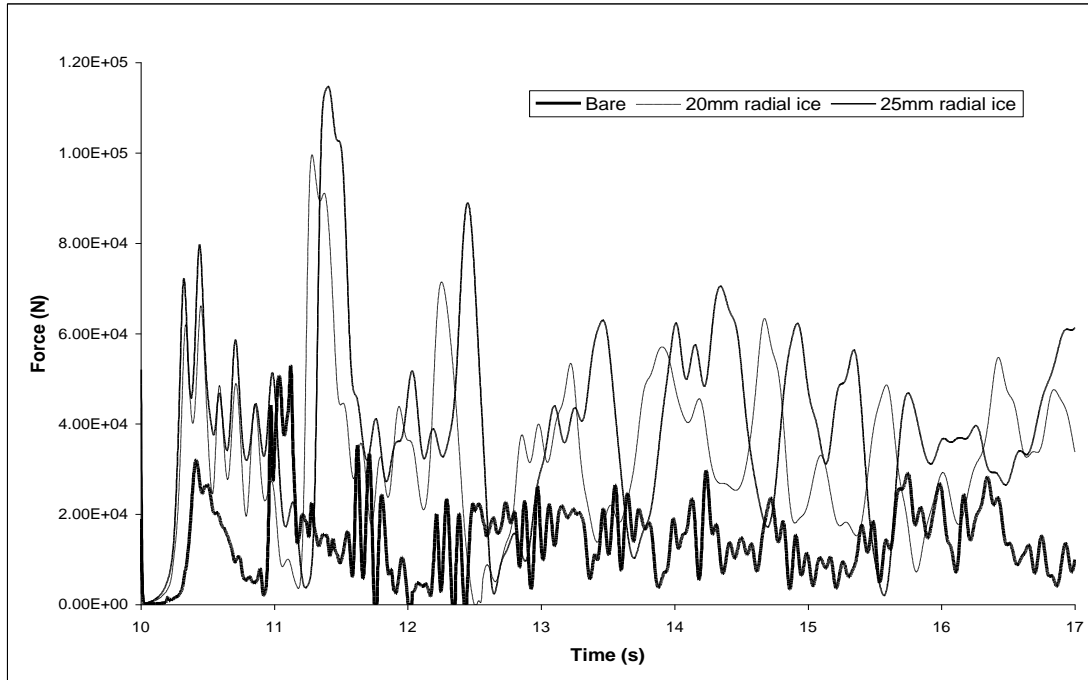
Figure 5.6 Conductor tension in Span #4:
ADINA simulation results from Lapointe (2003)
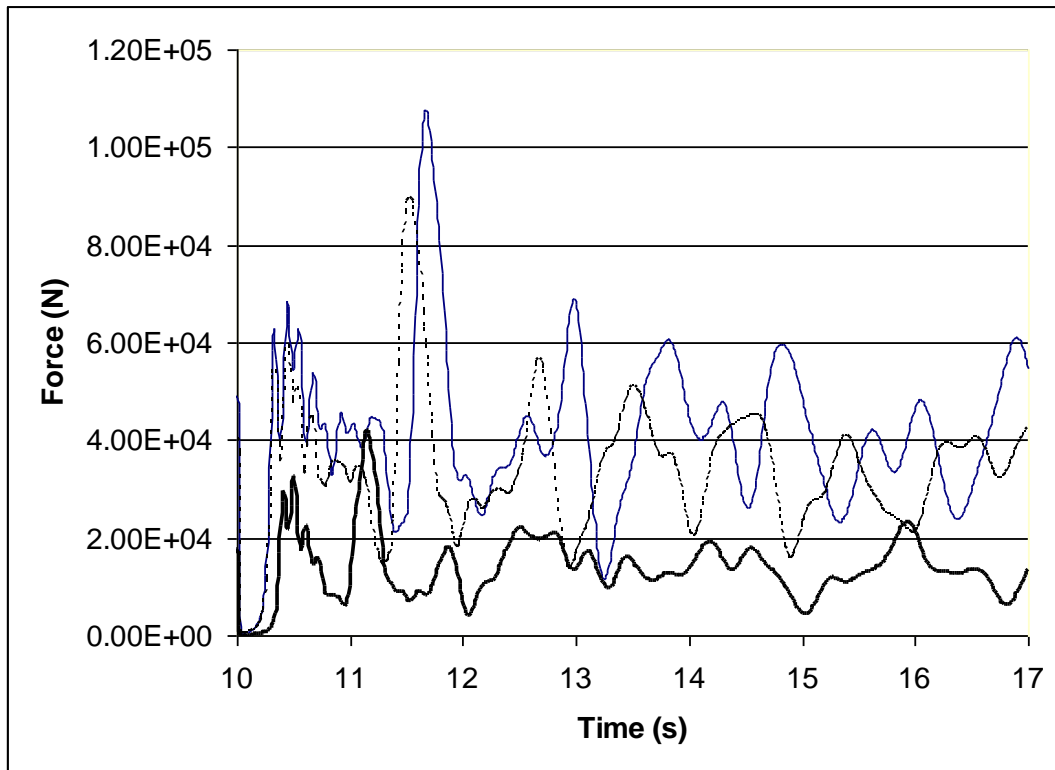
Figure 5.7 Conductor tension in Span # 4: USFOS simulation results
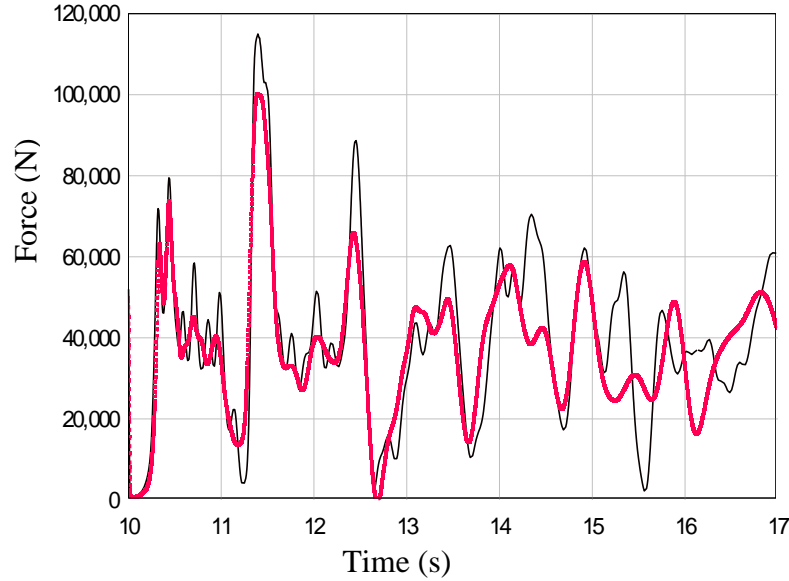
Figure 5.8 **Insulator string tension at right end of Span# 4:**
comparison between USFOS and ADINA results

Another series of simulations was carried out to verify the stress wave propagation along the cables.

The theoretical value of the velocity of a stress wave, V_{sw}, propagating along an elastic and homogeneous taut cable is given in Equation (5.1), where E is the elastic modulus and ρ is the material density.

$$V_{sw} = \sqrt{E/\rho} \tag{5.1}$$

For the cable loaded with different icing conditions, the elasticity remains the same but the density of material is modified to account for the presence of added ice mass.

Table 5.2 compares the theoretical values of the stress wave travel times on a complete span and the results calculated with the USFOS model in previous verifications. It is seen that USFOS results agree with the theory and this confirms that the cable element provides a good approximation of the conductor system.

Table 5.2 Verification of cable stress wave travel times

Stress wave Speed	Method (ms)	Span 1 334.6 m	Span 2 334.6 m	Span 3 332.7 m	Span 4 272.9 m
Bare cable $V_{sw} = 4392$ m/s	Theory	290	214	138	62
	USFOS	290	210	130	70
20 mm $V_{sw} = 2704$ m/s	Theory	471	348	224	101
	USFOS	460	340	220	100
25 mm $V_{sw} = 2425$ m/s	Theory	526	388	250	113
	USFOS	510	380	240	110

5.4 Post-Elastic Analysis of BBB Tower Section

The first series of numerical simulations on the BBB tower section models were done to prepare the full scale tests. Key parameters such as the maximum foundation reactions and overturning moment and the maximum displacement of the cross arm tip were obtained from the numerical simulations and were used for the design of the test set-up. The failure modes and load transmission paths obtained from the numerical simulations were also used for the design of the placement of the strain gauge on the tower prototypes. In Chapter 6, we will use the measured load time history during the dynamic tests as inputs to reanalyze the numerical models and results between the models and the tests will be compared in details thereafter.

5.4.1 Tower Geometry

Geometric details about the prototype design have been presented in Chapter 3. Figure 5.9 shows a three-dimensional view of the numerical model, as obtained from the USFOS graphical user interface.
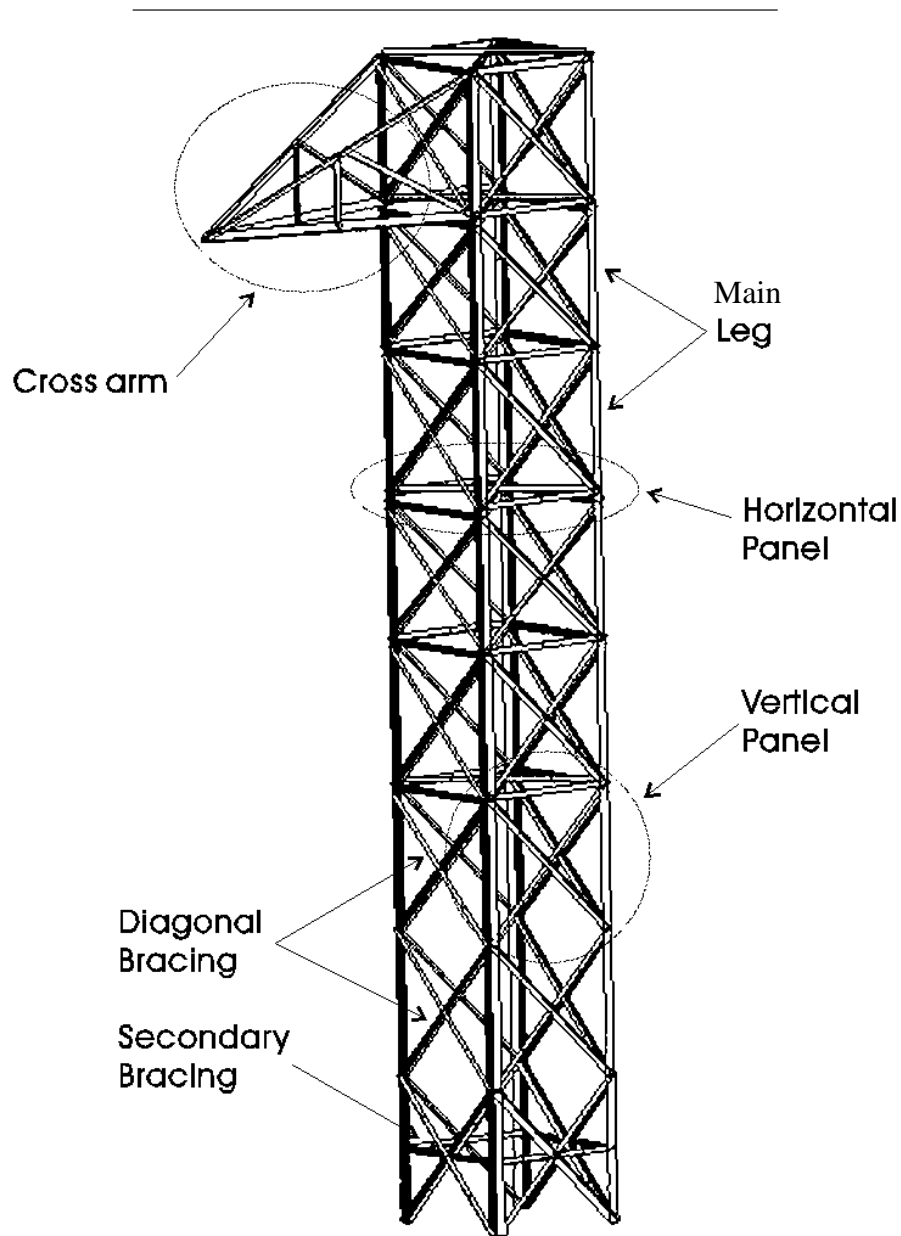
Figure 5.9 BBB tower geometry in USFOS model

The tower section was modeled with 121 nodes, 264 three-node frame (beam-column) elements, 64 non-linear springs to simulate the connections of the diagonals, and 54 offset vectors to simulate the connection eccentricity of angle members connected back-to-back on one leg. All the tower members were modeled as beam-columns, with appropriate end restraint releases for the diagonals.

5.4.2 Eccentricity of joint connections

It is well known by structural designers that eccentric connections affect the maximum capacity and failure mode of connected members. Small nominal eccentricities are inevitable and design provisions account for this. However, larger connection eccentricities must be taken into account explicitly, which is not normally done in space truss analysis. In latticed transmission towers made of angle shapes, the diagonal members are almost always loaded with eccentricity. This is shown schematically in Figure 5.10 for very common details: (a) back-to-back connected X-bracings; (b) diagonal connection on gusset plate to leg with or (c) without horizontal framing member.

(a)   (b)   (c)
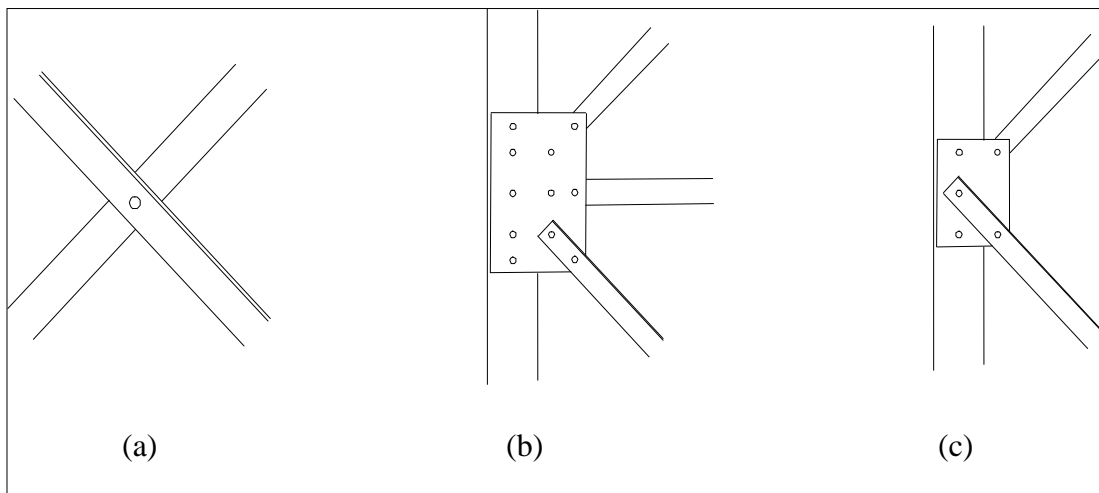
Figure 5.10 Common details of eccentric joints in latticed towers

108

Figure 5.11 shows another detail where the horizontal and diagonal bracing members are connected directly on one leg of the main (vertical) leg. The eccentricity of connection of the diagonal with respect to the horizontal is represented in a) by an offset vector that can be defined in USFOS. Other offset vectors are defined to model the out-of-plane eccentricities with respect to the centroidal axis of the main leg, as shown in b).

a)   b)
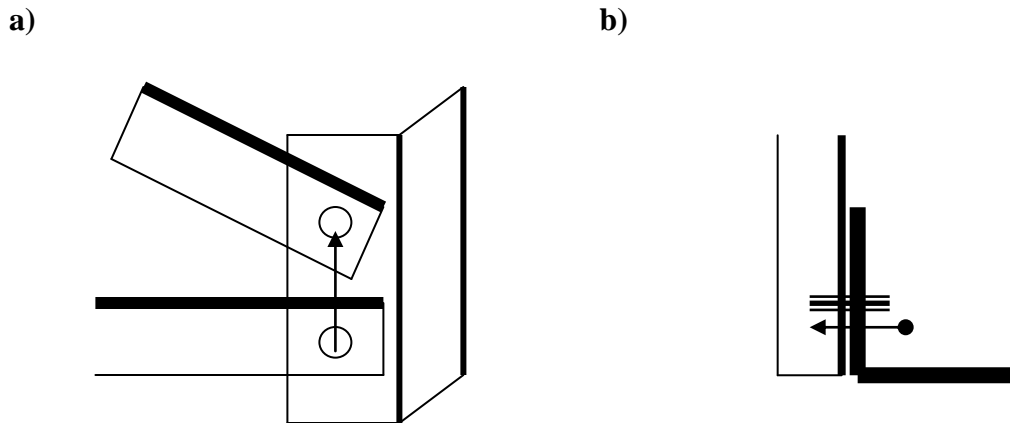
Figure 5.11 Offset vectors defining connection eccentricities

USFOS offset vectors provide a simple way to model members with complex connection eccentricity details. To the real joint coordinates defined when building the model geometry, "virtual joints" are added with the offset vectors, and rigid links are automatically introduced between the pair of joints. With these rigid links, the bolted connection is assumed free to rotate (ideal pin) within the plane defined while the translations are linked between the master nodes and slave nodes.

The slippage between the bolted connections is inevitable in reality when the loads are large and it will increase the global displacements of the structure. However, it is not

modeled here. In fact, when the tower reaches its ultimate capacity, most of the connection slippage has already occurred. However, connection slippage affects the calculated deflected shape significantly: this aspect will be further discussed in Chapter 6.

With rigid links representing the joint eccentricities, the USFOS analysis proceeds with the assumption that failure is governed by the members and no connection failure will occur. This assumption holds true for the BBB tower prototype and was carefully checked at the design stage – in fact diagonal-to-leg connections of the original design had to be strengthened to meet this requirement for the tests. Otherwise, the connection failure of diagonals would have governed the full scale tests and the post-elastic capacity of the prototypes would not have been fully developed.

In the pre-tests analyses used for test planning, no loading eccentricity was considered at the tip of the loaded cross arm. In reality, such an eccentricity could not be avoided, and it will be addressed in Section 5.5 on re-analysis.

Why are connection eccentricities of the structural members - and especially of diagonal members, so important? For the loading case of combined torsion and flexure on the BBB tower prototype, the structure was modeled with and without those eccentricities and a capacity 10 to 15% higher was obtained when the eccentricities were ignored. For the tower under bending only, where diagonals play a less important role in the failure mode, the difference was not significant and the joint eccentricities are not deemed

important overall. However, when measuring or calculating the stresses in eccentrically connected members, consideration of these eccentricities is always important.

The influence of modeling the eccentricities of back-to-back X-bracings was also investigated separately. The interface between each crossing pair was modeled by a linear elastic spring link: the material property of the link was defined by the shearing and tension capacity of the bolt used in the real structure. Because of the different member sizes, several offset vectors and links have to be defined and the procedure is rather tedious. However, introducing this eccentricity leads to an improved numerical prediction. As expected, this type of eccentricity is also more critical for the flexure-torsion loading case than for bending only under transverse loading. Without these eccentricities, the predicted ultimate strength is 10 to 20% higher than that obtained with consideration of these eccentricities for flexure-torsion, but the difference is again not significant for the bending case. Moreover, for flexure-torsion, the failure modes are changed without those eccentricities. The experiments have also confirmed that the X-bracings undergo significant bending in reality.

5.4.3 Loading and Boundary Conditions

The static pushover was modeled as an automatic load incremental approach without unloading, the load is increased monotonically till the collapse of the tower in both longitudinal and transverse directions.

For the dynamic tests, a cable-mass-tower system was modeled to simulate the dynamic effect of a weight dropping loading system. The gravity loading is applied in one time step (0.001s) and then the mass is dropped freely with the simulation of the breakage of the cable linking the mass to the cross arm.

Since the tower base conditions are not ideal in practice, two sets of boundary conditions were simulated: perfectly fixed or perfectly pinned. In fact, the foundation does provide some flexibility (this was observed in the test) and it was proven that the fixed boundary conditions provide a better model than the pinned conditions.

5.4.4 Results

5.4.4.1 Linear Elastic Analysis

To provide an additional verification of the USFOS model, a separate analysis was done using SAP2000 (CSI, 2003) only for the linear elastic portion of the analysis under the bending loading case with transverse (P_y) and downward (P_z) load components at the tip of the cross arm. The results of axial forces in selected members are summarized in Table 5.3 for two load cases. They show agreement but they cannot be identical since the USFOS model accounts for bracing eccentricities.

Table 5.3 Comparison of linear elastic analysis results SAP 2000 vs. USFOS

	Element ID	Load Case 1 $P_y = 70$ kN and $P_z = -17.5$ kN		Load Case 2 $P_y = 80$ kN and $P_z = -20$ kN	
		Axial Forces kN		**Axial Forces kN**	
		SAP2000	USFOS	SAP2000	USFOS
Elements at cross arm	133	85	85	97	102
	134	-119	-119	-136	-142
	135	-22	-22	-26	-26
	136	61	61	69	73
	137	85	85	97	102
	138	-119	-119	-136	-142
	139	0	0	1	1
	140	0	0	0	0
	141	60	61	69	73
	142	-22	22	-25	-27
Elements at base	101	194	197	222	232
	102	234	237	268	281
	103	-202	-205	-231	-242
	104	-243	-247	-278	-291
	186	194	197	222	232
	187	234	237	268	281
	188	-202	-205	-231	-242
	189	-243	-247	-277	290

Element ID numbers are shown in the Appendix A.
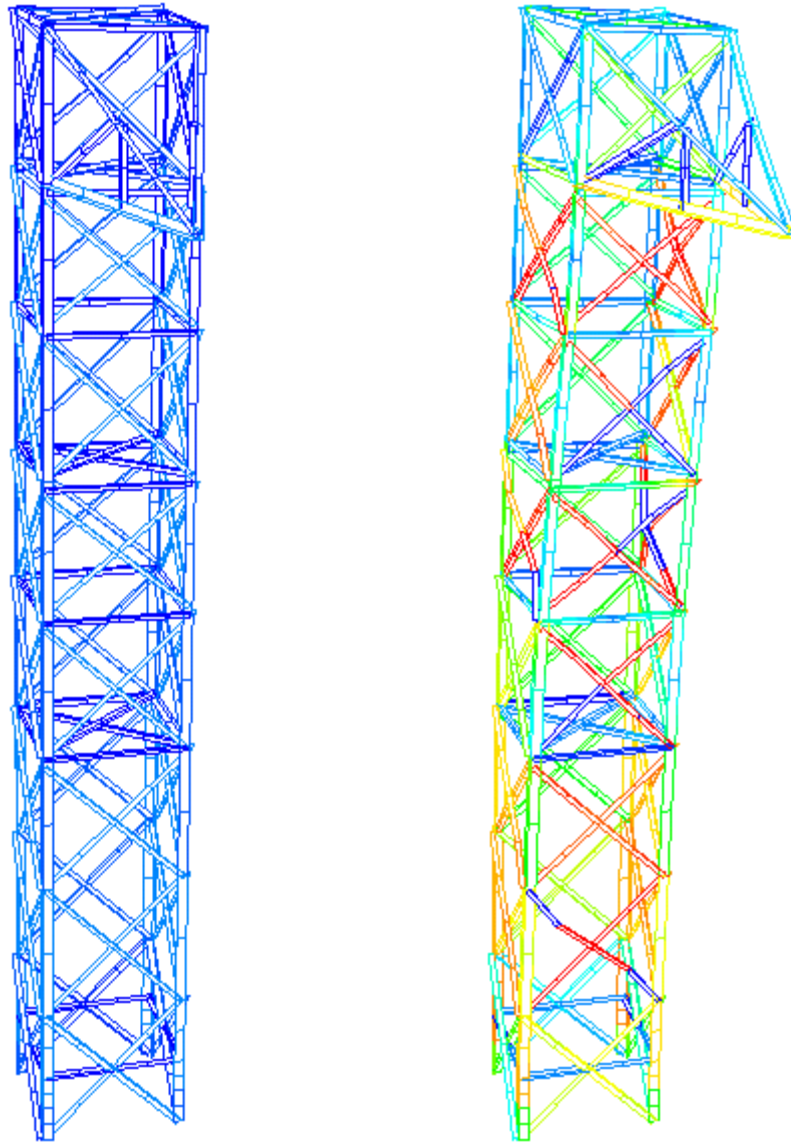
5.4.4.2 Torsion Pushover Test

The initial and final failure shapes of the prototype are shown in Figure 5.12. The input load vs. displacement curve at the tip of the cross arm is shown in Figure 5.13. From the detailed USFOS results, it was possible to determine the applied loads associated with different levels of progressive damage, as follows:

- First yielding: 42.4 kN (reference 1.00)

- First buckling: 44.0 kN (1.04)

- First plastic hinge: 46.0 kN (1.08)

- Ultimate strength of the structure (collapse load): 67.6 kN (1.59)

The failure starts from the diagonals of the panel below the cross arm and it propagates to the lower sections as the load increases. The colors in Figure 5.12 indicate that members in blue are stress free while members in red have yielded. From this analysis, a blind prediction of the failure sequences was obtained and the configuration of the instrumentation was designed and a decision was made upon where to place the 34 strain gauges used in the test. The members selected to be monitored are the four cross arm members (close to the loading point), and eight diagonal members (each with one strain gauge located 325mm away from the bolting location).

Also in order to locate the monitoring equipment, a realistic prediction of the maximum tip displacement has to be given in order to record the results, along its three orthogonal components, namely $D_X = 294$mm, $D_Y = 3$ mm and $D_Z = -3$mm. In view of prototype foundation design, the maximum main leg pull-out force at the base was found to be 265 kN while the maximum compression was 273 kN.

Figure 5.12 Initial and final model configurations for pushover torsion

Figure 5.13 Load vs. displacement at tip of cross arm in pushover torsion model

5.4.4.3 Bending Pushover Test

The initial and final failure shapes of the prototype are shown in Figure 5.14, and the total load vs. displacement curve at the tip of the cross arm is shown in Figure 5.15. From the detailed USFOS results, the following total applied load history was obtained:

- First yielding: 84.6 kN (reference 1.00)

- First buckling: 108.9 kN (1.29)

- First plastic hinge: 105.3 kN (1.24)

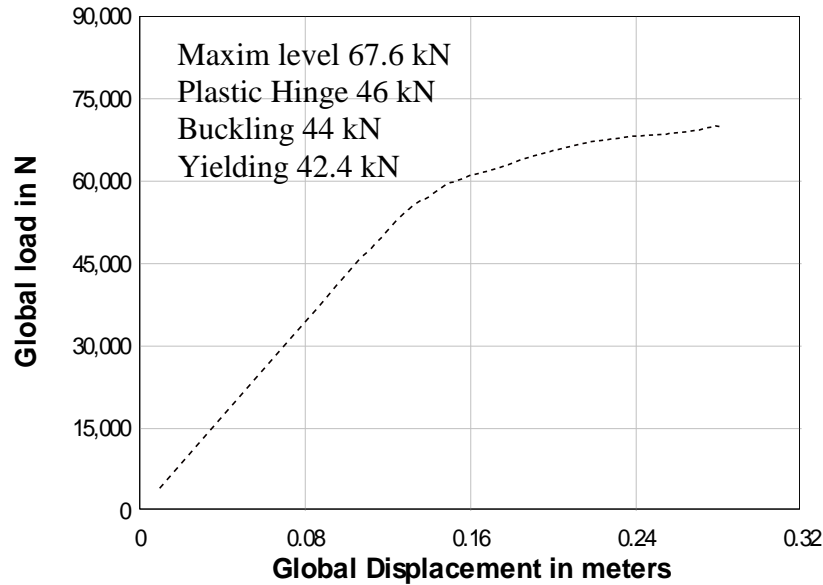- Ultimate strength of the structure (collapse load): 133.2 kN (1.57)

The maximum cross arm displacements are D_X = 95mm, D_Y = 455mm and D_Z = -12 mm. The maximum main leg pull-out force at the base is 483 kN and the maximum compression is 488 kN. It is seen that the bending loading case clearly governs the design of the foundation.
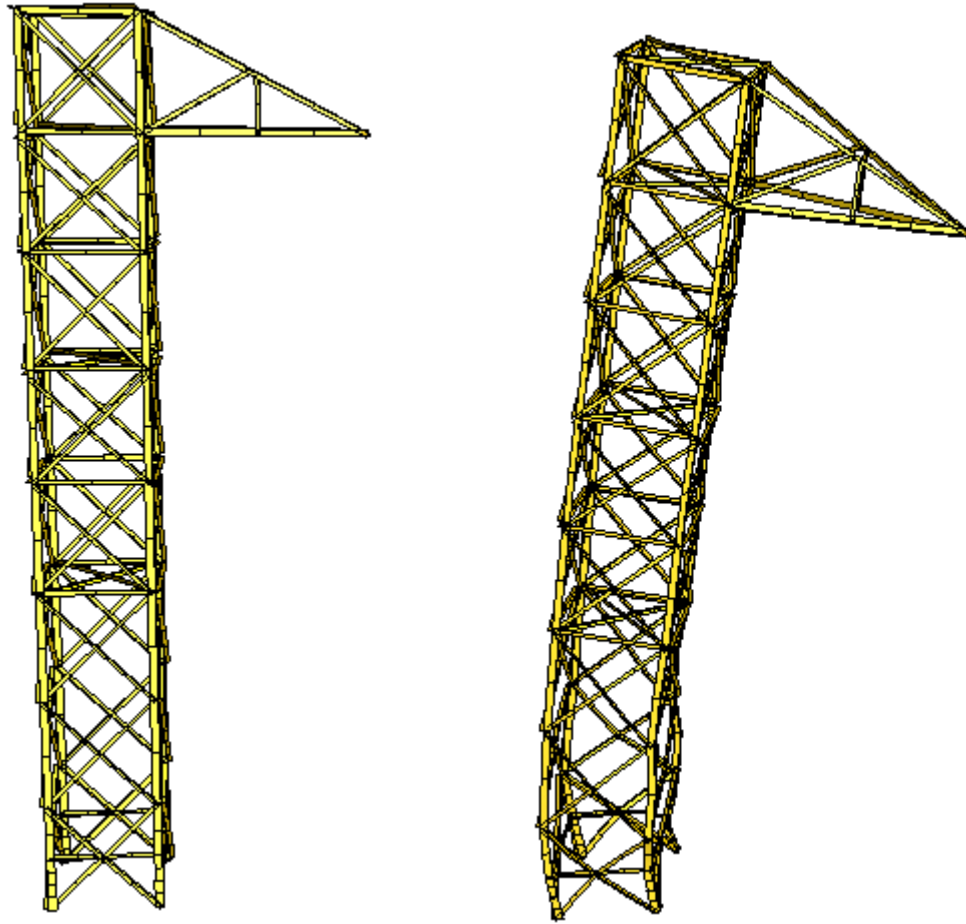
Figure 5.14 Initial and final model configurations for pushover bending tests

The numerical simulation of pushover bending indicated that the failure starts from the bottom section of the tower and propagates upwards. Therefore, a proper strain gauge layout was designed in order to capture the failure sequences as predicted by the simulations. As similar to the torsion case, four strain gauges on the cross arm members close to the loading point were installed to monitor the strain variation of those members.
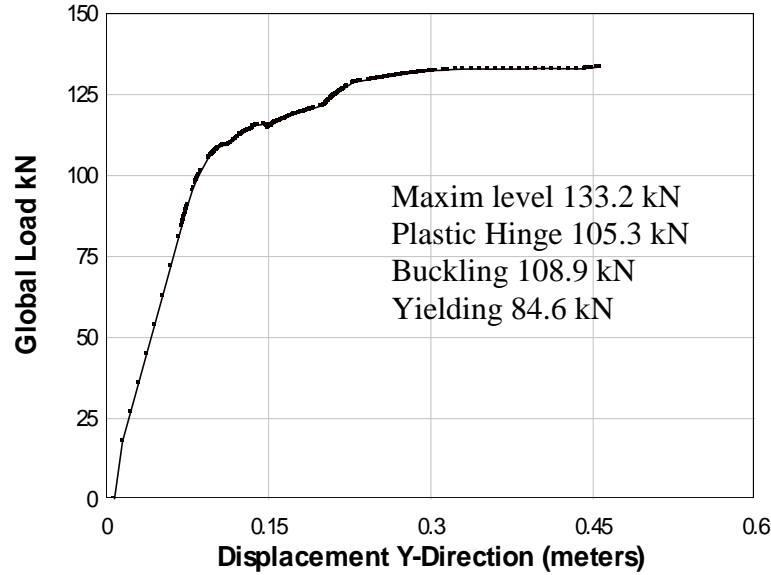
Figure 5.15 Load vs. displacement at tip of cross arm in pushover bending model

5.4.4.4 Natural Frequency Analysis

An important step before the dynamic load test is to verify the lowest natural frequencies and vibration modes of the tower section specimen. To simulate this test numerically, we have loaded the tip of the cross arm with the vertical pulse loading function shown in Figure 5.16, with maximum amplitude of 9.8kN (a one-ton mass), a slow rising time of t_r = 1.0 s and then the load was dropped suddenly at t_d = 4 s. The calculated response is shown in the time history curve of Figure 5.17, which can be used to extract the fundamental period of 0.12 s. It was verified that this load level was small enough to produce no permanent deformations in the structure.

A numerical frequency analysis has also been performed and the results are summarized in Table 5.4, with a comparison of the values obtained in the tests described in Chapter 4.
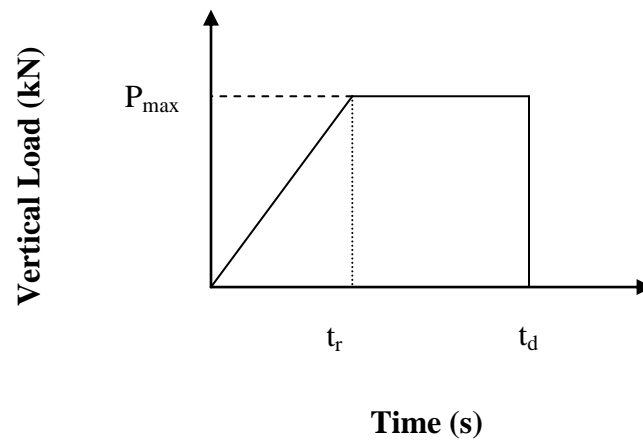
Figure 5.16 Pulse loading applied for tower pluck test
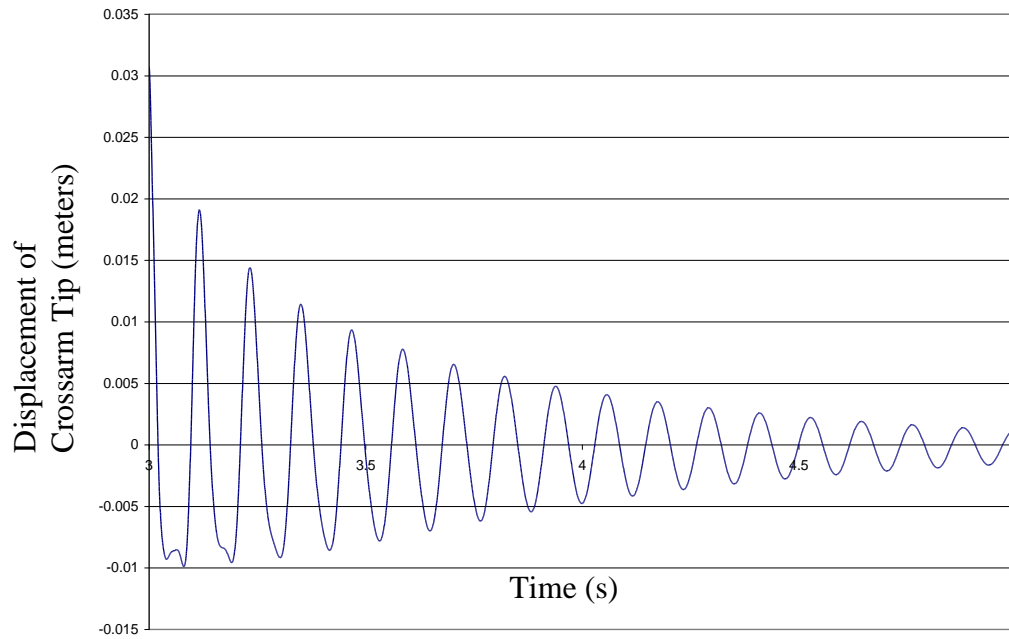
Figure 5.17 Vertical cross arm displacement due to pulse loading of Figure 5.16

Table 5.4 Natural frequency analysis results

Mode of vibration	Period (s)	Natural Frequency (Hz)
1st Transverse Bending	0.135 (0.110)*	7.4 (9.1)
2nd Longitudinal Bending	0.125 (0.106)	8.0 (9.4)
3rd Torsion	0.068 (0.053)	14.8 (18.8)

* Values in () are from the numerical simulations

The natural frequencies measured from the pluck tests for all the three lowest-frequency modes were approximately 20% smaller than calculated values, which confirms that the real test structure is more flexible than its numerical model, mainly due to the fact that foundation flexibility was not modelled.

5.4.4.5 Dynamic Torsion Test

As mentioned in Section 5.4.3, load modelling to represent the mass dropping test required special consideration. In order to apply the shock load in the correct direction (longitudinally for the torsion test), the weight was assumed to drop along that direction with the direction of gravity redefined. Figure 5.18 represents the geometry of this loading set-up. The cable loop in the figure represents the length of the drop height, and the dynamic shock loading of the cross arm will proceed with the sudden release of the loop.

A free drop length of 600 mm
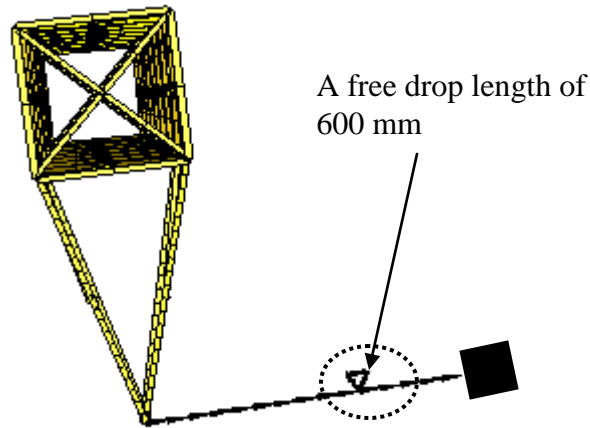
Figure 5.18 Dynamic torsion loading scheme in the USFOS model

Previous analysis had shown that actual gravity effects due to self weight of the tower were practically negligible, and the proposed loading scheme was found adequate. The loading cable was modeled using 33 three-node isoparametric truss elements with end rotational restraint to avoid the singularity of the element stiffness matrix. The effect of different dropping heights could be simulated by changing the length of the cable loop, and the total energy of the loading pulse could be determined. In numerical simulations, there is no consideration of the energy transfer efficiency issue (η parameter in Equation 4.1) so the theoretical dropping height obtained from the simulations should be adjusted for the physical tests. Estimates of the amount of strain energy required to damage the tower were obtained from taking the area below the load-displacement curve of the torsion static pushover simulation (Figure 5.13). To form the first plastic hinge, at 46.0 kN, the external work needed will be 2.11 kN-m. To form two plastic hinges, at 48.0 kN, the external work is 2.76 kN-m. The latticed tower being highly redundant, it will be able to take more load even with more than two plastic hinges. In the limit, at 67.6 kN, the total external work input necessary to collapse the tower is 13.2 kN-m, which is 5 times the elastic strain energy absorbed by the tower. With the 600 mm dropping height, the

121

total potential energy is 5.88 kN-m However, according to basic theory of solid mechanics, the potential energy will be transferred into three categories of energy: kinetic energy in the motion of the dropping mass and the structure, damping/friction energy, and strain energy that will deform the structure. Some of the strain energy will also be absorbed by the secondary structures of the experimental set-up and the tower foundation and soil. With these considerations in mind, we estimated the efficiency parameter η could vary between 0.30 and 0.8 and we calculated a drop height of 2000 mm for the physical test (strain energy of 7.59 kN-m absorbed by the tower for $\eta = 0.3$). With this external work level, the structure will have more than one plastic hinge.

Figures 5.19 and 5.20 show the initial and deformed configurations obtained from the numerical simulations of the weight dropping test with $h = 600$ mm. Figure 5.21 shows the longitudinal pulse load at the tip of the cross arm.
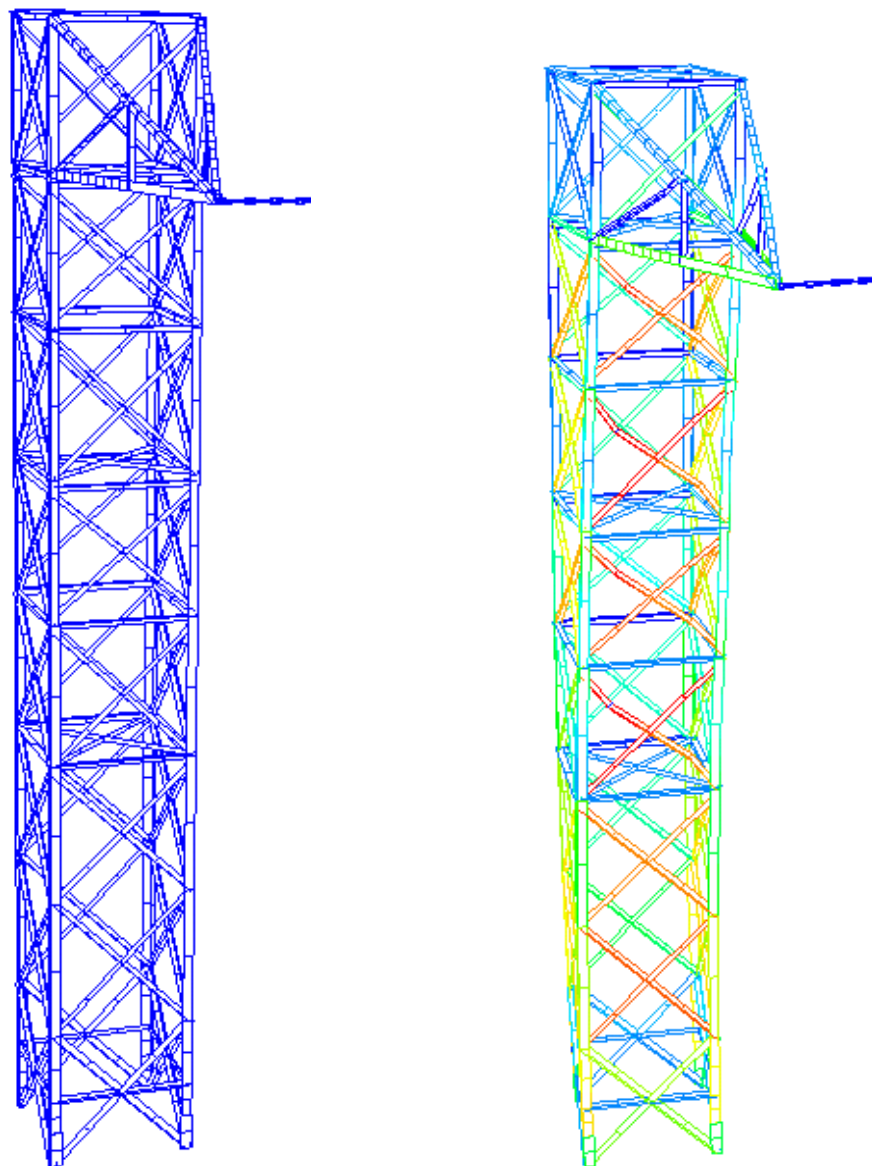
Figure 5.19 Initial and final model configurations for dynamic torsion

From the detailed USFOS model results, the following load-damage history is obtained:

- First yielding: 42.4kN (reference 1.00)

- First buckling: 46.0kN (1.08)

- First plastic hinge: 46.0kN (1.08)

- Maximum load: 49.0kN (1.17)

These results confirm that the pulse load simulated indeed pushed the structure beyond the first plastic hinge, which is created in the first longitudinal panel below the loading point. It is noted that the tower has not fully collapsed under this pulse load.

From the simulation, it was clear that the dynamic failure modes under this particular loading scenario are almost the same as the static ones. Therefore, the same strain gauge layout adopted in the static pushover test was applied for monitoring the dynamic response of the structure. Since there were no failure predicted in the lower section of the tower due to the limitation of the data acquisition system, the bottom section diagonal strain gauges were relocated to the diagonal members in the upper panel (4 diagonals with strain gages on both legs of each member) to monitor the stress distribution on the cross section of the angle members.
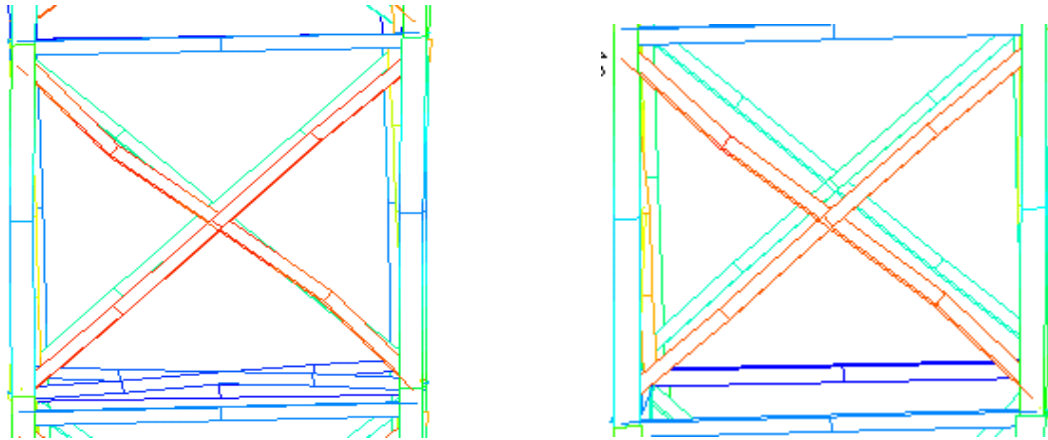
Figure 5.20 Close-up views of tower deformations in dynamic torsion simulation
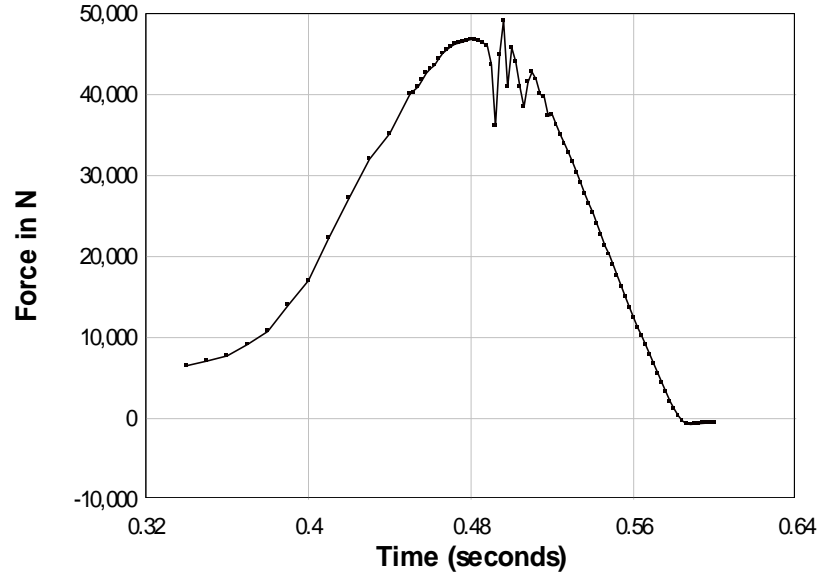
Figure 5.21 Pulse loading at tip of cross arm in dynamic torsion model

The maximum cross arm tip displacements are DX = 110 mm, DY = 1 mm and DZ = -1 mm. The maximum vertical forces on the leg are ± 203 kN.

Figure 5.22 shows the time histories of (a) the movement of the dropping mass used to simulate the dynamic load and (b) the longitudinal displacement of the tip of the cross arm. It is seen that the two motions are synchronized and that the steady-state of the dropping mass will eventually be reached at 600 mm.

a)

Dropping Mass
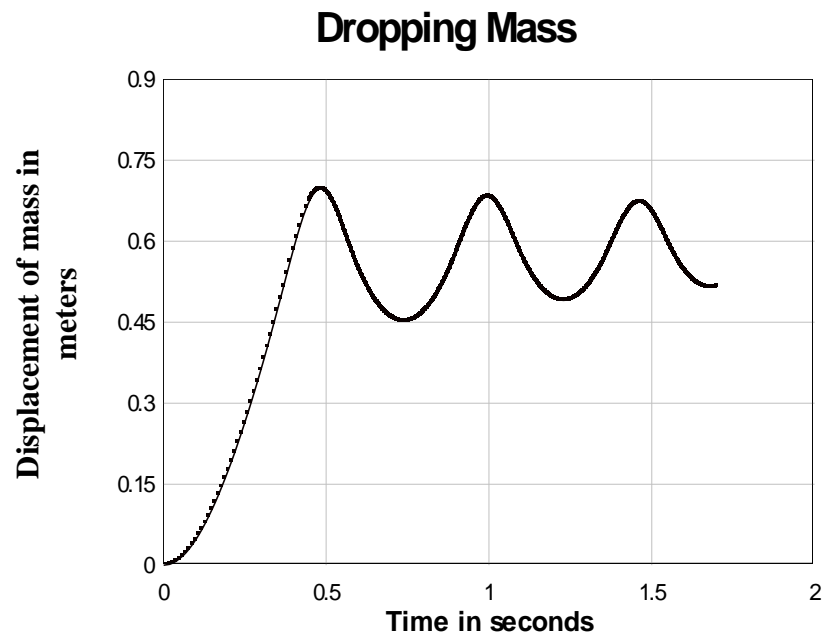
b)
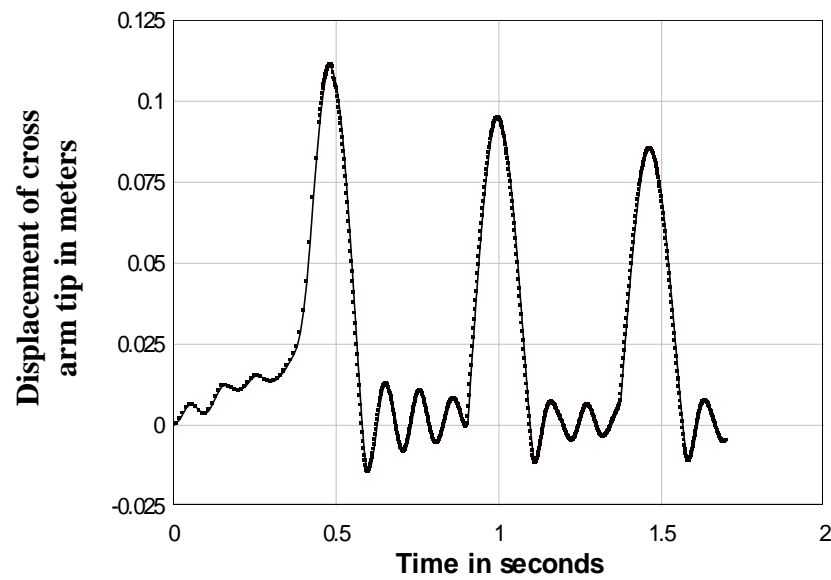
Figure 5.22 Longitudinal motions of the dropped mass (a) and cross arm tip (b)

5.4.4.6 Dynamic Bending Test

The same pulse load modeling approach as used in the dynamic torsion simulations was applied to the bending case. As illustrated in Figure 5.23, this time the gravity direction was changed to the transverse direction (-Y) in order to represent the bending loading scenario. The dynamic simulation used a one-ton mass with a dropping height of 3 m (length of cable loop in Figure 5.23). The loading cable is modelled with 50 elements as used in the torsion dynamic test.
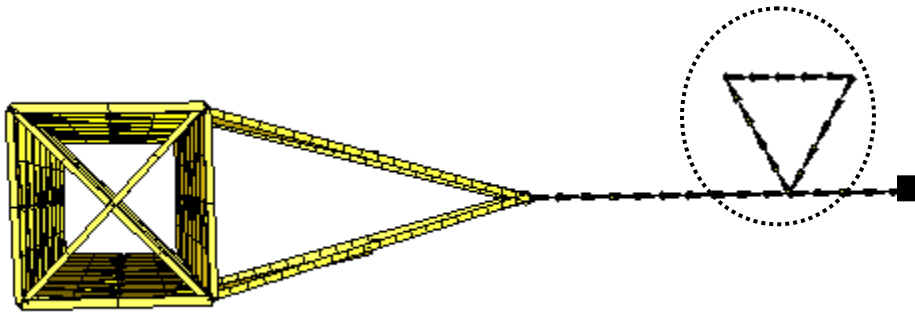
Figure 5.23 Dynamic bending loading scheme in the USFOS model

The selection of the drop height in the physical test was based on similar considerations as explained above for the torsion test, referring now to the bending static pushover load-displacement curve in Figure 5.15. If one plastic hinge was developed (at 105.3kN) the strain energy is 5.27 kN-m. If two plastic hinges were developed (at 106.2kN), the strain energy is 5.84 kN-m. Even with two or more plastic hinges, because of structural redundancy, the tower remains standing and can resist a higher load. In the static simulation, the total strain energy at the collapse load (133.2kN) amounts to 46.5 kN-m, which is 10 times more than the elastic strain energy absorbed by the tower (strain energy up to the first yield level).

As discussed for the dynamic torsion simulation, the energy transfer efficiency has to be taken into consideration during the full scale tests. With a simulated drop height of 3m, the total potential energy is mgh=37.7 kN-m. Considering that the connection eccentricities of the diagonal members to the main legs are not modeled and are less influent in the bending case, we have assumed $\eta = 0.5$ (note that d = 6 m is also a practical limit of the experimental set-up). This energy level should be large enough to get more than one post-elastic event (yielding, buckling and plastic hinge formation). Figure 5.24 shows the deformed shape obtained from the USFOS model with a one-ton drop height of 3 m. It is seen that the failure mode is similar to the static one illustrated in Figure 5.14, so the same strain gauging layout as the static ones were designed.
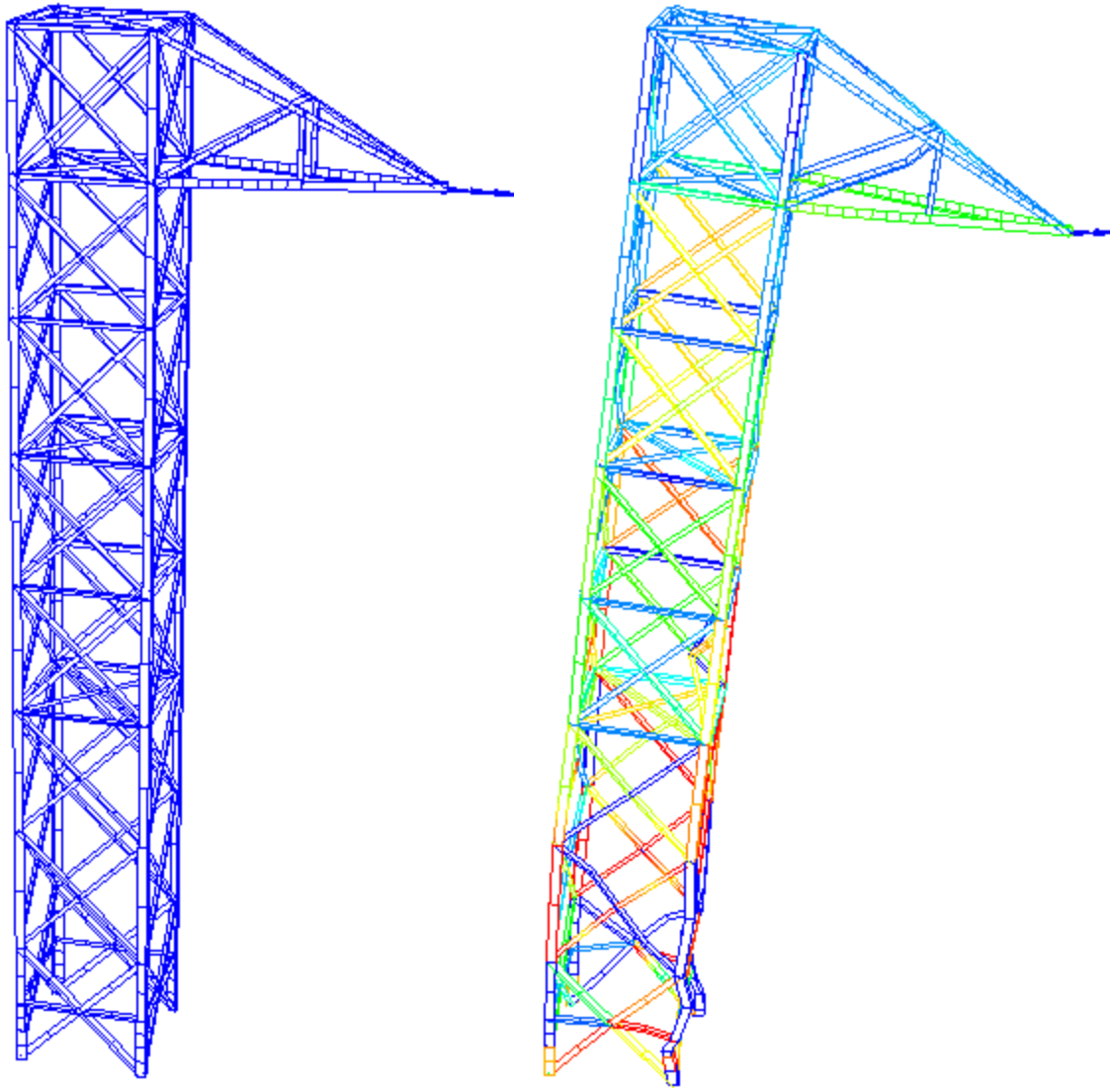
Figure 5.24 Initial and final model configurations for dynamic bending

Figure 5.25 shows the transverse pulse load at the tip of the cross arm. In comparison to Figure 5.21 showing the torsion loading pulse, it is seen that the bending loading resulting from the drop of the one-ton mass creates a sharper peak with maximum amplitude of 158 kN in a much shorter time duration, which means the loading rate is much higher than in the torsion case.
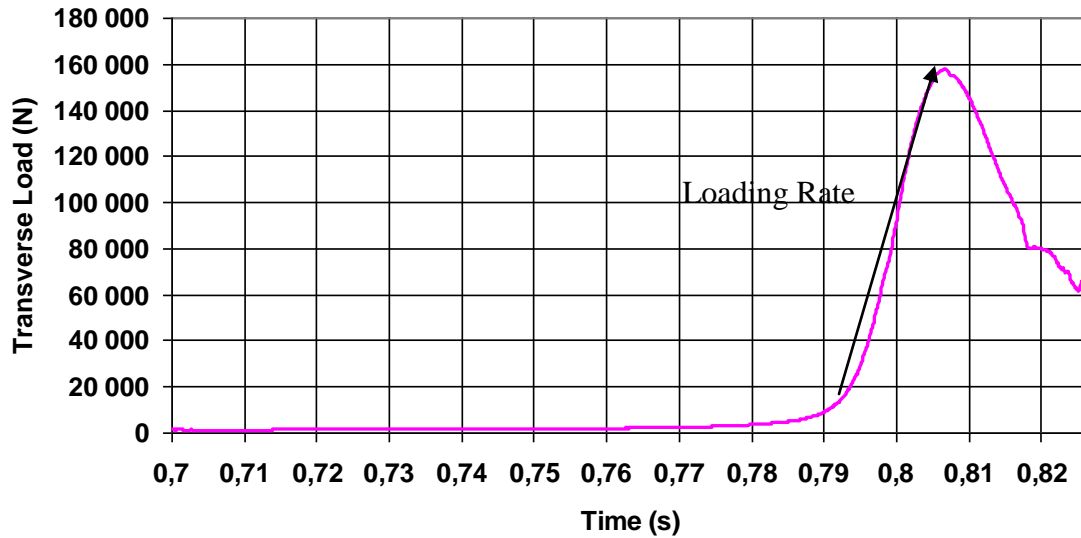
Figure 5.25 Pulse loading at tip of cross arm in dynamic bending model

From the detailed USFOS results, the following load-damage history is obtained:

- First yielding: 120.5 kN (0.8133 second)

- First buckling: 85.1 kN (0.8178 second)

- First plastic hinge: 97.2 kN (0.8166 second)

- Maximum load: 157.6 kN (0.8067 second)

The maximum cross arm tip displacements are DX = 1mm, DY = -115 mm and DZ = -51 mm. The loading rate obtained as shown in Figure 5.25 is 10,000 kN/s. The maximum vertical forces on the main legs are ± 453 kN.

It is noticed that in the dynamic simulation the maximum base reactions were lagging behind the peak external load by approximately 50 to 200 ms. This may be explained by the stress wave propagation from the top to the bottom of the tower.

5.5 Conclusion:

At this stage, the purpose of the computer simulations is to provide as complete as possible the information for the experimental tests such as the failure load levels, the failure sequences etc.; without this information, it would be difficult to plan the tests and to obtain the relevant information from these very expensive full scale tests.

Comparing results of the four simulations, it was concluded that the maximum foundation reaction was approximately 500kN for each main leg. Applying a safety factor of 2 the foundation was designed to resist an uplift force of 1,000kN for each leg and a maximum overturning moment of 2,500 kN-m. This data was a direct input into our facility infrastructure design as shown in Figure 5.26.

Figure 5.26 Construction of foundation for the testing prototypes.

Also the installation of all the instrumentation and monitoring system were carried out according to the predicted failure sequences from the numerical simulations. For the dynamic bending case (dropping of a mass), because of the very high speed of the deformation and loading rate, high speed cameras and high speed data acquisition are both critical for obtaining valuable data.

Figure 5.27 High speed cameras

The sampling frequency of the high speed camera is 2500 fps (frames per second) and the strain gauge sampling frequency is 200 pps (measurements per second). From the simulation results, due to the limitation of the resources, the high speed camera was focused on the bottom sections where the failure is predicted to begin, in order to capture the failure sequences.

Chapter 6 Comparison of Numerical and Experimental Results of BBB Tower Tests

6.1 Re-Analysis of BBB Tower Models

After the four full scale tests were completed on the BBB tower section prototypes, several adjustments were done to our numerical models in order to obtain more realistic simulations of the test results. Firstly, some modifications related to the input of the real (or more realistic) material properties of the tested prototypes, which were obviously not available during the initial modeling phase. Changes also included modeling of the connection eccentricities of all the horizontal and vertical diagonals. Also, the dynamic models were improved by the knowledge of the damping ratio obtained from the dynamic tests. Finally, the load functions measured from the experiments were used as input on the numerical models. These model adjustments are described next.

6.1.1 Material Properties

When the tower material was ordered, some uniaxial loading tests were requested and these stress strain data were used to input the steel material properties specific to each member group in the numerical models. In particular, the material tests indicated that smaller angle shapes had higher yield stresses and ultimate stresses than larger members. Two examples of stress-strain curves are provided in Appendix B. The uniaxial loading test results used in the models are provided in Table 6.1. The material properties used in the numerical model are the average values listed in Table 6.1 for 8 member groups. The global average yield stress was found to be 370 MPa compared to nominal 350 MPa,

while the average ultimate stress was found to be 527 MPa compared to nominal of 550

MPa specified in CSA-G40.21-04/G40.21-04 for 350W steel (CSA, 2004).

Table 6.1 Material properties obtained from axial loading tests

Angle Size (WXHXT) in mm	Test No.	Yield Stress (MPa)			Ultimate Stress (MPa)		
		Test 1	Test 2	Average	Test 1	Test 2	Average
88.9X88.9X6.4	B26514	363.30	364.18	363.74	502.68	502.92	502.80
76.2X76.2X9.5	P7770	348.83	348.15	348.49	530.15	517.05	523.60
76.2X76.2X6.4	B23907	350.22	354.42	352.32	518.41	528.43	518.42
76.2X76.2X4.8	B24317	393.06	394.64	393.85	515.53	517.25	516.39
63.5X50.8X4.8	B23748	365.13	370.52	367.83	505.61	505.48	505.55
50.8X50.8X4.8	B26102	381.23	380.88	381.06	552.51	552.37	552.44
50.8X50.8X3.2	3071325	361.25	367.22	364.32	565.02	563.07	564.05
44.5X44.5X3.2	3121303	360.99	354.85	357.92	506.24	505.30	505.77
			Average	369.55		Average	527.10

6.1.2 Eccentricity of Connections of Diagonal Members

As discussed in Chapter 5, the nominal connection eccentricities were modeled to plan the tests. After the prototypes were built, the precise measurements of these eccentricities were taken into consideration into the in the numerical models. These measurements were tedious and their model implementation at times cumbersome, but it is necessary to implement those eccentricities into the numerical model for the reliable simulation of the prototype as the physical models.

As discussed earlier, the connection eccentricities of the X-bracings play an important role in the torsional tower response because the failure is due to the collapse of these bracing members. Though a few researchers (Kitipornchai et al. 1994) have tried to identify the effects of those eccentricities, but modeling those eccentricities were still very challenging. In this study, a simple method of introducing these eccentricities in numerical simulations of latticed towers were proposed and it was found that the simulation results of the lattice towers subjected to static and dynamic loads was on good agreement with the results from the full scale tests.

6.1.3 Loading Time History Functions

For the two cases of static pushover simulations, the loading were changed from load control (automatic load increments) to displacement control as the latter is more representative of the test conditions. The displacement was applied monotonically to the loading point at a constant speed of 2 mm/s, until the analysis is stopped due to collapse instability. The USFOS software provided this feature and it was convenient for the re-analysis of the towers. With a displacement-controlled loading, the structure will undergo large deformations until the maximum displacements are reached, no matter how many failure events occur. The analysis is stopped by the loss of numerical stability due to global collapse mechanism or excessive distortions.

For the dynamic simulations, the pulse loading time histories measured during the experiments were applied, as shown in Figures 4.19 (for torsion) and Figure 4.33 (for bending), directly to the tip of the cross arm.

6.1.4 Rigid Foundation

As expected, the experiments indicated that the tower foundation was not perfectly rigid and residual displacements have been measured after the tests. However, we did not adjust the numerical models since this should affect mainly the kinematics of the tower and not its internal load distribution. We felt that due consideration of the foundation flexibility would require more explanations of the geotechnical context and foundation design, which was outside the scope of this research. Therefore, all the numerical models assume a fully rigid connection of the four main leg members at the base, as in the pre-test runs. The rigid gusset plate connection at the bottom section of the tower was introduced in the re-analysis models.

6.2 Comparison of Numerical and Experimental Results

6.2.1 Torsion Pushover Test

Figure 6.1 shows the load-displacement curve resulting from the displacement-controlled loading of the tip of the cross arm in the revised analysis, while Figure 6.2 compares the numerical and experimental load-displacement curves for the complete test. It is seen in Figure 6.2 that the initial torsional stiffness of the tower (which is related to the slope of the load-displacement curve) is less in the physical test than in the model. This is explained by the relative flexibility of the foundation that is not modeled (see Section 6.1.4), which causes a rigid body tilting of the tower, and also by the slippage of the bolted connections in lap-splice joints of the leg members. This means that the numerical model will systematically underestimate the cross arm displacements. In fact, a simple correction can be applied to the predicted displacement if this rigid body rotation is

estimated from the test: this was not done here but it is suggested as further work to follow this research in the concluding chapter. The joint slippage occurs gradually and then stops (likely around 45 kN) when all the geometric looseness of the connections is taken up. Joint slippage was observed in the preliminary physical tests when the prototypes were unloaded and did not return to their original configuration. Kitipornchai (Kitipornchai, et al. 1994) also reported that bolting slippage might contribute 20% or more of the total displacement. In the torsion test, such displacements have only a secondary effect on the ultimate capacity (overestimated in the model) and do not affect the failure mode.
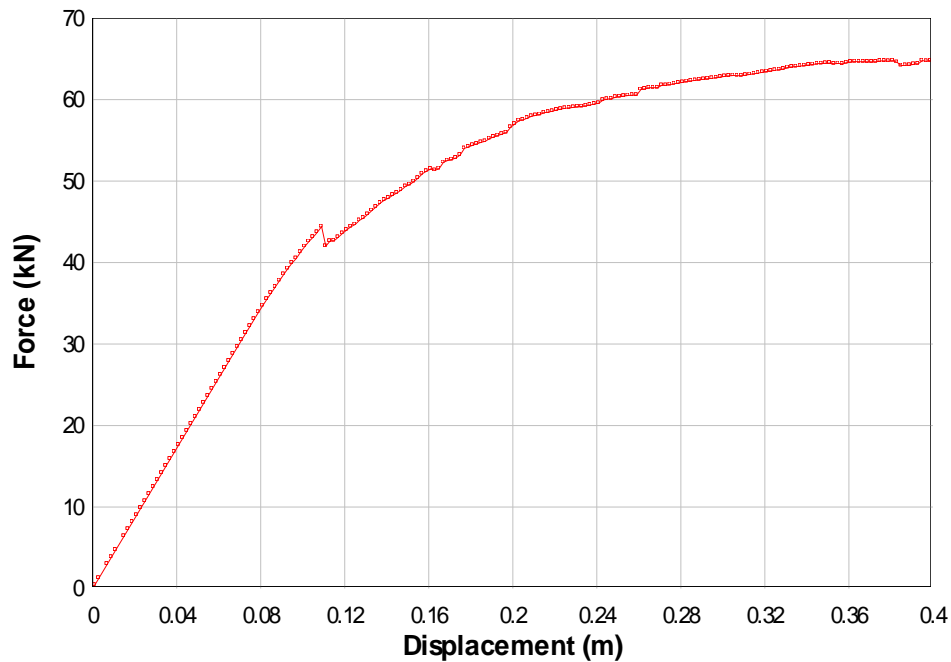

Figure 6.1 Load vs. displacement at tip of cross arm (numerical simulation)
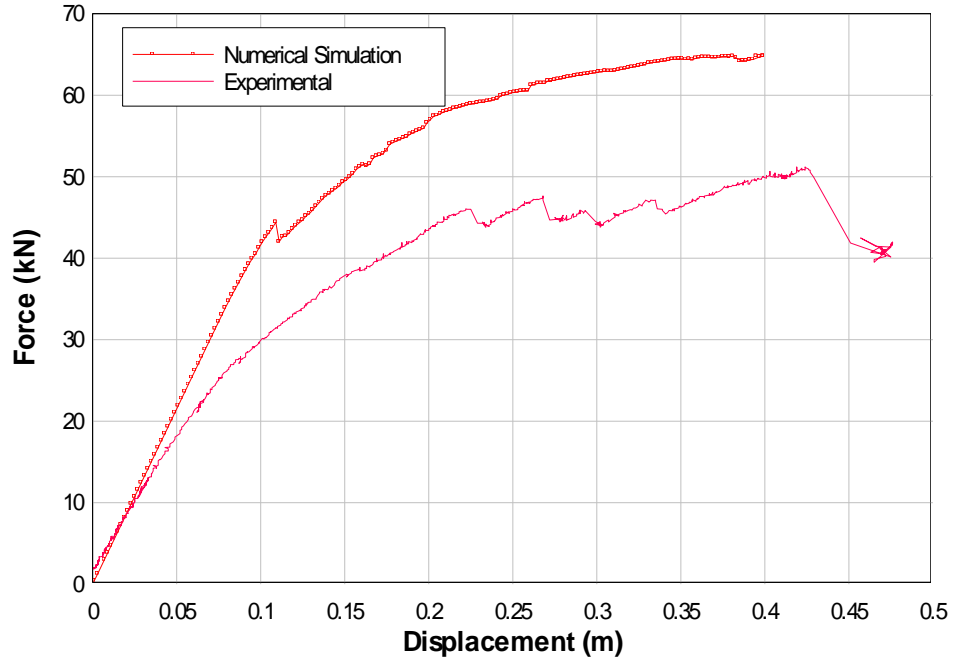
Figure 6.2 Load vs. displacement at tip of cross arm in static pushover torsion

The initial and final deformed configurations obtained from the numerical model are shown in Figure 6.3, which should be compared to the photograph of the physical test in Figure 4.15. Figure 6.3 should be interpreted with the member failure sequence presented in Table 6.3; the failed members near the bottom of the prototype (shown in red in Figure 6.3) had developed plastic hinges after the diagonal members failed. Close-up views of the distorted numerical configurations are shown in Figure 6.4. Figure 6.4 a) is a top view showing the total twisting of the tower while Figures 6.4 b) and c) show the deformations of the first panels below the cross arm in the longitudinal and transverse faces, respectively. Comparing these calculated deformed shapes with the photographs (and videos) taken during the full scale test, we can confirm that the experimental failure modes are the same as predicted by the numerical simulations. The plastic hinges formed in the diagonal members are closer to the leg connection in the physical tests, whereas

they can appear only at a defined node in the numerical model, as shown in Figures 6.4 b) and c). It is of course possible to refine the mesh of each member in the numerical model, but the simulation shows that this is not necessary to capture the essential features of the tower response.
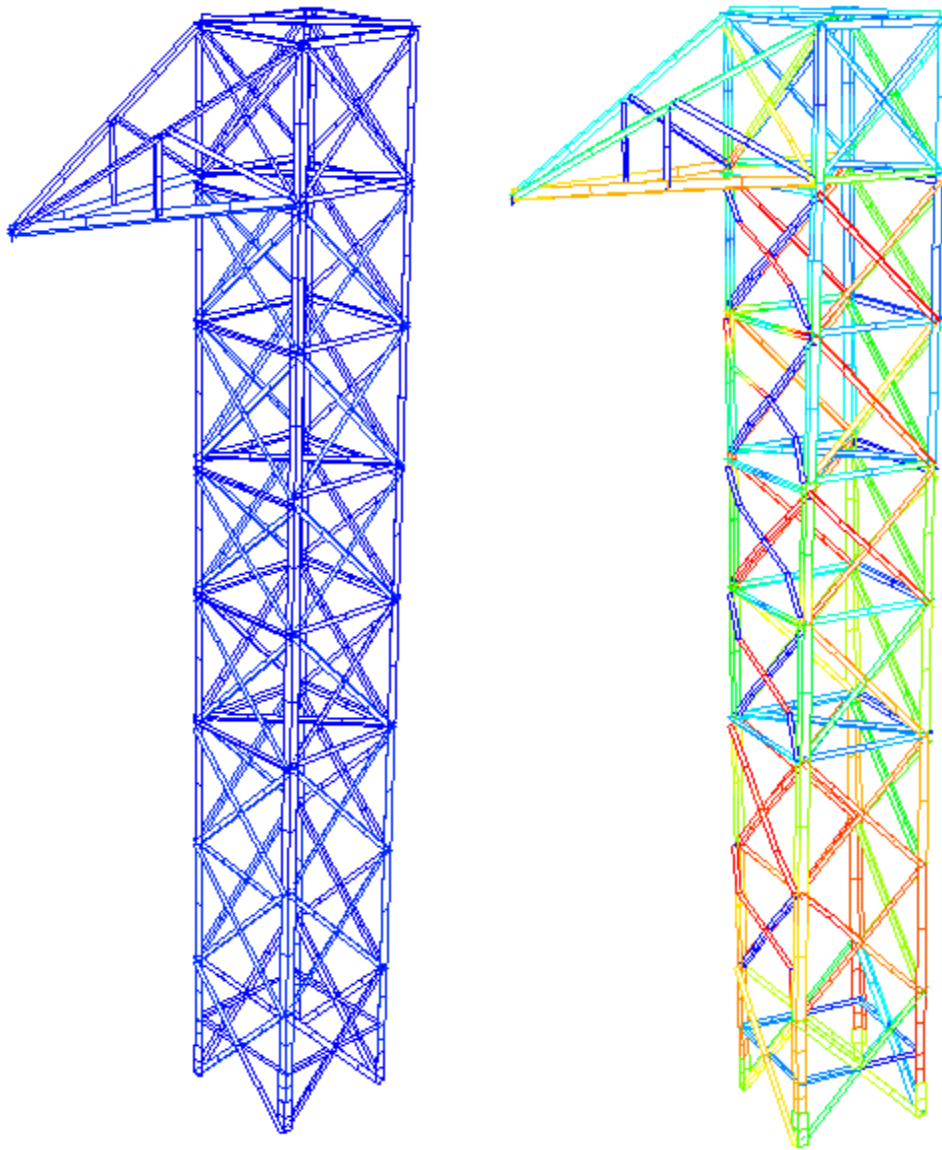
Figure 6.3 Initial and final model configurations for pushover torsion

a)
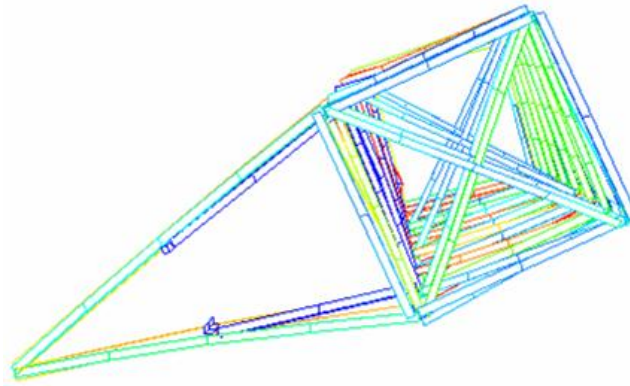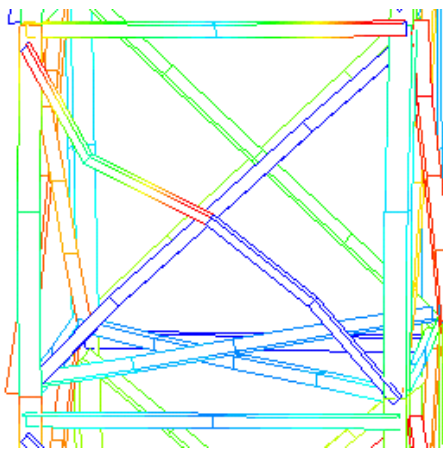
b)   **c)**
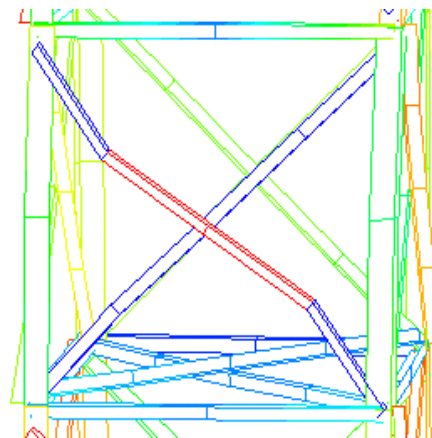
Figure 6.4 Close-up views of the numerical tower deformations in torsion

The numerical analysis provided a very clear and consistent representation of the post-elastic behaviour of the tower. The results for the static pushover torsion are as follows:

- First yielding: 42.8 kN (reference 1.00)

- First plastic hinge: 51.2 kN (1.20)

- First buckling: 57.5 kN (1.34)

- Ultimate strength (collapse load): 67.2kN (1.57)

Tables 6.2 and 6.3 compare the experimental and numerical simulation results including the failure sequence, the related load level and time history. With the installation of four digital video cameras (with 30 fps sampling frequency) facing each tower side, it was possible to identify from the video records the sequence of the failure events and compare them with the strain gauge readings.

Table 6.2 Experimental results in torsion pushover

Strain Gauge No.	Time (s)	Applied Force At Cross Arm (kN)	Failure Position From the Video
GT08	187.61	**45.9**	
GT07	187.64	**45.4**	D4
The 1st failure observed			
GT10	197.81	**47.0**	
GT09	197.84	**44.7**	E4
The 2nd failure observed			
GT12	201.66	**44.5**	
GT11	201.68	**44.5**	F4
The 3rd failure observed			
GT02	210.30	**47.0**	
GT01	210.33	**46.0**	C4
The 4th failure observed			
GT13	237.60	**50.9**	
GT14	238.06	**50.5**	G4
The 5th failure observed			

Table 6.3 Numerical results in torsion pushover

Strain Gauge No.	Time (s)	Applied Force At Cross Arm (kN)	Failure Position From the Tower Configuration	Element No.
GT08	55.717	49.1		43
GT07	56.753	50.0	D4	44
The 1st failure was obtained			↓	
GT10	56.753	56.3	↓	41
GT09	70.470	65.9	E4	42
The 2nd failure was obtained				
GT12	63.162	61.7	↓	39
GT11	76.053	61.7	F4	40
The 3rd failure was obtained				
GT02	59.809	61.7	↓	45
GT01	75.000	64.3	C4	46
The 4th failure was obtained			↓	
GT13	56.753	56.3	↓	36
GT14	70.470	65.9	G4	35
The 5th failure was obtained				

From the numerical simulation, it was concluded that the diagonal members should be modeled as beam-column with joint eccentricities for the correct prediction of both the failure modes and the collapse load level. The two-bolt connections should be regarded as framing connections and the single-bolt connections as pin-ended. A more refined model would also take into account the factor of joint flexibility and bolt slippage. However, it appears that consideration of the foundation flexibility is more important in this case.

6.2.2 Bending Pushover Test

As for the torsion test, a controlled velocity of 2 mm/s was applied to increase the transverse displacement of the cross arm tip in the numerical model used for re-analysis, and the global force-displacement curve shown in Figure 6.5 was obtained from the numerical simulation.

Once again, the comparison with the experimental curve indicates that the initial stiffness of the real prototype is less than that of the numerical model. This is attributed to the flexibility of the foundation and the slippage of the bolted connections. This slippage is more important in bending than in torsion because the splice connections of the main legs are directly affected. The ultimate capacity predicted by the model is only 5% larger than the measured value and the failure modes are identical in the model (Figures 6.6 and 6.7) and the test (Figures 4.26 and 4.27). The failure starts from the bottom section of the tower and this was confirmed by both the numerical simulation and full scale test.

We obtained the following failure sequence from the simulation:

- First yielding: 95.4 kN (reference 1.00)

- First buckling: 122.4 kN (1.28)

- First plastic hinge: 118.8 kN (1.25)

- Ultimate strength (collapse load): 124.20 kN (1.30)

The benefit of the post-elastic strength is evident from these results. This comes at the expense of additional displacement but this is not a major concern as long as the failure mode allows for the tower to remain standing (although much deformed).
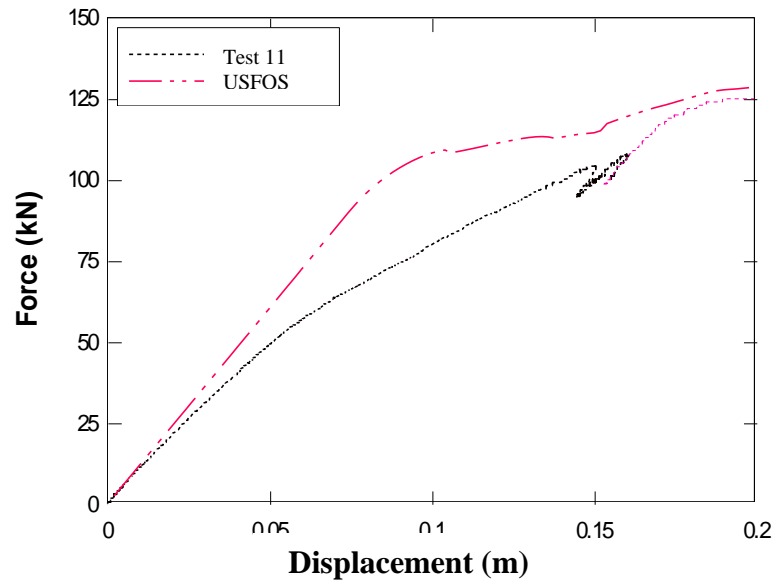
Figure 6.5 Load vs. displacement at tip of cross arm in pushover bending
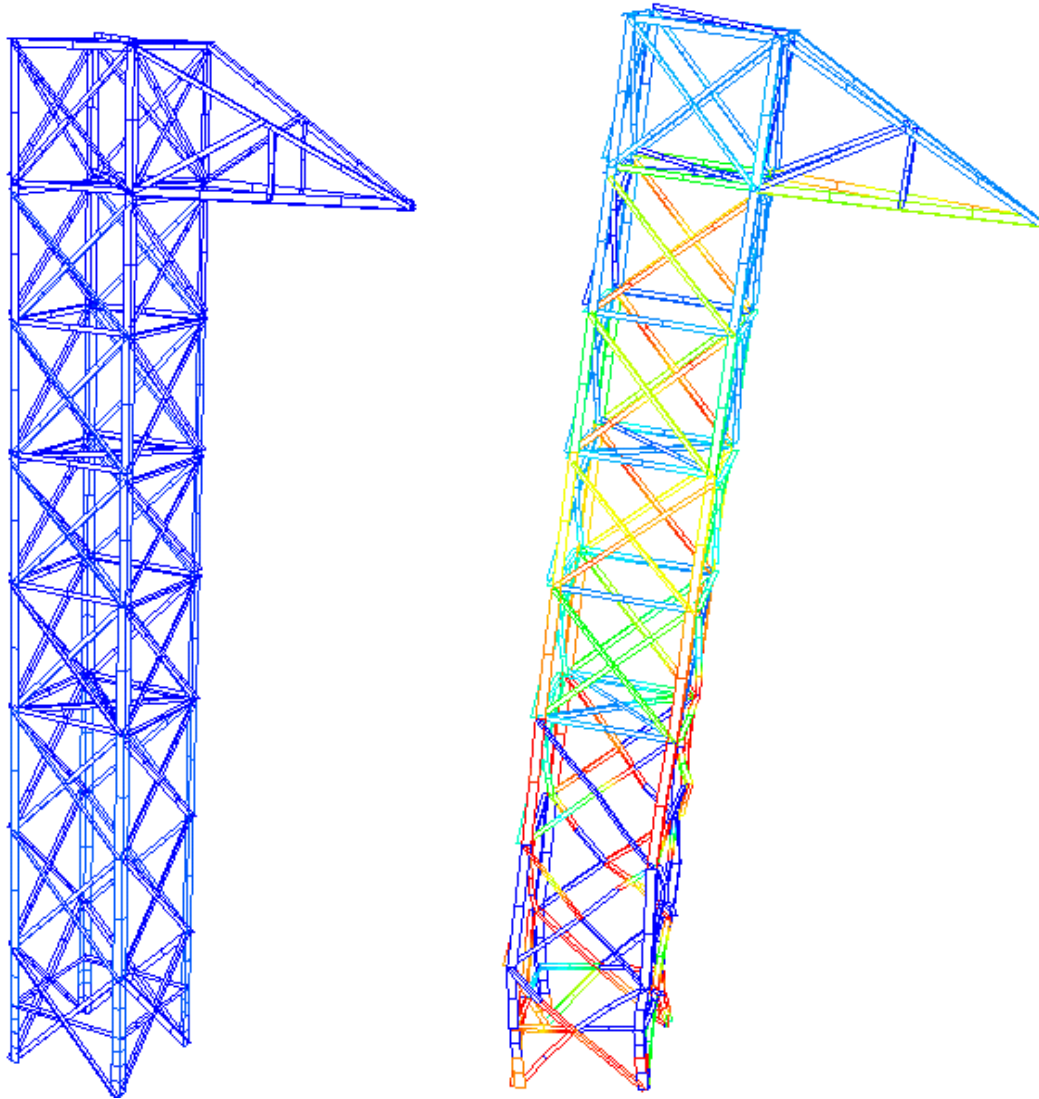
Figure 6.6 Initial and final model configurations for pushover bending
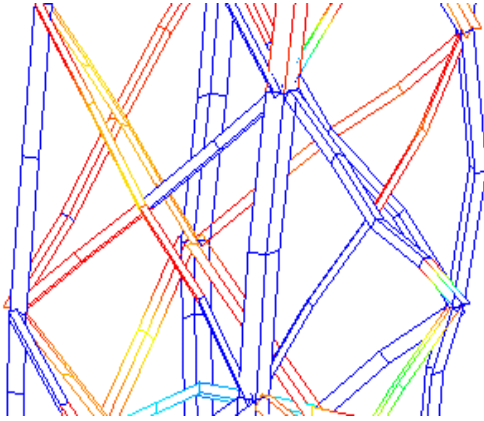
a)   b)
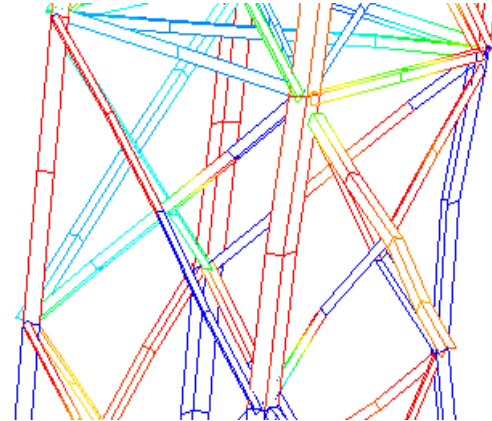
Figure 6.7 Close-up views of tower deformations in bending

Table 6.4 compares the failure sequence and the related load level for the tested

prototype and the numerical model. Element ID numbers are shown in Appendix A.

Table 6.4 Experimental and numerical results in bending pushover

Strain Gauge No.	Element No. (ref. numerical model)	Applied Force at cross arm in test (kN)	Force at cross arm in model (kN)
GB02 GB01	189	115.6	119.7
GB07 GB08	186	106.6	118.8
	1052	106.6	118.8
	4058	106.6	119.7
GB05 GB06	187	108.4	119.7
GB03 GB04	188	108.4	120.6
	2054	108.4	120.6
	3056	108.4	120.6
	107	114.3	124.2
	105	120.0	127.8

6.2.3 Dynamic Torsion Test

Figure 6.8 shows the loading function applied to the tip of the cross arm in the numerical model, which was measured by the load cell in Test 6. Figure 6.9 shows the corresponding displacement calculated (in USFOS) during the first pulse of the excitation (between time t = 0.5 s and 1.5 s) and the value measured during the test. As explained for the static test, the displacement measured is much larger than the model prediction, owing essentially to the slippage in the main leg connections and the elastic movement of the foundation. It is seen that the differences in displacements between the two sets of results build up gradually as the load increases and remain constant after the peak response.
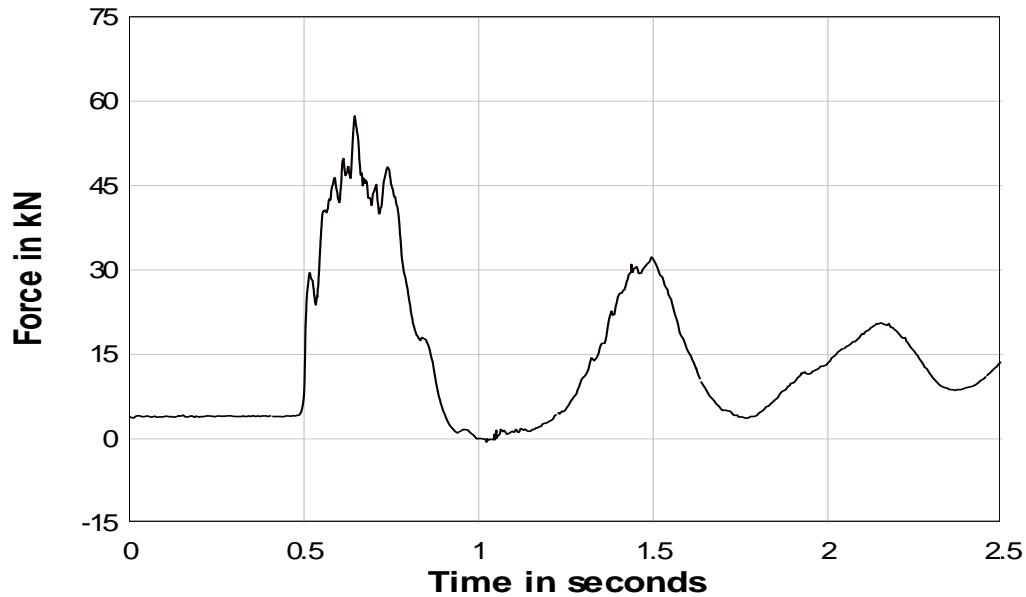
Figure 6.8 Loading time history at tip of cross arm in dynamic torsion
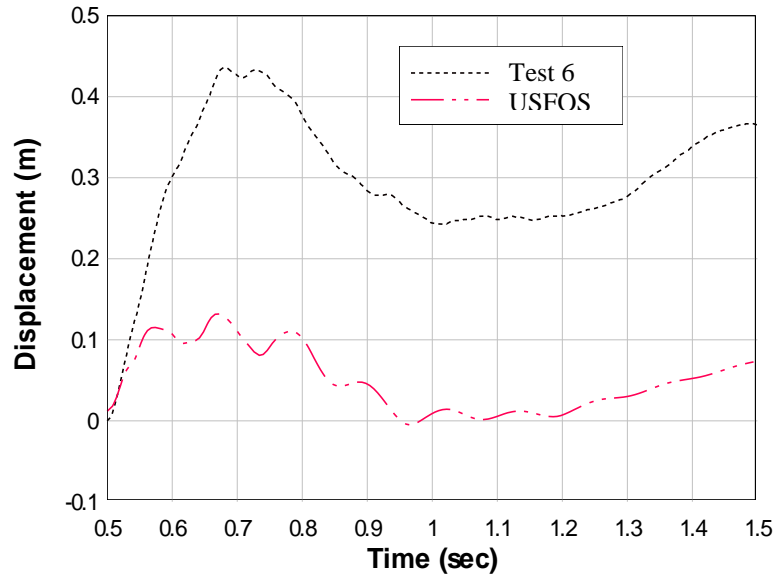
Figure 6.9 Longitudinal displacement time histories at tip of cross arm

It was noted in Chapter 4 that the structure did not collapse under this loading case. As such, this test does not represent the maximum dynamic capacity of the tower which could still sustain more loads. In Chapter 5, we have shown that the numerical model can be used to search for this ultimate capacity. The selection of a larger drop height in Test 6 would have imparted more input energy to the system: in retrospect, the efficiency coefficient we had selected (η = 0.30) was overly conservative. Nonetheless, the numerical model can replicate the failure sequence and maximum load observed in the test.

From the numerical model, we have the following sequence of damage:

- First yielding: 43.0 kN (reference 1.00)

- First buckling: 45.0 kN (1.05)

- First plastic hinge: 55.0 kN (1.28)

- Maximum load (without collapse): 57.5 kN (1.34)

Tables 6.5 and 6.6 present the failure sequence and the related load level for the numerical model and the tested prototype, respectively.

Table 6.5 Numerical simulation results in dynamic torsion

Gauge No.	Element No.	Time (s)	Force at cross arm (kN)	Reference to first yield
GT08	43	0.570	43	1.00
GT07	44	0.656	56	1.30
GT10	41	0.560	43	1.00
GT09	42	0.560	43	1.00
GT12	39	0.564	45	1.05
GT11	40	0.654	55	1.28

Table 6.6 Experimental results in dynamic torsion

Strain Gauge No.	Time (s)	Force at cross arm (kN)	Failure Sequence	Reference to first yield
GT08	0.5992	42.6		1.00
GT07	0.6164	47.8	D4	1.12
GT10	0.6016	42.0		0.99
GT09	0.6220	47.2	E4	1.11
GT12	0.6236	47.1		1.11
GT11	0.6284	47.8	F4	1.12
GT14	0.6664	46.5		1.10
GT33	0.6716	45.9	C4	1.08

As for connection slippage, friction damping in the joints varies with the amplitude of loading and displacements. When the loading is large enough so that most of the possible joint slippage has occurred, this form of friction damping is exhausted. At present, there is no practical way to model this type of friction effect in the dynamic regime, although it

is possible to model static nonlinear slippage at joints using prescribed load-slippage link elements. At low load level, we may consider that structural damping in such a bolted lattice structure is of the order of 3% to 5% as far as there is no joint slippage. Once the load increases enough to cause some slippage in the joints, the effective damping ratio increases. Finally, when all the slippage has occurred, the damping ratio returns to the level of 3% to 5%. It is not possible to predict the damping ratio in the intermediate loading range and we ignored this effect in our numerical analysis.

Figure 6.10 illustrates the residual displacements measured at the top of the prototype after the application and the release of various load levels. The figure indicates the initial displacement after the erection of the prototype and subsequent pre-loading at 5 kN. The other measurements correspond to the residual after the dynamic and static pushover tests, respectively.
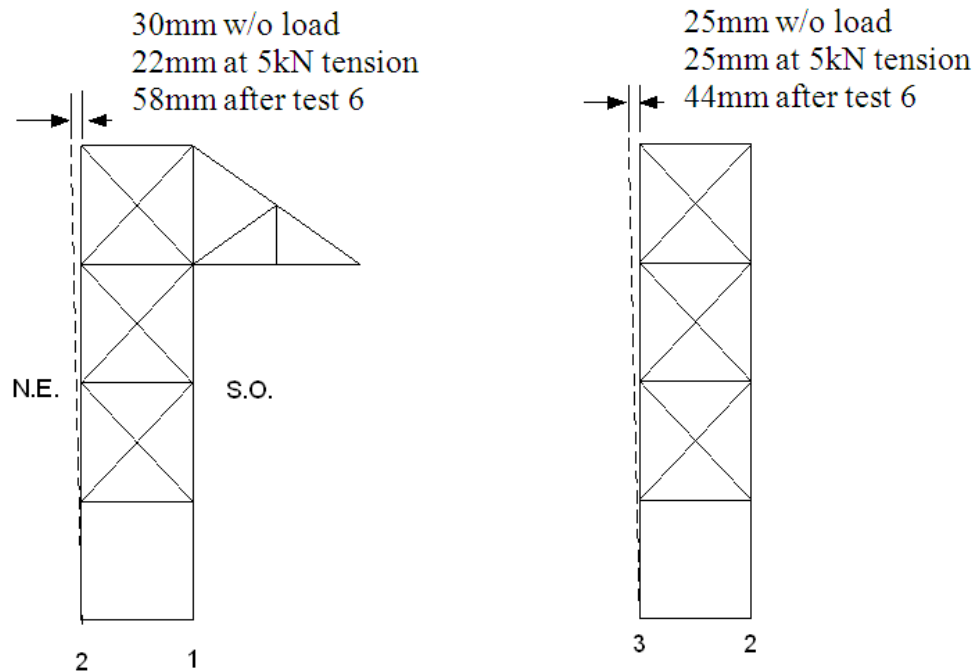
Figure 6.10 Residual displacements after torsion loading tests

6.2.4 Dynamic Bending Test

The force time history measured from the load cell (Figure 6.11) was used as the external load input to the cross arm tip of the tower in the numerical model.
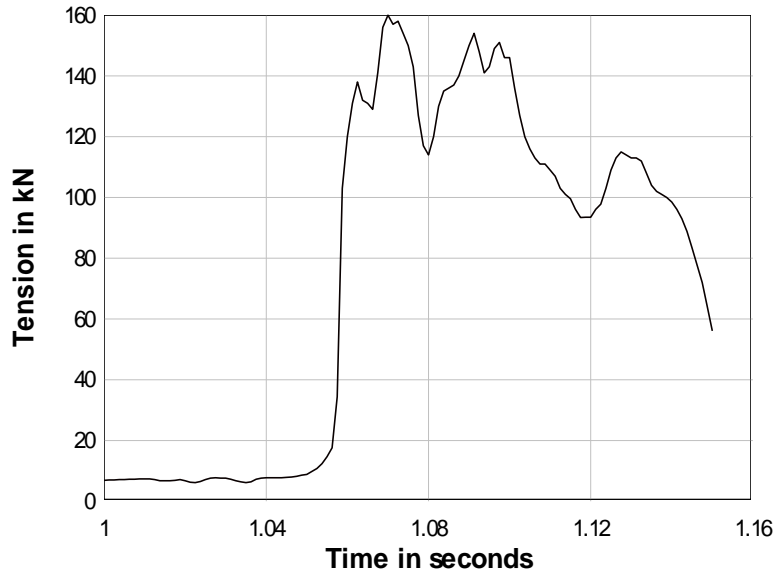
Figure 6.11 Loading time history at tip of cross arm in dynamic bending

Under this dynamic pulse loading case, much attention had to be paid to the selection of an appropriate integration time step. As was observed in Test 12, the loading rate is very high - the average is 40,000kN/s and the highest is 63,000kN/s. For instance, for a loading rate of 63,000 kN/s, a time increment of 0.1 ms increases the load by 6.3 kN in one single step, which might result in a large deformation if the structure is in its post-elastic range of response.

Another observation from the test is that the peak displacement was lagging 50 to 100 ms behind the peak value of the maximum force measured at the loading point. Since the impulse was very severe, after t = 0.130 s on Figure 6.12, the numerical model

experienced the rupture of several members almost simultaneously and it was no longer possible to get a converged solution and the analysis stopped. This is because the finite element model created cannot capture the effects of these high strain rates and the fast propagation of the failure shock in the members of the tower; a much finer mesh would be necessary to replicate these effects. However, it is not necessary to predict this post-failure response very precisely since the tower has already collapsed, and the numerical model can predict the force response before the collapse of the tower and up to its ultimate capacity. The failure sequences and the modes are well predicted and validated by the full scale test.
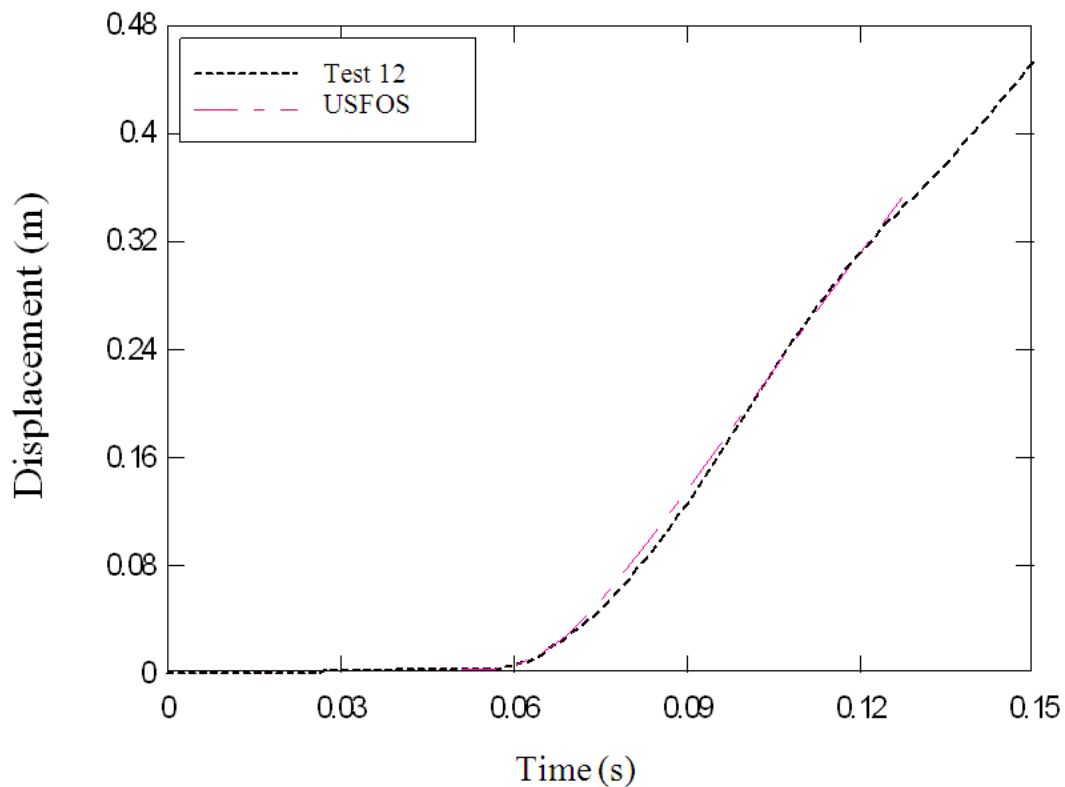
Figure 6.12 Cross arm transverse displacement during the initial loading phase of the dynamic bending test
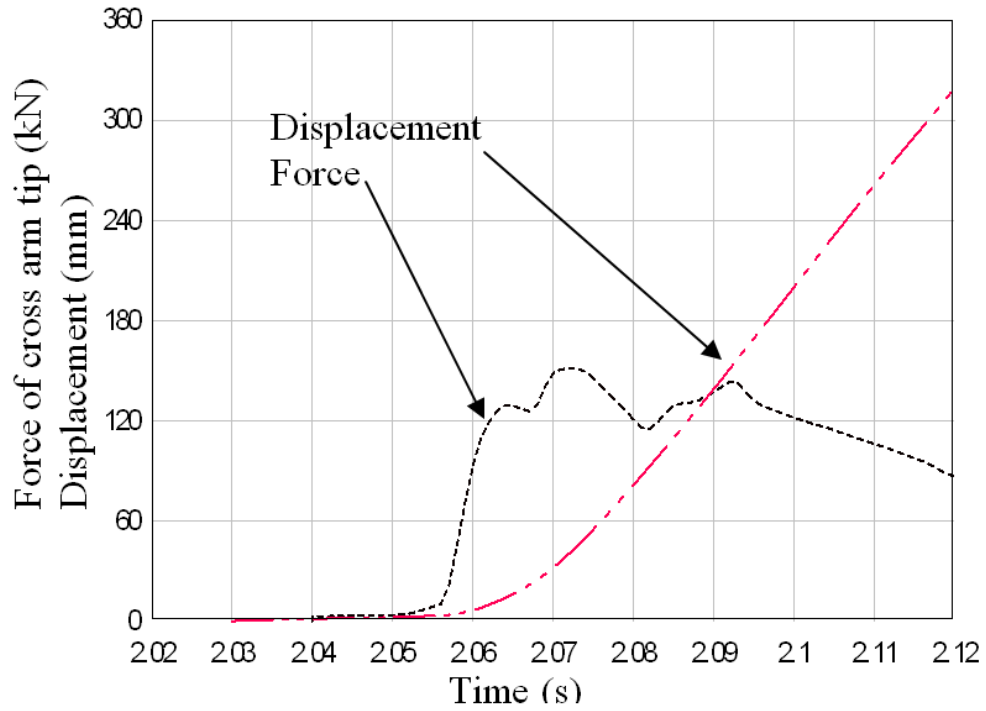
Figure 6.13 Time history of applied load and displacement at tip of cross arm in

numerical simulation

Figure 6.13 shows that the displacement was increased monotonically to collapse and the force reached its peak very quickly and then decreased. Figure 6.14(a) shows the final deformed structure, with the detailed views of lower damaged sections in (b) and (c). Referring to Figures 4.30 and 4.31, it can be seen that the simulation can predict the failure modes both in global and local levels.

154
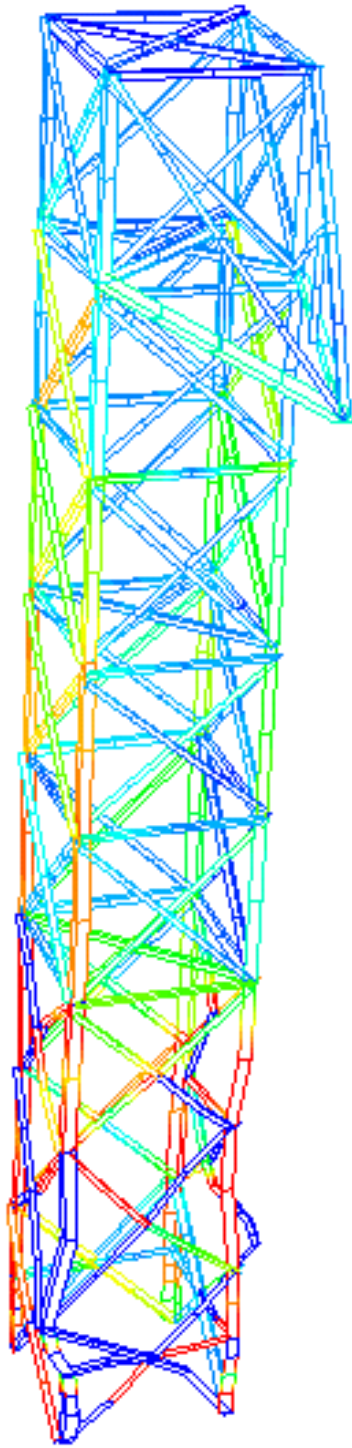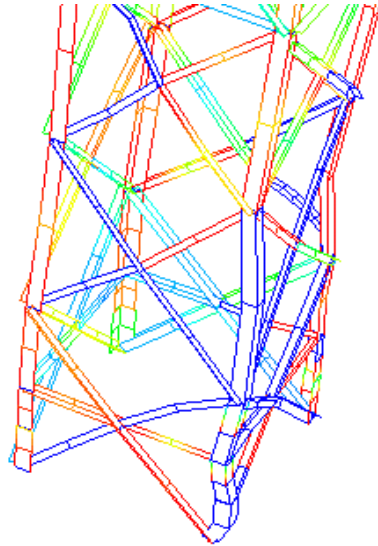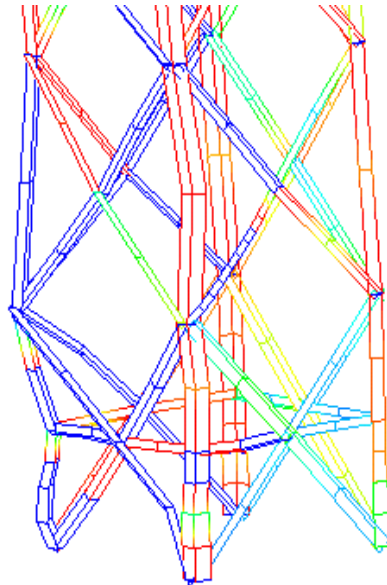
Figure 6.14 Calculated deformed shapes in dynamic bending

It is difficult to explain the dynamic results because of the delay between the tower response and the applied loading pulse; this is observed in both the physical test and the numerical simulation. According to the model, the first yield starts at time 0.082 s, which is lagging 10 ms behind the peak force reached at t = 0.0732 s. The overall dynamic failure modes are very similar in both the dynamic and static tests, but additional diagonal member failures were observed which were not obtained from the static loading. This was also confirmed by our numerical simulations.

Comparing the maximum dynamic load, 160 kN, to the collapse load of 133.5 kN in the static bending pushover, a factor of 1.20 is obtained. For mild steel, considering the widely used Cowper-Symonds equation of strain rate effects on stresses (Alves 2000), there might have an increase in dynamic stress by a factor of

$$\frac{\sigma_{0d}}{\sigma_{0s}} = 1 + \left(\frac{\dot{\varepsilon}}{C}\right)^{1/q} \quad \text{(C=550.43 S}^{-1}\text{ and q=3.439)} \tag{6.1}$$

Substituting the measured strain rate of 0.14 s^{-1} in (6.1), the increased dynamic stress is 1.09 times the static stress. The element ID numbers used in Table 6.7 and 6.8 are shown in Appendix A.

Table 6.7 Numerical simulation of dynamic bending

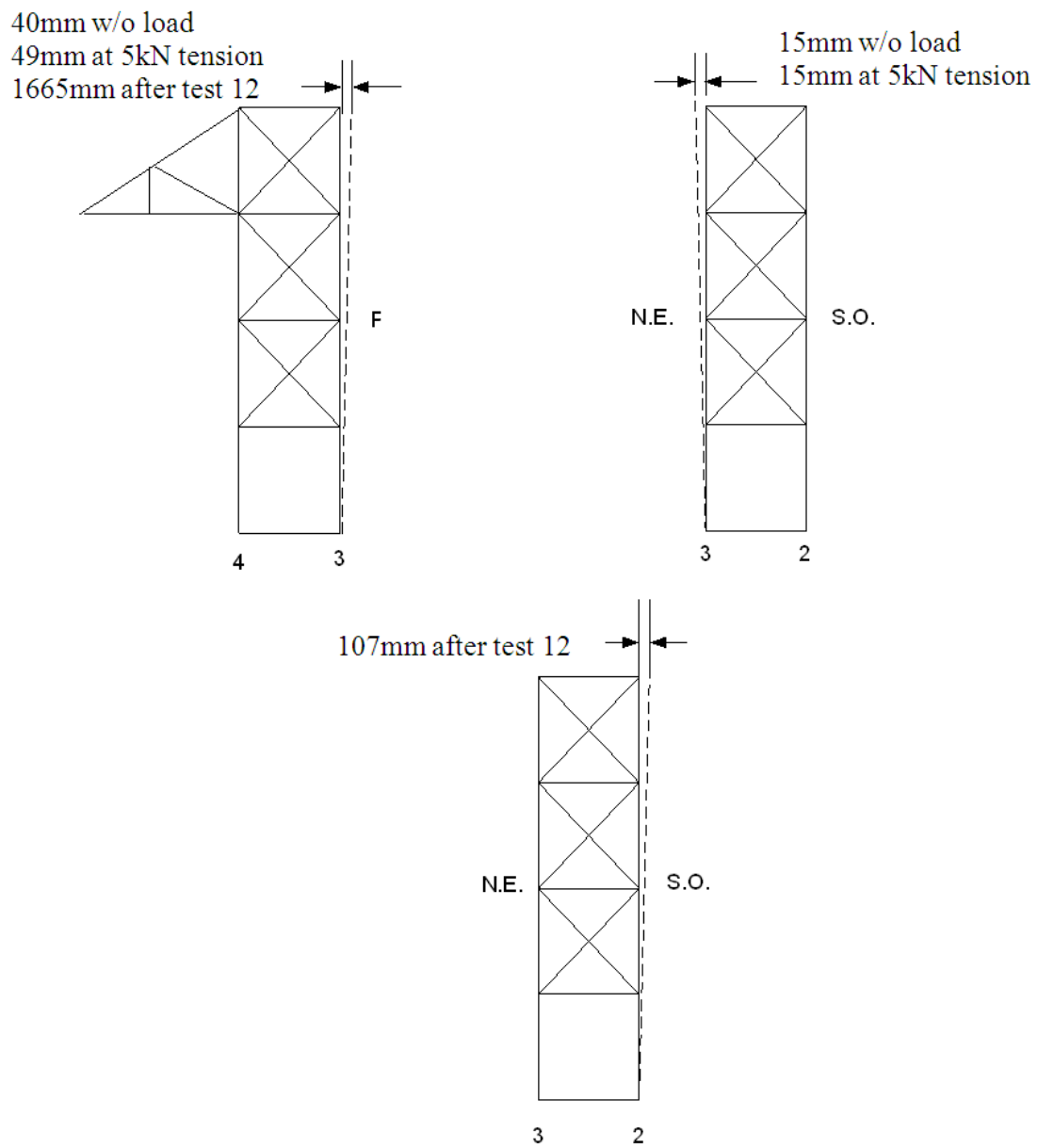| Element No.	Time (s)	Applied load at cross arm (kN)
107	0.083	119.3
106	0.084	129.0
105	0.088	137.5
336	0.089	136.8
108	0.088	129.1
185	0.094	127.1

Table 6.8 Experimental results of dynamic bending

Strain Gauge No.	Element No.	Time (s)	Applied load at cross arm (kN)	Failure Sequence	
GB03	188	0.083	**119.3**		
	106	0.085	**129.0**		
	105	0.090	**137.5**		
No Strain gage	336	0.094	**136.8**		localized failure
	4058	0.096	**129.1**		
	108	0.097	**127.1**		
	112	0.103	**117.3**		
No Strain gage	335	0.104	**115.9**		Rupture of connection
	185	0.105	**114.2**		
	401	0.106	**112.5**		

Residual displacements after the test

Similarly to Figure 6.10, Figure 6.15 illustrates the residual displacements measured at the top of the prototype after the application and the release of various load levels for the bending test. The figure indicates the initial displacement after the erection of the prototype and subsequent pre-loading at 5 kN. The other measurements correspond to the residual after the dynamic and static pushover tests, respectively.

Figure 6.16 shows the foundation movement during the dynamic test and Figures 6.17 to Figure 6.20 show the strain distribution along one main angle member in compression which illustrates the stress wave effects in the dynamic test.

40mm w/o load
49mm at 5kN tension
1665mm after test 12

F

4   3

15mm w/o load
15mm at 5kN tension

N.E.   S.O.

3   2

107mm after test 12

N.E.   S.O.

3   2

Figure 6.15 Residual displacements after dynamic bending loading tests
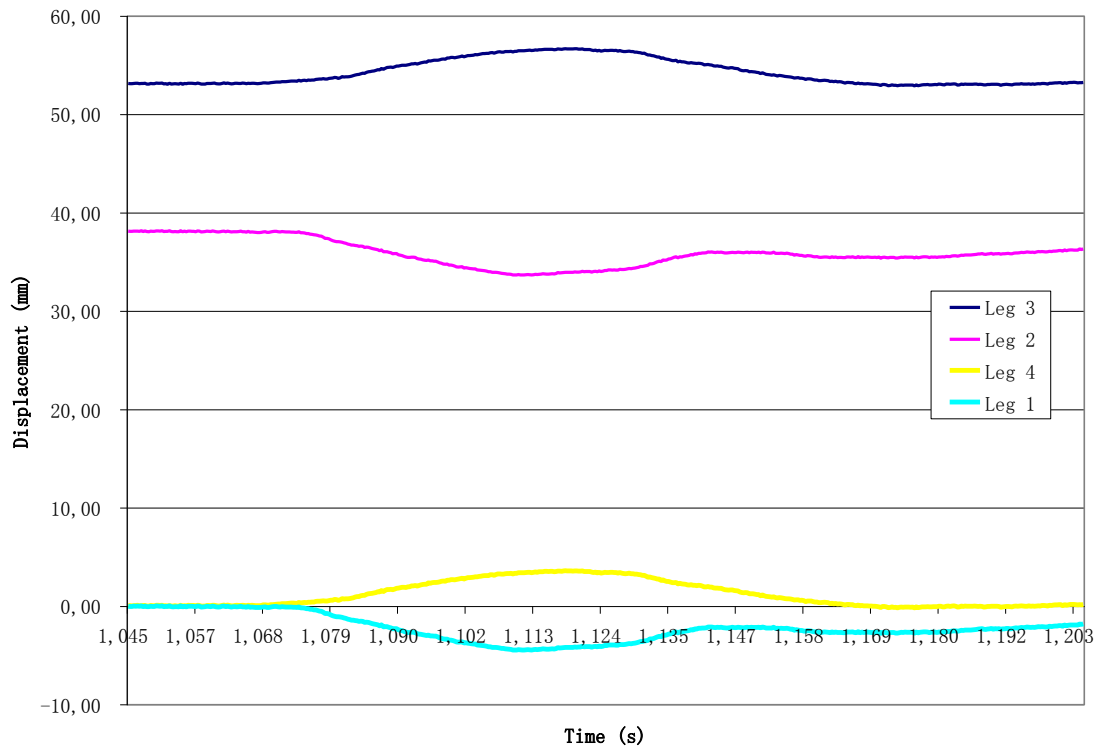
Figure 6.16 Foundation displacements during dynamic bending test
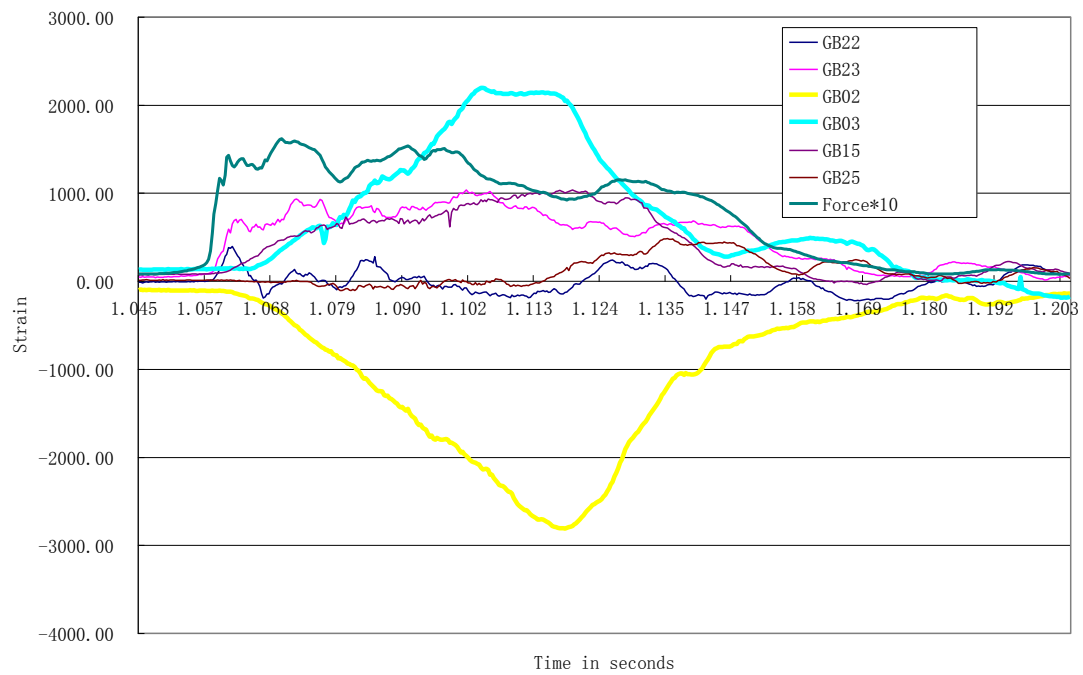
Figure 6.17 Strain in leg members under bending pulse loading

159
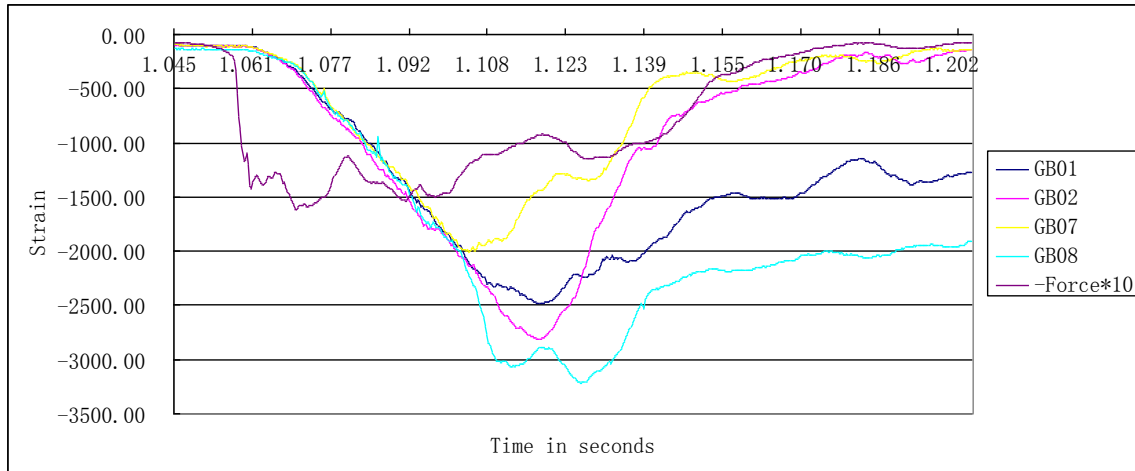
Figure 6.18 Main leg strains on compression side
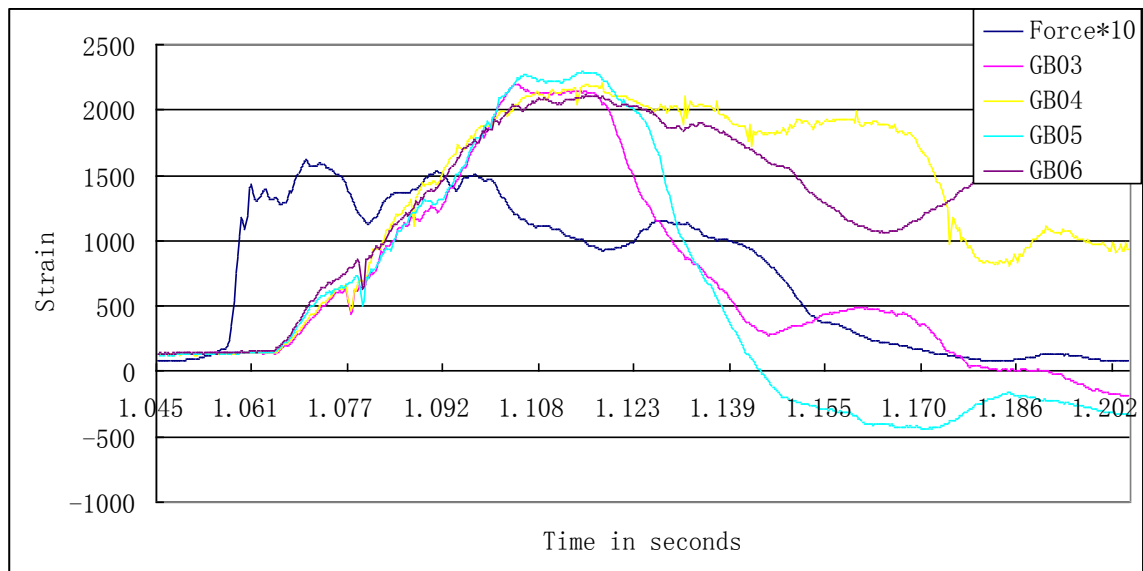
Figure 6.19 Main leg strains on tensile side
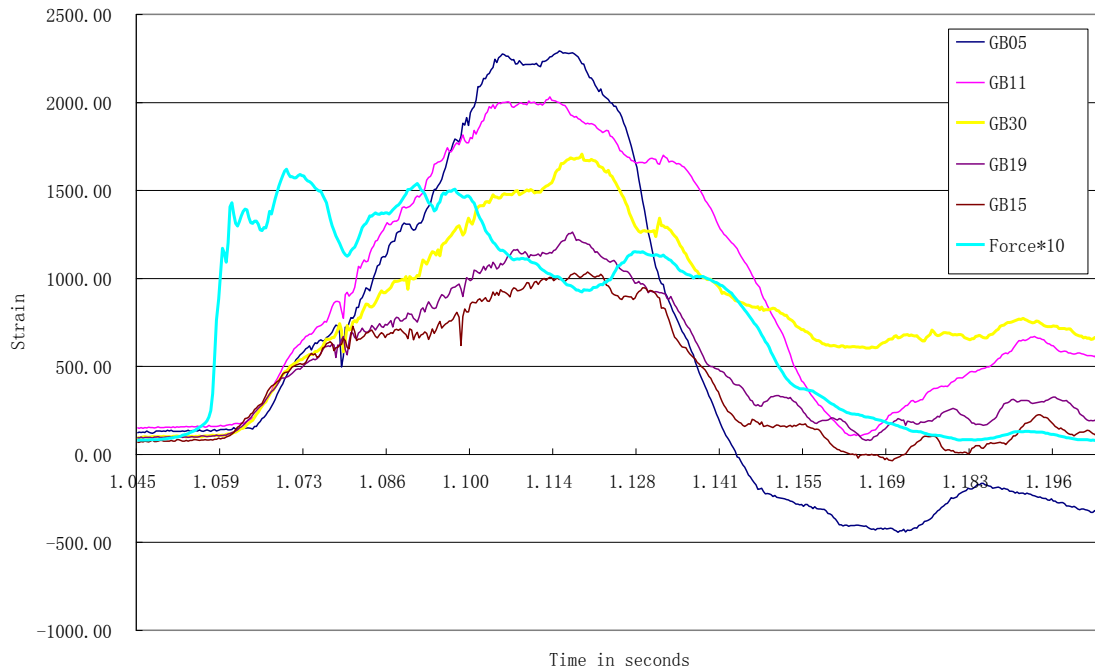
Figure 6.20 Vertical stress wave propagation along main leg 3 (Test 12)
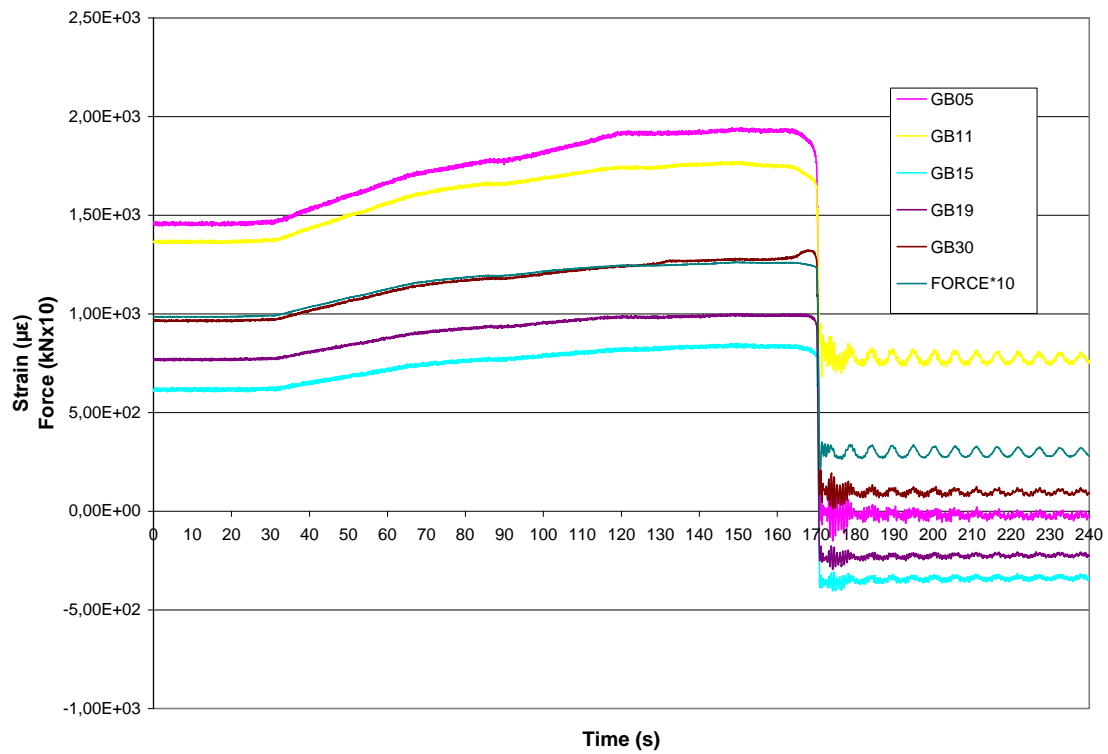
Figure 6.21 Strain measurements along main leg 3 (Test 11)

161

Comparing Figure 6.20 with Figure 6.21, we can observe that the stress pattern in the dynamic response is quite different than the static or quasi-static distribution obtained in the static pushover bending test. Under static loading, all the strains in those members are increased at the same pace and proportion with the external loading, very minor differences are observed, which can be ignored. But in the high rate dynamic loading case, at the initial stage, the strains in all the gauges are almost same, then the stress levels vary very fast immediately after the maximum load is reached and the structure has begun to collapse: the closest member to the collapse location takes more stresses than that away from the collapse location. We believe that there is a stress wave propagating in this main leg member.

6.3 Discussion

### 6.3.1 Post-elastic Reserve Strength

Whereas in traditional elastic design, redistribution of loads is not normally considered, collapse or plastic limit state design allows for local failure in yielding or buckling and even partial (localized) collapse, provided the overall integrity of the structure is maintained. By utilizing the inherent redundancy found in most latticed transmission structures, the progressive collapse limit state can be used to assess and mitigate the risk of accidental damage under extreme loads. Considerable post-elastic reserve strength is available in these structures provided that premature connection failures are prevented. Under the idealized conditions of the numerical simulation, we can get as much as 50% higher capacity compared with the elastic limit. As for the full scale test, we observed some increase of 20 to 40% depending on the loading scenario. The numerical modelling methodology applied in this research can be extended to other examples to estimate this

reserve strength and the nature of the failure modes governing the design, with the objective of eliminating unsafe failure modes that can lead to progressive tower collapses.

6.3.2 Static vs. Dynamic Response at Failure

For the failure modes, we can conclude that in the torsion loading case with reasonably low loading rate, the failure modes are the same in both the static and dynamic regime: this is verifies in both the tests and the numerical simulations. However, the dynamic load observed at failure in the test cannot be considered as the dynamic collapse load: the maximum dynamic load that the tower can sustain depends on the energy content of the input and not solely on the amplitude of the load per se.

In the impulse bending test, the loading rate of 60,000kN/s is regarded as very high from a structural engineering viewpoint, and the resulting strain rate in the steel tower members is approximately 0.14/s. We believe there is a significant rate effect on the strength in this case, but this is not representative of the dynamic accidental loads likely to solicit a tower. Further research is needed to verify this conclusion. Another phenomenon of interest is the stress wave propagation which might cause the local failures observed in the dynamic bending experiment.

6.3.3 Reliability and Performance of Numerical Models

In this research, USFOS is proved to be a very efficient tool for post-elastic analysis of lattice transmission towers. First of all, using post-elastic analysis was very useful to obtain the basic experimental parameters to plan the full scale static and dynamic tests. Without those preliminary simulations, we would not have been able to monitor the

appropriate member and forces as required, which might have lead to a waste of effort and money. The detailed analysis has the additional advantage of providing response indicators at any degree of freedom of the model, and as such it was used also to complement the analysis of the experimental results. Second, by using such software, design engineers can document the reserve strength of a structure and identify its failure modes. Good control of the tower failure modes is paramount to efficient line design. Furthermore, re-analysis of existing designs may help in assessing the overall vulnerability of lines to progressive collapse.

Since full-scale experiments are costly, we recommend that additional verifications of the software be done using destructive test results available from the usual prototype verification tests. Such verifications are under way at McGill University in a collaborative project with Chinese researchers. With the advances in computational technology, especially with high-performance laptop computers, the numerical simulation of the post-elastic response of a full transmission tower under several loading scenarios is feasible in only a few hours and the results can be very reliable with careful model preparation.

Chapter 7 Conclusion

Summary of main observations

The first part of this research was to adapt USFOS, a post-elastic structural analysis software originally developed for offshore platform structures, to transmission tower and line applications. After successful validation of the modeling approach, especially with the introduction of connection eccentricities, with both static an dynamic analysis examples, four detailed models of a prototype tower section were developed to design and plan full scale destructive tests.

Four full-scale prototypes were tested under four loading conditions: 1) static pushover flexure-torsion; 2) static pushover bending; 3) dynamic pulse in flexure-torsion; and 4) dynamic pulse in bending. The static test results and the numerical modeling results were in agreement, in terms of failure modes, member stresses and maximum load at collapse. However, the numerical models cannot predict the displacement response with accuracy because connection slippage occurring in the lap splice bolted joints of the tower legs are not accounted for. No model exists in USFOS at the moment to include this effect since joint models for offshore platforms involve welded details for tubular members. This joint slippage effect may also cause variations in structural damping under dynamic loads. Another important contribution to the discrepancies in displacement predictions relates to the prediction of the rigid body displacements of the tested prototypes subjected to foundation displacements. The correction was not made to the numerical models because the main focus of the research was the prediction of the strength reserve in the

post-elastic regime and the characterization of the failure modes, and none of these is significantly affected by such displacements. Furthermore, transmission towers do not have very stringent serviceability criteria in terms of displacements, which do not affect their good performance.

The detailed stress analysis of some individual angle sections has confirmed the need to consider the connection eccentricities in angle shapes, especially for diagonal members connected only on one leg. Some local failures in diagonal members, in particular, confirmed that connections are vulnerable (small end distances; loading eccentricities) and they could be obstacles for existing towers to develop their full post-elastic strength reserves in case of overloading.

The powerful graphical interface of the software (as pre-processor and post-processor) was appreciated to display animated failure sequences and time responses, giving the user a good sense of the real response of structure.

Planning of the physical tests at the Hydro-Québec experimental line of the research institute in Varennes, Québec, was very challenging as the test facilities had never been used for such tests in the past. Decisions on the dynamic testing parameters were difficult to make because of the novelty of the tests. Dynamic response monitoring with normal video cameras was not sufficient, and high speed cameras were used for displacement measurements on several targets. The dynamic impact tests were essentially load-controlled (impact due to dropping a large mass), therefore, it was not possible to predict

166

the displacements as measured during the tests. In such impulse loading conditions, the displacements are usually delayed with respect to the load and stress wave propagation takes place which may affect the local damage inflicted to the tower members.

Conclusions

In the interest of transmission tower design, the main conclusions are as follows:

- It is possible to use post-elastic analysis to accurately predict the reserve strength of bolted lattice towers provided connection eccentricities are properly modeled at peaks or cross arms loading points and in diagonals connected only on one leg.

- Consideration of the tower post-elastic capacity is necessary for realistic assessment of tower vulnerability to extreme loads.

- Accurate pushover post-elastic analysis is an essential design tool to ensure that the tower capacity is adequate and that failure modes are safe, i.e. not leading to progressive collapse. With appropriate training, such analysis is feasible in a design office.

- In the tower prototypes tested in this research, the post-elastic reserve strength was 1.22 for flexure-torsion (i.e. tower under longitudinal loading) governed by diagonals, and 1.37 for bending (i.e. tower in transverse loading) governed by inelastic buckling of the main legs.

- Observations from physical tests, confirmed by numerical simulations, suggest that failure modes under pushover static and dynamic pulse loading are similar.

- Some rate effects may exist - we observed a "strength gain" of approximately 9% for a strain rate of 0.14 s^{-1}. However, these gains may not be significant at the

167

lower strain rates corresponding to dynamic loads likely to affect transmission towers, and we recommend that they be ignored in the evaluation of the tower strength.

- Diagonal members affect the failure modes of transmission towers and their connection design may be a weak link in the development of their post-elastic capacity. Diagonal members connected on one leg only are subject to biaxial bending, they cannot develop the full strength of their cross section since the unconnected leg takes much less stress on its entire length.

References

ADINA (Automatic dynamic incremental nonlinear analysis). 2003. Version 8.0. ADINA R&D, Inc. Watertown, MA.

Abdel-Rahim, A.B. and Polyzois D. 1996. Effect of temperature and galvanization on cold-formed steel, Journal of materials in civil engineering August 1996 114-122.

Adluri, S.M.R. and Madugula, M.K.S., 1996a. Flexural buckling of steel angles – experimental investigation, Journal of structural engineering, ASCE, 122(3) 309-317.

Adluri, S.M.R. and Madugula, M.K.S., 1996b. Development of column curves for steel angels, Journal of structural engineering, ASCE, 122(3) 318-325.

Albermani, F.G.A. and Kitipornchai, S. 1992. Nonlinear analysis of transmission towers. Engineering Structures, 14(3), 139-151.

Albermani, F.G.A. and Kitipornchai, S. 1997. Predicting the ultimate structural behavior of transmission towers, Steel Construction, 24(4), 2-19.

Albermani, F.G.A. and Kitipornchai, S. 2003. Numerical simulation of structural behavior of transmission towers, Thin-walled structures, 41, 167-177.

Al-Mashary, F. and Chen, W.F. 1990. "Elastic second-order analysis for frame design." Journal of Construction Steel Research, 15, 303-322.

Alves, M. 2000. Material constitutive law for large strains and strain rates, Journal of Engineering Mechanics, 126 (2), 215-219

Andrew, K.K.So. and Chan, S.L. 1991. Buckling and geometrically nonlinear analysis of frames using one element/member, Journal of construction steel research, 20(1991) 271-289.

ASCE Manual 74, American Society of Civil Engineering, USA, 2001. "Guidelines for electrical transmission line structural loading," June 2001 Draft revision, ASCE manuals and reports on engineering practice, ASCE, Reston, VA

ASCE/SEI (2005). Minimum Design Loads for Buildings and Other Structures, ASCE/SEI 7-05.

Bathe, K.J. 1996. Finite Element Procedures, Prentice-Hall, Englewood Cliffs, NJ.

Ben Kahla, N. 1994. Dynamic analysis of guyed towers. Engineering Structures, 16(4), 293-301.

Blandford, G.E. 1997. Review of Progressive failure analysis for truss structures, Journal of structural engineering, 123(2), 122-129.

Bonar, P.P., 1968. "Dynamic Testing of Lattice Steel Masts" International Conference on large high tension electric system, June 10-20, Paris.

Canadian Standards Association, CSA-G40.20-04/G40.21-04, 2004. General requirements   for rolled or welded structural quality steel, Toronto, Ontario.

CENELEC EN-50341-1, 2000. European Committee for Electrotechnical Standardization, Overhead electrical lines exceeding AC 45 kV.

Charbonneau, M., Banville, D., Guilbault, P., Lemieux, S., Vincent, P., McClure, G., Zhang, X. and Holmas, T. 2006. Overhead Transmission Lines Evaluation of the post-elastic behavior of line components. *41st General Session of CIGRÉ*, 27 August-1 September, Paris, France. Paper no. B2-303, 8 p.

Commission - 1998 Icestorm, 1999: Facing the unforeseeable, lessons from the icestorm of 1998, Les Publications du Quebec, Quebec, 434.

Computers and Structures, Inc. (CSI). 2003. SAP®2000. Version 8.1.2 Integrated structural analysis and design software, SCI Berkeley, CA.

Earls, C.J. 2001. "Geometric axis compactness criteria for equal leg angles: horizontal leg compression." Journal of Construction Steel Research, 57, 351-373.

EPRI, 1986. Structural development studies at the EPRI transmission line mechanical research facility, Interim report No, 1: EPRI EL-4756. Sverdrup Technology Inc, Tullahoma, TN.

Fung, Y.C. 1965. Foundations of Solid Mechanics, Prentice-Hall, Englewood Cliffs, NJ.

Govers, A. 1970. "On the impact of uni-directional forces on High-Voltage Towers Following conductor breakage" International conference on large electric systems at high tension (CIGRE), Paris

Guilbault, P. 2004. Essais dynamiques post-elasticques sur treillis metalliques, TransÉnergie, Report No. 53024187, December 2004, IREQ, Quebec.

Guilbault, P., Leblanc, J.L., Leveille, J. and Louwet, C. 2003. Essais dynamiques en ligne de transport: Ligne experimentale de St-Luc de Vincennes, TransÉnergie Report No. 53014683, June 18. IREQ, Quebec.

Guilbault, P. and Picard, J. 2000. Essais Mechaniques du chevalet de cable de garde du pylone 735kV type SAE1968 Conception 2000 No. 53005840. Transegergie, 2000.

Guo, L. 2003. Strain rate effects on the dynamic response of steel trusses. Department of Civil Engineering and Applied Mechanics, McGill University, M.Eng. Project Report G03-03. 87p.

Hilbert, H.M., Hughes, T.J.R., Taylor, R., 1977. Improved numerical dissipation for time integration algorithms in structural dynamics, Earthquake engineering and structural dynamics, 5, 283-292.

Hughes, T. 1987. The Finite Element Method, Prentice-Hall, Englewood Cliffs, NJ.

International Electrotechnical Commission (IEC), 2003: Design Criteria of overhead transmission lines, International standard IEC 60826-2003, 3rd Edition, Geneva, Switzerlan.

Kemp, A.R. and Behnke, R.H., 1998. Behavior of Cross-Bracing in Latticed Towers, Journal of Structural Engineering, February, 360-367.

Kempner, L.Jr. 1997. Longitudinal impact loading on electrical transmission line towers: A scale model study, Ph.D. Thesis, Systems Science: Civil Engineering, Portland state university, Portland, Oregon.

Kempner, L.Jr., Mueller, W.H., Kitipornchai, S., Albermani, FGA., Menezes, R.C. and Silva, J.BGF. 2002. Lattice transmission tower analysis: beyond simple truss model. Proceedings of the conference electrical transmission in a new age, ASCE, Sept 9-12, 2002 Omaha, NE, USA, 175-187.

Kenny, S., Taheri, F. and Pegg, N. 2001. "Experimental investigations on the dynamic plastic buckling of a slender beam subject to axial impact." International Journal of Impact Engineering, V27(1), p1-17.

Kitipornchai, S. 1983. Torsional-flexural buckling of angles: A parameter study, Journal of construction steel research, 3(3), 27-31.

Kitipornchai, S. and Lee, H.W. 1986. Inelastic experiment of angle and tie struts Journal of constructional steel research, 6(1), 219-236

Kitipornchai, S., Al-Bermani, F.G.A, and Peurot, A.H. 1994. "Effect of Bolt Slippage on Ultimate Behavior of Lattice Structures." Journal of Structural Engineering, 120(8), 2281-2287.

Kitipornchai, S., Zhu, K., Xiang, Y. and Albermani, F.G.A., 1991. Single-equation yield surface for monosymmetric and asymmetric sections, Engineering Structures, Vol 13, October, 366-370.

Kulak, G.L. and Grondin, G.Y. 2006. Limit states design in structural steel 8th edition. Canadian Institute of Steel Construction, Willowdale, ON, 387p.

Lapointe, M. 2003. Dynamic analysis of a power line subjected to longitudinal loads, Master of Engineering Thesis, Dept. of Civil Engineering and Applied Mechanics, McGill University, Montreal, Quebec.

Lee, P.-S. and McClure, G. 2005. A general 3D L-section beam finite element for elastoplastic large deformation analysis, *Proceedings of the 20th CANCAM Conference*, Montreal, Canada, 30 May-2 June.

Lee, P.-S., and McClure, G. 2006. A general three-dimensional L-section beam finite element for elastoplastic large deformation analysis. *Computers & Structures*, 84: 215-229.

Lee, P.-S., and McClure, G. 2007. Elastoplastic large deformation analysis of a lattice tower structure and comparison with full-scale tests. *International Journal of Constructional Steel Research*. 63(5), 709-717.

Lee, P.-S., Zhang, X.H., and McClure, G. 2005. Development of a general three-dimensional L-section beam finite element for elastoplastic large deformation analysis and its application to the analysis of a transmission tower, *Proceedings of the Third MIT Conference on Computational Fluid and Solid mechanics*, Cambridge, MA, USA, 14-17 June. Abstract only.

Liew, J.Y.R., Chen, W.F. and Chen, H. 2000. Advanced inelastic analysis of frame structures. Journal of construction steel research, 55(2000) 245-265

Madugula and Kennedy 1985: Single and Compound Angle Elsvier applied science publisher, London,

McClure, G. and Lapointe, M. 2003. Modeling the structural dynamic response of overhead transmission lines, Computers and structures 81(2003) 825-834.

McClure, G. 2006. Recent advances in modeling the dynamic response of overhead transmission lines. Chapter 18 *Innovation in Computational Structures Technology, Saxe-Coburg - (Invited presentation): Proceedings of the 8th International Conference on Computational Structures Technology*, 12-15 September, Las Palmas de Gran Canaria, Spain, 371-392.

McClure, G. Lapointe, M., 2003 "Modeling the structural dynamic response of overhead transmission lines" Computers and Structures, 81, 825-834.

McClure, G., Johns, K.C., Knoll, F., and Pichette, G. 2002. Lessons from the ice storm of 1998 Improving the structural features of Hydro-Québec's power grid. *International Workshop on Atmospheric icing of Structures IWAIS 2002*, Brno, Czech Republic, 17-20 June, 7 p.

Mizuno, E. and Liu, Q.Y. 1998. A two-surface model in force space for steel members, Journal of construction steel research, 48, 107-122.

Mozer, J.D. 1978. "longitudinal unbalance loads on transmission line structures." EPRI Project 1096-1, Palp Alto, CA.

Newmark, N.M. 1959. "A method of computation for structural dynamics." Proce. ASCE, 85(EM3), Part 1, 67-94.

Peabody, A.B. 2001. Transmission line longitudinal loads: A review of design philosophy. Structural Engineering Series No. 2001-02, Dept. of Civil Engineering and Applied Mechanics, McGill University, Montreal, Quebec.

PLS-CADD, 2006 Madison, WI, Power Line System.

Ramesh B.Malla, Baihai Wang, and Butchi B.Nalluri 1993. Dynamic effects of progressive member failure on the response of truss structures. Proceedings of the technical sessions on response of truss and truss-type structures during progressive failure and dynamic loading and analysis of structures, Charlottesville, VA, June 6-9, 1993.

Rao, N.P. and Kalyanaraman, V. 2001. "Non-linear behavior of lattice panel of angle towers." Journal of Constructional Steel Research 57 (2001) 1337-1357.

Reilly R.J. and Sutton E.L. 1973. "An iterative solution for geometrically nonlinear truss." Computers and Structures Vol 3 1053-1061.

Robert, V. and Lemelin, D.R. 2002. "Flexural consideration in steel transmission tower design." Proceedings of the conference electrical transmission in a new age, ASCE, Sept 9-12, 2002 Omaha, NE, USA, 149-165.

Roy, S., Fang S.J. and Rossow, E. 1984. "Secondary stresses on transmission tower structures." Journal of energy engineering, ASCE 110(2) 157-172.

Roy, S. and Fang, S.J. 1992. "Designing and testing heavy dead-end towers." Proceedings of conference in electrical transmission, Chicago, Illinois.

Savory, E. 2001. "Modeling of tornado and microburst-induced wind loading and failure of a lattice transmission tower." Engineering structures 23(2001) 365-375.

Sekulovic, M., Salatic R. and Nefovska, M. 2002. Dynamic analysis of steel frames with flexible connections. Computers and structures 80(2002) 935-955.

Do, T.T., Miller, M.D., Kempner L.Jr., Lyver T.D. and Mueller III W.H., 1993. Collapse load calculation by probability based analysis compared to full scale tower test results, Proceedings of the technical sessions on response of truss and truss-type structures during progressive failure and dynamic loading and analysis of structures, Charlottesville, VA, June 6-9.

Urbano, C.A. 2001. "Steel transmission towers: some current topics." progress in structural engineering and materials, 3(1), 36-47.

USFOS, 2001. A computer program for progressive collapse analysis of steel offshore structures, version 7-8, SINTEF, Trondheim, Norway.

USFOS, 1994. Theory manual TF71 F88038.Trondheim, Norway.

Vincent, P., Huet, C., Charbonneau, M., Guilbault, P., Lapointe, M. and McClure, G. 2004. Testing and numerical simulation of overhead transmission lines dynamics under component failure conditions. *40th General Session of CIGRÉ*, Paris, France, 29 August- 3 Sept., Paper No. B2-308.

White D. 1993. Plastic-hinge methods for advanced analysis of steel frames, Journal of construction steel research, 24(1993) 121-152.
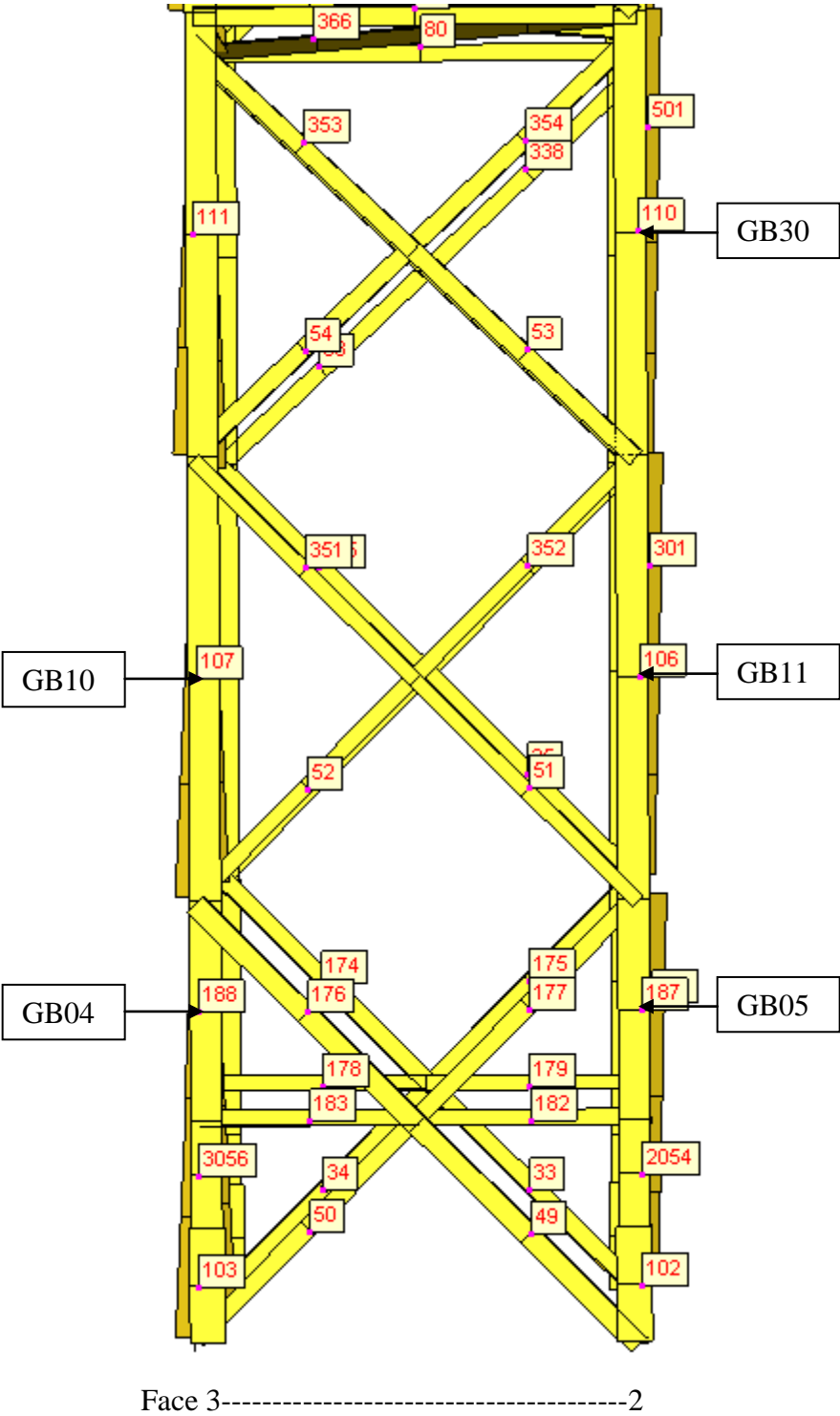
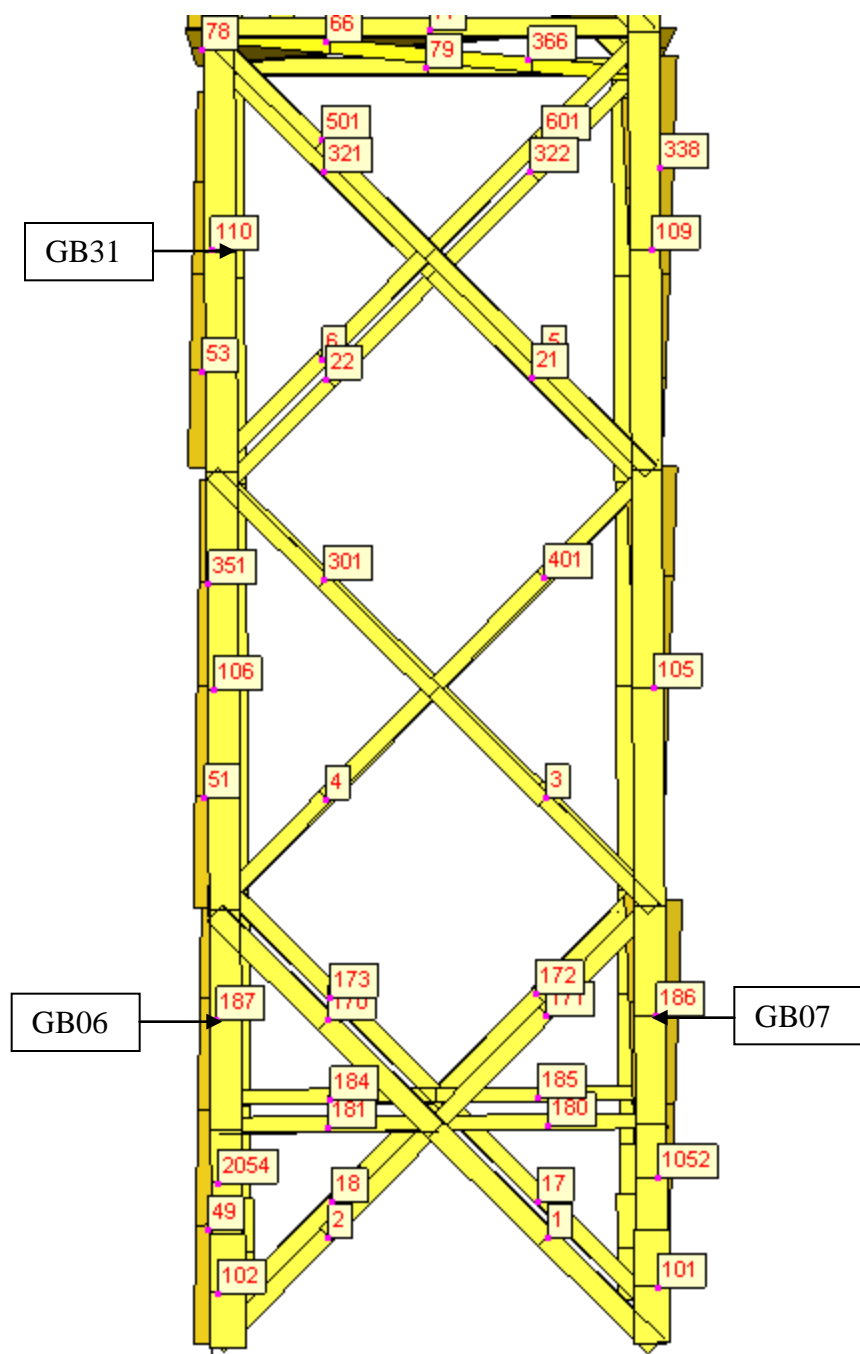# Appendix A: Element numbering in numerical model

Also the associated strain gauge numbering in experiments are shown
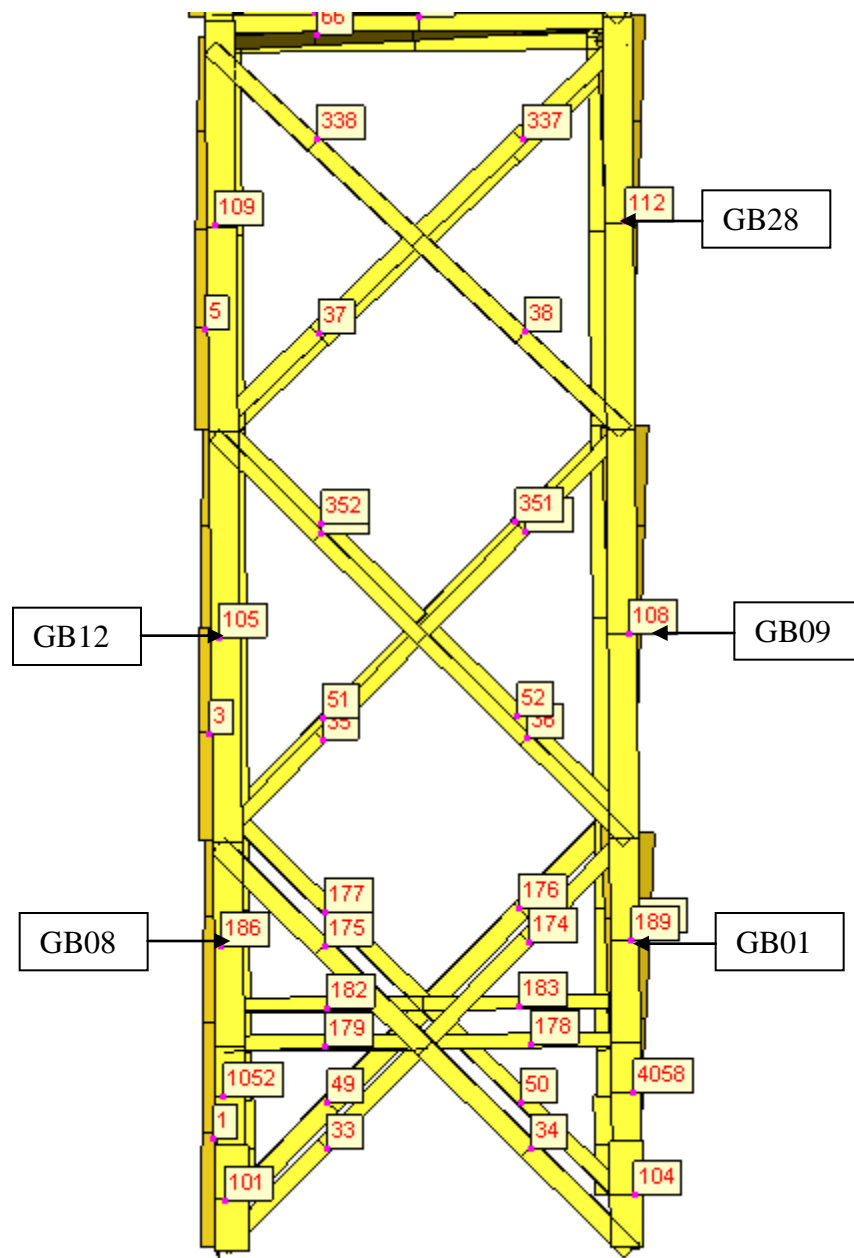
Element numbering for cross arm:
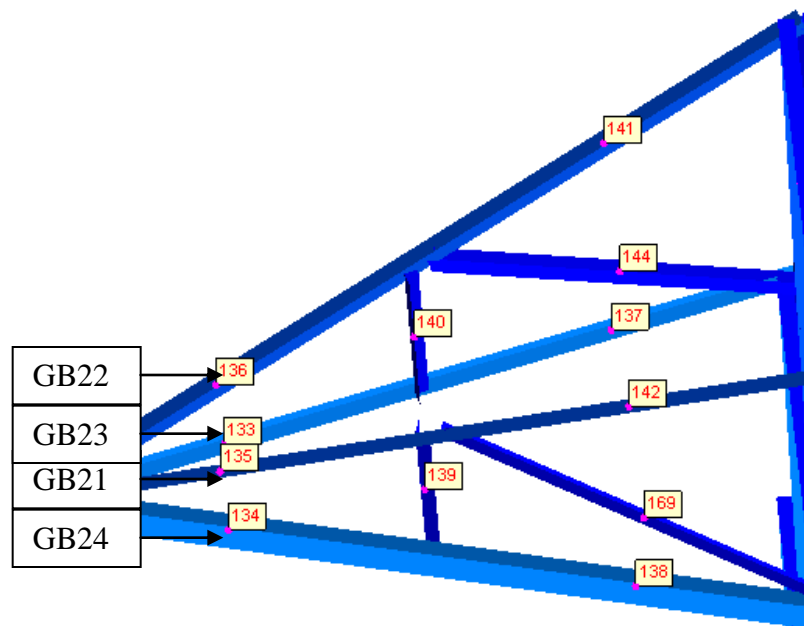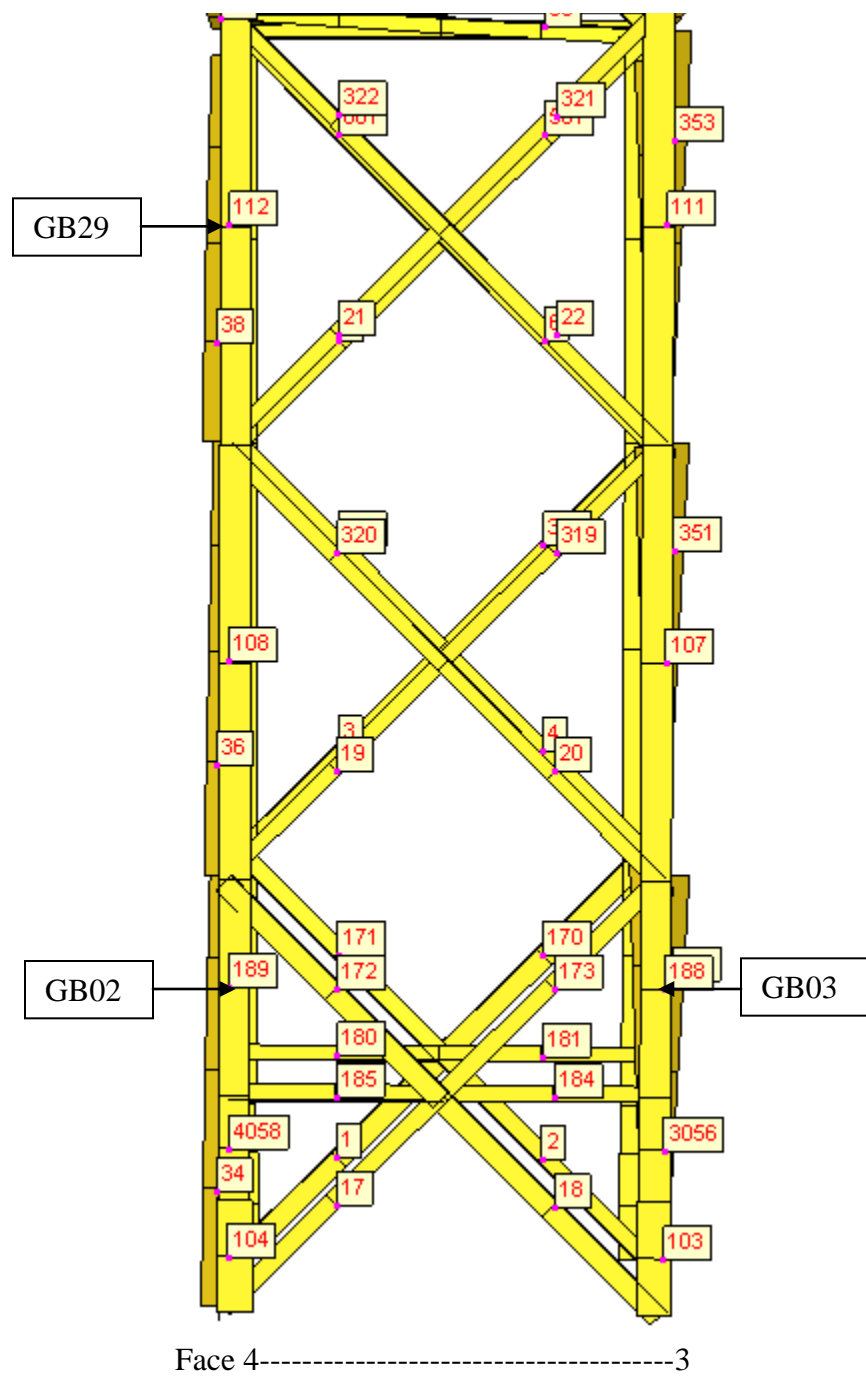
Element numbering for main leg members:

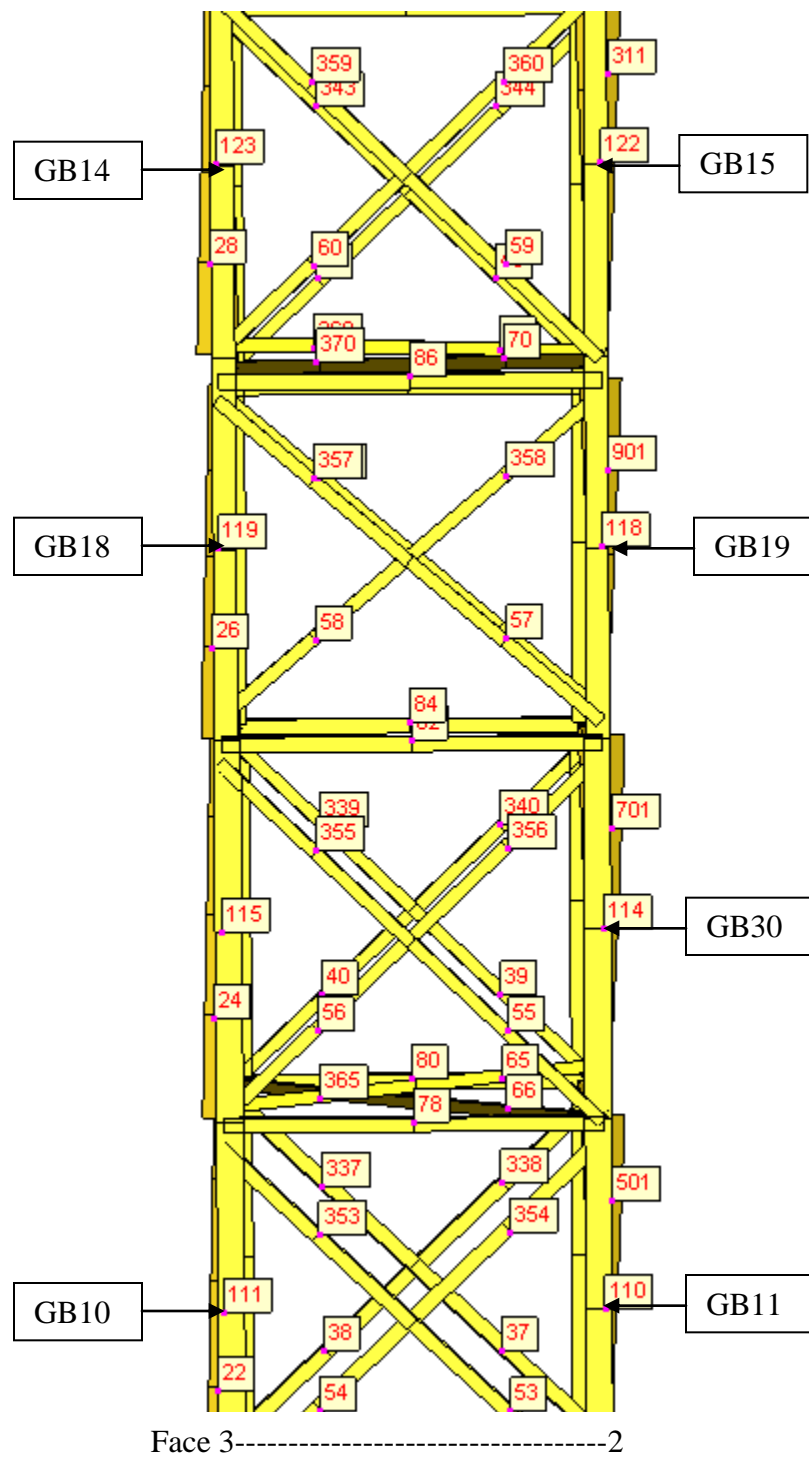Face 3---2

Face 2--1

Face 1--------------------------------4

Face 4---------------------------------------3

Face 3------------------------------------2
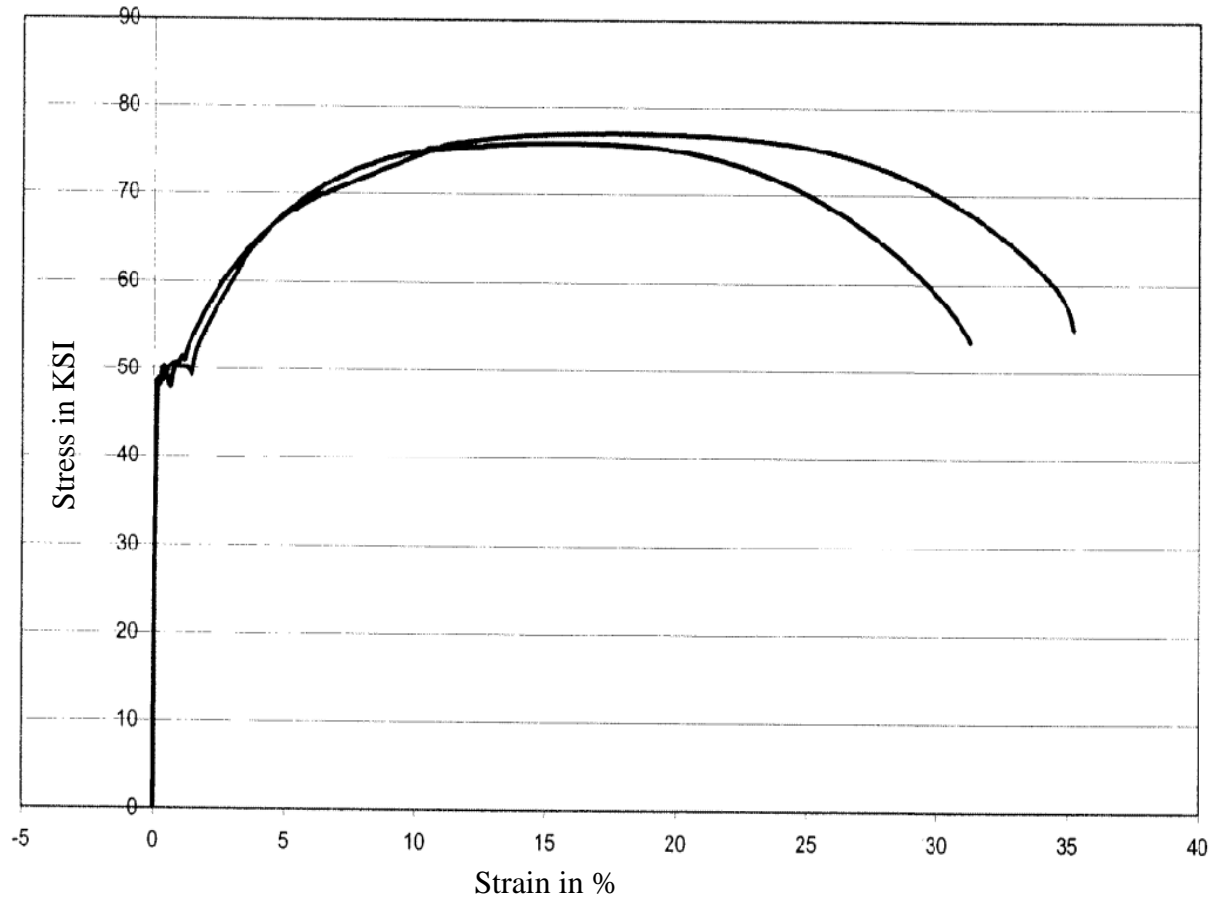
181

Appendix B: Uniaxial test of angle member stress strain curve.

Angle member size: 76.2X76.2X6.4mm

Angle member size: 50.8X50.8X4.8mm

Stress in KSI

Strain in %